Aalborg University

Master project

Analysis of Terahertz Waves in Waveguides

Written by:
Kasper H. Jørgensen
Simon F. Jensen

Supervised by:
Thomas M. Søndergaard

Group 5.330 D
Department of Materials and Production

Spring semester 2020

June 3rd 2020

AALBORG UNIVERSITY
STUDENT REPORT

Title:
Analysis of Terahertz Waves in Waveguides

Theme:
Master

Project period:
Spring semester 2020

Project group:
Group 5.330 D

Participants:
Kasper Hoffmann Jørgensen
Simon Faurholt Jensen

Supervisor:
Thomas Møller Søndergaard

Number of pages: 65

Date of completion:
June 3rd 2020

Abstract
The aim of this project is the modelling of single-mode step-index fibre and slab waveguides in the terahertz range. This will be done by a combination of several analytical and numerical methods and we will derive the relevant theory. We will look into mode profiles, mode coupling by evanescent waves and transmission and reflection in several geometries. For a 200 μm diameter air-silica step-index fibre, we find that single-modes exist for frequencies below 0.607 THz. The coupling length between two identical silica slab waveguides of thickness 200 μm ranges from a few hundred micrometres to several meters due to substantial evanescent waves. The reflection of slab waveguide in several geometries remains low usually below 1 %. Whereas the transmission of the guided mode in a layer of a waveguide suspended in the air to a layer with foam instead of air is highly dependent on the refractive index of foam. The same holds when the guided mode is incident from the waveguide-foam layer to the waveguide-air layer.

Contents

Preface

This report was written by Kasper J. and Simon S. during the spring semester of 2020 at Department of Materials and Production at Aalborg University as a master project. We would like to thank our supervisor Thomas Møller Søndergaard for his guidance during this period.

_____   _____
       Kasper Hoffmann Jørgensen   *Simon Faurholt Jensen*

1 Introduction

The purpose of this report is to examine waveguide which can support guided single modes in the terahertz range. Despite the many applications of waves in the terahertz domain, one may often encounter problems with the high material absorption for waves in this frequency range. However a fairly new method was discovered by *Dominik Walter Vogt* and *Rainer Leonhardt* in [1], where they obtained a Q-factor of 1.5×10^4. We will in this report have a focus on examining similar waveguides as the one presented in the before mentioned text. We will look into single-mode step-index fibre and slab waveguides and investigate several properties of said waveguides.

Our report starts by introducing a general theory about Maxwell's equation and waveguides. Several numerical methods are used such as finite difference, which is applied to Maxwell equations to derive the finite difference frequency domain for a computational Yee Mesh for which the optical field can be calculated. This numerical approach is then optimised by introducing a tensor averaging approximation, which allows us to model circular waveguides more accurately.

The numerical method, the modal method in the frequency domain is presented in chapter 4. The idea behind this approach is to use that the structure in question is piecewise constant along the propagation axis. The eigenmodes are then calculated in each of the constant layers and used to expand the field in their respective layers. To investigate two-dimensional structures, we introduce the Fourier modal method. Furthermore, we will also derive and discuss the theory about the coupling between two waveguides, which can be found in chapter 5. This chapter builds upon coupled-mode theory.

Chapter 6 will then present and discuss the different results obtained from the derived theory in the previously mentioned chapters. This includes; examination of the mode profile, coupling, reflection and transmission.

2 Preliminary theory

2.1 Maxwell's Equations

The Maxwell's equations will serve as the fundamental building block for most of the theory and calculation presented in this report and hence this section will work as an introduction to these equations. Their differential formulation is given by

$$\nabla \times \mathbf{E}(\mathbf{r}, t) = -\frac{\partial}{\partial t}\mathbf{B}(\mathbf{r}, t) \tag{2.1a}$$

$$\nabla \times \mathbf{H}(\mathbf{r}, t) = \frac{\partial}{\partial t}\mathbf{D}(\mathbf{r}, t) + \mathbf{J}_f(\mathbf{r}, t) \tag{2.1b}$$

$$\nabla \cdot \mathbf{D}(\mathbf{r}, t) = \rho_f(\mathbf{r}, t) \tag{2.1c}$$

$$\nabla \cdot \mathbf{B}(\mathbf{r}, t) = 0, \tag{2.1d}$$

where $\mathbf{E}$ and $\mathbf{H}$ are the electric and magnetic field, respectively, ρ_f is the free electron charge density and $\mathbf{J}_f$ is the free current density. Furthermore, the displacement field $\mathbf{D}$ and the magnetic induction $\mathbf{B}$ are defined by the following equations

$$\mathbf{D}(\mathbf{r}, t) = \varepsilon_0 \mathbf{E}(\mathbf{r}, t) + \mathbf{P}(\mathbf{r}, t) \tag{2.2}$$

$$\mathbf{B}(\mathbf{r}, t) = \mu_0 \mathbf{H}(\mathbf{r}, t) + \mathbf{M}(\mathbf{r}, t). \tag{2.3}$$

The vacuum permittivity ε_0 and vacuum permeability μ_0 are connected by the speed of light in vacuum, c, as

$$c = \frac{1}{\sqrt{\varepsilon_0 \mu_0}}. \tag{2.4}$$

The polarisation density, $\mathbf{P}(\mathbf{r}, t)$, and the magnetisation density, $\mathbf{M}(\mathbf{r}, t)$, describes the density of electric and magnetic dipole moments in a material. Assuming that the media is linear, local and isotropic. Then the polarization and magnetisation densities can be expressed as linear response functions leading [2, 3]

$$\mathbf{D}(\mathbf{r}, t) = \varepsilon_0 \mathbf{E}(\mathbf{r}, t) + \varepsilon_0 \int_0^\infty \chi_e(\mathbf{r}, t - \tau)\mathbf{E}(\mathbf{r}, \tau)\, \mathrm{d}\tau \tag{2.5}$$

$$\mathbf{B}(\mathbf{r}, t) = \varepsilon_0 \mathbf{H}(\mathbf{r}, t) + \mu_0 \int_0^\infty \chi_m(\mathbf{r}, t - \tau)\mathbf{H}(\mathbf{r}, \tau)\, \mathrm{d}\tau, \tag{2.6}$$

where χ_e and χ_m are the electric and magnetic susceptibilities respectively. Due to causality, it is required that $\chi_i(\mathbf{r}, t - \tau) = 0$ for $\tau > t$ for $i \in \{e, m\}$.

The Maxwell's equations introduced in eq. (2.1) all contain time derivatives, but it can often be convenient to consider the Fourier transform of these equations and thereby work

in the frequency domain. For example, in finite difference frequency domain (FDFD) uses Maxwell's equations in the frequency domain and will be described further in chapter 3. Starting by Fourier transforming the electric and magnetic fields;

$$\mathbf{E}(\mathbf{r}, \omega) = \int_{-\infty}^{\infty} \mathbf{E}(\mathbf{r}, t) \, \mathrm{e}^{\mathrm{i}\omega t} \, \mathrm{d}t; \qquad \mathbf{E}(\mathbf{r}, t) = \frac{1}{2\pi} \int_{-\infty}^{\infty} \mathbf{E}(\mathbf{r}, \omega) \, \mathrm{e}^{-\mathrm{i}\omega t} \, \mathrm{d}\omega \qquad (2.7)$$

$$\mathbf{H}(\mathbf{r}, \omega) = \int_{-\infty}^{\infty} \mathbf{H}(\mathbf{r}, t) \, \mathrm{e}^{\mathrm{i}\omega t} \, \mathrm{d}t; \qquad \mathbf{H}(\mathbf{r}, t) = \frac{1}{2\pi} \int_{-\infty}^{\infty} \mathbf{H}(\mathbf{r}, \omega) \, \mathrm{e}^{-\mathrm{i}\omega t} \, \mathrm{d}\omega. \qquad (2.8)$$

Consider the Fourier transformation of the displacement field eq. (2.6)

$$\mathbf{D}(\mathbf{r}, \omega) = \int_{-\infty}^{\infty} \mathbf{D}(\mathbf{r}, t) \, \mathrm{e}^{\mathrm{i}\omega t} \, \mathrm{d}t \qquad (2.9)$$

$$= \int_{-\infty}^{\infty} \left(\varepsilon_0 \mathbf{E}(\mathbf{r}, t) + \varepsilon_0 \int_{0}^{\infty} \chi_e(\mathbf{r}, t - \tau) \mathbf{E}(\mathbf{r}, \tau) \, \mathrm{d}\tau \right) \mathrm{e}^{\mathrm{i}\omega t} \, \mathrm{d}t \qquad (2.10)$$

$$= \varepsilon_0 \mathbf{E}(\mathbf{r}, \omega)(1 + \chi_e(\mathbf{r}, \omega)). \qquad (2.11)$$

In the second step, we applied the convolution theorem of Fourier theory, which states [3]

$$F(\omega)G(\omega) = \int_{-\infty}^{\infty} \mathrm{e}^{\pm \mathrm{i}\omega t} \int_{-\infty}^{\infty} F(t - \tau)G(\tau) \, \mathrm{d}\tau \mathrm{d}t. \qquad (2.12)$$

One can in a similar way obtain a relation between $\mathbf{B}$ and $\mathbf{H}$ by applying the same steps to the magnetic induction, $\mathbf{B}$, in eq. (2.6);

$$\mathbf{B}(\mathbf{r}, w) = \mu_0 \mathbf{H}(\mathbf{r}, \omega)(1 + \chi_m(\mathbf{r}, \omega)). \qquad (2.13)$$

The free current density $\mathbf{J}_f$ can be separated into two variables; the source current density $\mathbf{J}_s$ and the currents induced by the electric field $\mathbf{J}_c$ [2, 3]:

$$\mathbf{J}_f(\mathbf{r}, t) = \mathbf{J}_s(\mathbf{r}, t) + \mathbf{J}_c(\mathbf{r}, t) \qquad (2.14)$$

$$= \mathbf{J}_s + \int_{0}^{\infty} \sigma(\mathbf{r}, \tau)\mathbf{E}(\mathbf{r}, t - \tau) \, \mathrm{d}\tau, \qquad (2.15)$$

where σ is the electric conductivity. Applying the Fourier transformation on the free current density gives

$$\mathbf{J}(\mathbf{r}, \omega) = \mathbf{J}_s(\mathbf{r}, \omega) + \sigma(\mathbf{r}, \omega)\mathbf{E}(\mathbf{r}, \omega). \qquad (2.16)$$

The next step is to express eq. (2.1b) in the frequency domain;

$$\nabla \times \mathbf{H}(\mathbf{r}, \omega) = \int_{-\infty}^{\infty} \nabla \times \mathbf{H}(\mathbf{r}, t) \, \mathrm{e}^{\mathrm{i}\omega t} \, \mathrm{d}t \qquad (2.17)$$

$$= \int_{-\infty}^{\infty} \left(\frac{\partial}{\partial t} \mathbf{D}(\mathbf{r}, t) + \mathbf{J}_f(\mathbf{r}, t) \right) \mathrm{e}^{\mathrm{i}\omega t} \, \mathrm{d}t \qquad (2.18)$$

$$= \mathbf{J}_s(\mathbf{r}, \omega) - \mathrm{i}\omega\varepsilon_0 \left(1 + \chi_e(\mathbf{r}, \omega) + \frac{\mathrm{i}\sigma(\mathbf{r}, \omega)}{\omega\varepsilon_0} \right) \mathbf{E}(\mathbf{r}, \omega) \qquad (2.19)$$

$$= \mathbf{J}_s(\mathbf{r}, \omega) - i\omega\varepsilon_0\varepsilon(\mathbf{r}, \omega)\mathbf{E}(\mathbf{r}, \omega). \tag{2.20}$$

The last step can be performed by defining the complex dielectric function as

$$\varepsilon(\mathbf{r}, \omega) = \left(1 + \chi_e(\mathbf{r}, \omega) + \frac{i\sigma(\mathbf{r}, \omega)}{\omega\varepsilon_0}\right). \tag{2.21}$$

Similarly performing the above calculations for eq. (2.1a) yields

$$\nabla \times \mathbf{E}(\mathbf{r}, \omega) = i\omega\mu_0\mu(\mathbf{r}, \omega)\mathbf{H}(\mathbf{r}, \omega). \tag{2.22}$$

For most materials the magnetisation density $\mathbf{M}$ have a small contribution, hence it stands to reason that it can be neglected i.e. $\mu(\mathbf{r}, \omega) = 1$. Under this assumption, the above equation reduces to

$$\nabla \times \mathbf{E}(\mathbf{r}, \omega) = i\omega\mu_0\mathbf{H}(\mathbf{r}, \omega). \tag{2.23}$$

Maxwell's equations in the frequency domain can then be expressed as

$$\nabla \times \mathbf{E}(\mathbf{r}, \omega) = i\omega\mu_0\mathbf{H}(\mathbf{r}, \omega) \tag{2.24a}$$
$$\nabla \times \mathbf{H}(\mathbf{r}, \omega) = \mathbf{J}_s(\mathbf{r}, \omega) - i\omega\varepsilon_0\varepsilon(\mathbf{r}, \omega)\mathbf{E}(\mathbf{r}, \omega) \tag{2.24b}$$
$$\nabla \cdot \mathbf{D}(\mathbf{r}, \omega) = \rho_s(\mathbf{r}, \omega) \tag{2.24c}$$
$$\nabla \cdot \mathbf{B}(\mathbf{r}, \omega) = 0, \tag{2.24d}$$

where $\rho_s(\mathbf{r}, \omega) = \nabla \cdot \mathbf{J}_s(\mathbf{r}, \omega)/i\omega$. In this report we will primarily use Maxwell's equations in the frequency domain and will often use a shortened notation where the argument ω is made implicit.

2.2 Wave Equations

Maxwell's equations in the frequency domain can be used to derive a second-order wave equation, which only involves one of either the magnetic or the electric field. The derivation for the electric field will be performed in this chapter, but the principle can be used similarly to derive the wave equation for the magnetic field. Taking the curl of eq. (2.24a) and substitute eq. (2.24b) into this equation gives

$$\nabla \times \nabla \times \mathbf{E}(\mathbf{r}, \omega) - k_0^2\varepsilon(\mathbf{r}, \omega)\mathbf{E}(\mathbf{r}, \omega) = i\omega\mu_0\mathbf{J}_s(\mathbf{r}, \omega), \tag{2.25}$$

where $k_0^2 = \omega^2\varepsilon_0\mu_0$. In this report we will primarily work with regions far from source currents, therefore the source current will be neglected in the following calculation. Furthermore by applying the identity $\nabla \times (\nabla \times \mathbf{A}) = -\nabla^2\mathbf{A} + \nabla(\nabla \cdot A)$ to the above equation yields

$$\nabla^2\mathbf{E}(\mathbf{r}, \omega) - \nabla(\nabla \cdot \mathbf{E}(\mathbf{r}, \omega)) + k_0^2\varepsilon(\mathbf{r}, \omega)\mathbf{E}(\mathbf{r}, \omega) = 0. \tag{2.26}$$

Assuming that there are no free-charges, $\rho_s(\mathbf{r}, \omega) = 0$, then from eq. (2.24c) the following expression can be derived

$$\nabla \cdot \mathbf{E}(\mathbf{r}, \omega) = -\mathbf{E}(\mathbf{r}, \omega) \cdot \nabla \ln(\varepsilon(\mathbf{r}, \omega)), \tag{2.27}$$

where we have used the identity

$$\nabla \cdot (c\mathbf{A}) = c\nabla \cdot \mathbf{A} + (\nabla c) \cdot \mathbf{A} \tag{2.28}$$

and $\frac{1}{c}\nabla c = \nabla(\ln(c))$. In the case where $\varepsilon(\mathbf{r}, \omega)$ varies slowly, then the term in eq. (2.27) can be neglected and eq. (2.26) is reduced to

$$(\nabla^2 + k_0^2 \varepsilon(\mathbf{r}, \omega))\mathbf{E}(\mathbf{r}, \omega) = 0. \tag{2.29}$$

Taking the curl of eq. (2.24b) and substitute eq. (2.24a) and repeating the above steps for the magnetic field gives a similar wave equation

$$(\nabla^2 + k_0^2 \varepsilon(\mathbf{r}, \omega))\mathbf{H}(\mathbf{r}, \omega) = 0. \tag{2.30}$$

It should be noted that the wave equation for the magnetic and electric fields are identical and that the components of both fields decouple, which means that the wave equation can be reduced to a scalar equation

$$\nabla^2 \Psi + \varepsilon k_0^2 \Psi = 0, \tag{2.31}$$

where Ψ can denote any component of $\mathbf{H}$ and $\mathbf{E}$.

In the case where the material is homogeneous and the material functions ε and μ do not depend on the coordinates, these wave equations can be reduced to Helmholtz equations [3]

$$\nabla^2 \mathbf{H}(\mathbf{r}) + k_0^2 \varepsilon \mu \mathbf{H}(\mathbf{r}) = 0 \tag{2.32a}$$

$$\nabla^2 \mathbf{E}(\mathbf{r}) + k_0^2 \varepsilon \mu \mathbf{E}(\mathbf{r}) = 0. \tag{2.32b}$$

In the case where ε and μ are piecewise constant, the Helmholtz equations can still be locally valid in regions where ε and μ are constant. By matching the local solutions from these equations across the material interfaces with appropriate boundary conditions, then solutions can still be found.

2.3 Waveguides

The main topic of this project is to study waveguides in the terahertz band and their properties will be investigated in this section. Waveguides are those geometries featuring uniformly along one axis. This class of geometries is especially interesting because they are widely used in e.g. single and multi-mode step-index optical fibres or slab waveguides.

In this section the uniform axis of the waveguides is taking to be the *z*-axis. In this case the dielectric constant $\varepsilon(\mathbf{r}) = \varepsilon(\mathbf{r}_\perp)$ only depends on the transverse coordinates. In this case $\mathbf{r}_\perp = (x, y)$.

In this section, we will consider non-magnetic waveguides without free charges and currents and a monochromatic optical field on the form

$$\mathbf{E}(\mathbf{r},t) = \mathbf{E}(\mathbf{r})\,\mathrm{e}^{-\mathrm{i}\omega t}, \quad \mathbf{H}(\mathbf{r},t) = \mathbf{H}(\mathbf{r})\,\mathrm{e}^{-\mathrm{i}\omega t}, \tag{2.33}$$

and with this time convention the Maxwell's equations is given by eq. (2.24) with $\mathbf{J}_s = \mathbf{0}$ and $\rho_s = 0$. Since the z-axis is uniform, the electric and magnetic field can be written on the form

$$\mathbf{E}(\mathbf{r}) = \mathbf{e}(\mathbf{r}_\perp)\,\mathrm{e}^{\mathrm{i}\beta z} \tag{2.34}$$

$$\mathbf{H}(\mathbf{r}) = \mathbf{h}(\mathbf{r}_\perp)\,\mathrm{e}^{\mathrm{i}\beta z}, \tag{2.35}$$

where β is the propagation constant and is used to describe the z-dependency of the field. Within the assumptions made so far one can combine eqs. (2.26) and (2.27) into

$$\nabla^2 \mathbf{E}(\mathbf{r},\omega) + \nabla(\mathbf{E}(\mathbf{r},\omega) \cdot \nabla \ln(\varepsilon(\mathbf{r},\omega))) + \varepsilon(\mathbf{r},\omega)k_0^2 \mathbf{E}(\mathbf{r},\omega) = 0, \tag{2.36}$$

which holds generally. If we apply the assumptions of uniform z-axis and with the electric field presented earlier, this can be written as a second-order eigenvalue problem [3]

$$\nabla_\perp^2 \mathbf{e} + (\nabla_\perp + \mathrm{i}\beta\hat{\mathbf{z}})(\mathbf{e} \cdot \nabla \ln(\varepsilon(\mathbf{r}_\perp))) + \varepsilon(\mathbf{r}_\perp)k_0^2 \mathbf{e} = \beta^2 \mathbf{e}. \tag{2.37}$$

This equation can be simplified to a standard eigenvalue problem by noticing that the z-derivative of ε is zero, which indicates that the transverse field is not coupled to e_z hence

$$\nabla_\perp^2 \mathbf{e} + \nabla_\perp(\mathbf{e} \cdot \nabla \ln(\varepsilon(\mathbf{r}_\perp))) + \varepsilon(\mathbf{r}_\perp)k_0^2 \mathbf{e} = \beta^2 \mathbf{e}. \tag{2.38}$$

When solving this equation one obtain the eigenvalues $\lambda_m = \beta_m^2$ and the eigenmodes $\mathrm{e}_{\perp,m}(\mathbf{r}_\perp)$. If β is real-valued, then there will exist a solution for both positive and negative values of β. With the time convention, $\exp(-\mathrm{i}\omega t)$ and ω positive, the negative values of β will represent to backward travelling waves and the positive values of β will represent to forward travelling waves. This will be reversed if ω changed sign. For the case where the eigenvalues are negative the propagation constants will assume complex values, which leads to modes that either increase or decrease exponentially along the propagation axis. The modes with exponential decreasing fields make physical sense and these modes are called evanescent modes.

The transverse electric field $\mathbf{e}_\perp$ can be calculated by solving eq. (2.38). In the case where there are no free charges one can connect e_z and $\mathbf{e}_\perp$ with Gauss law

$$\nabla \cdot (\varepsilon \mathbf{E}) = 0. \tag{2.39}$$

Since $\nabla = (\nabla_\perp, \nabla_z)$ where $\nabla_\perp$ is the transverse part of the nabla operator and using that ε only depend on the lateral coordinates, the following identity can be derived

$$e_z = \frac{-\nabla_\perp \cdot (\varepsilon \mathbf{e}_\perp)}{\mathrm{i}\beta\varepsilon}. \tag{2.40}$$

Similarly one can use eq. (2.24d) with the assumption that the material is non-magnetic to derive

$$h_z = \frac{\mathrm{i}}{\beta}\nabla_\perp \cdot \mathbf{h}_\perp. \tag{2.41}$$

Using e_z's expression in eq. (2.40), the magnetic field can be calculated from eq. (2.24a) as

$$\mathbf{H} = \frac{1}{\mathrm{i}\omega\mu_0}\left(-\hat{\mathbf{x}}\left(\mathrm{i}\beta E_y - \frac{\partial E_z}{\partial y}\right) + \hat{\mathbf{y}}\left(\mathrm{i}\beta E_x - \frac{\partial E_z}{\partial x}\right) + \hat{\mathbf{z}}\left(\frac{\partial E_y}{\partial x} - \frac{\partial E_x}{\partial y}\right)\right). \tag{2.42}$$

The lateral coordinates of $\mathbf{H}$ can be extracted with $\mathbf{H}_\perp = \hat{\mathbf{z}} \times \mathbf{H} \times \hat{\mathbf{z}}$ and the z-component with $H_z = \hat{\mathbf{z}} \cdot \mathbf{H}$, which leads to [3]

$$\mathbf{h}_\perp = \frac{1}{\mu_0\omega}\hat{\mathbf{z}} \times \left(\beta\mathbf{e}_\perp - \nabla_\perp\left(\frac{\nabla_\perp \cdot (\varepsilon\mathbf{e}_\perp)}{\beta\varepsilon}\right)\right) \tag{2.43}$$

$$h_z = \hat{\mathbf{z}} \cdot \frac{\nabla \times \mathbf{e}_\perp}{\mathrm{i}\mu_0\omega}. \tag{2.44}$$

As mentioned earlier. there are both forward and backward travelling solutions for the same eigenmode $\mathbf{e}_\perp$ of the eigenvalue problem. The forward mode profile for the magnetic and electric field is given by

$$\mathbf{E}^+(\mathbf{r}) = (\mathbf{e}_\perp(\mathbf{r}_\perp) + e_z(\mathbf{r}_\perp)\hat{\mathbf{z}})\,\mathrm{e}^{\mathrm{i}\beta z} \tag{2.45}$$

$$\mathbf{H}^+(\mathbf{r}) = (\mathbf{h}_\perp(\mathbf{r}_\perp) + h_z(\mathbf{r}_\perp)\hat{\mathbf{z}})\,\mathrm{e}^{\mathrm{i}\beta z}. \tag{2.46}$$

Since the transverse part of the electric field for a forward and backward propagating wave is derived from the same eigenmode $\mathbf{e}_\perp$, then $\mathbf{e}_\perp$ is independent on β's sign. This is however not the case for e_z as can be seen from eq. (2.40). This is reversed for the magnetic field as can be seen from eqs. (2.43) and (2.44), hence leading to the following expression for the backward travelling mode

$$\mathbf{E}^-(\mathbf{r}) = (\mathbf{e}_\perp(\mathbf{r}_\perp) - e_z(\mathbf{r}_\perp)\hat{\mathbf{z}})\,\mathrm{e}^{-\mathrm{i}\beta z} \tag{2.47}$$

$$\mathbf{H}^-(\mathbf{r}) = (-\mathbf{h}_\perp(\mathbf{r}_\perp) + h_z(\mathbf{r}_\perp)\hat{\mathbf{z}})\,\mathrm{e}^{-\mathrm{i}\beta z}. \tag{2.48}$$

The wave equation for a waveguide can be reduced to a scalar wave equation [3]

$$\nabla_\perp^2\Psi + \varepsilon k_0^2\Psi = \beta^2\Psi, \tag{2.49}$$

where Ψ is any of the lateral components of the electric or magnetic field. One should keep in mind that the field still needs to satisfy the divergence constraints.

2.3.1 Slab Waveguides

In this section, the focus point will be slab waveguides which is a structure where the permittivity only depends on one lateral coordinate, which is taken to be the x-coordinate.

We look at the class of solutions $\mathbf{e}(x)$ independent of the y coordinate. This assumption allows us to rewrite eq. (2.38) into two equations, one for e_x and one for e_y given by

$$\frac{\partial^2 e_x}{\partial x^2} + \frac{\partial}{\partial x}\left(e_x \frac{\mathrm{d}\ln(\varepsilon(x))}{\mathrm{d}x}\right) + \varepsilon(x)k_0^2 e_x = \beta^2 e_x \qquad \text{(TM)} \tag{2.50}$$

$$\frac{\partial^2 e_y}{\partial x^2} + \varepsilon(x)k_0^2 e_y = \beta^2 e_y \qquad \text{(TE)}, \tag{2.51}$$

respectively, where it was used that $\partial \mathbf{e}/\partial y = \mathbf{0}$. In order to calculate e_z one can use eq. (2.40). It should here be noted that only the solution from eq. (2.50) gives a contribution to e_z, because $\partial e_y/\partial y = 0$. For the case where the solution is polarised along the y-axis, then $e_z = 0$ and therefore these type of modes is often known as transverse electric (TE) modes.

2.3.2 Boundary Conditions and Eigenmode Classes

In many cases, it is useful to divide the different types of eigenmodes into groups separated by their eigenvalues. A simple waveguide with real-valued relative permittivity profiles will be considered. The classification will be done through examples with three classes of geometries, which are all shown in fig. 2.1. The first case of interest is the open geometry shown in fig. 2.1a. The modes in an open geometry may be separated into two different groups: The discrete set of guided modes and the continuum of radiation modes. The discrete modes satisfies the equation $\varepsilon_1 k_0^2 < \beta^2 < \varepsilon_2 k_0^2$ and the radiation modes satisfies $\beta^2 < \varepsilon_1 k_0^2$. The second geometry is a periodic structure with period L_x as shown in fig. 2.1a. While the domain is infinite, the periodicity reduces the computational domain to a single period by applying the Bloch theorem

$$\mathbf{E}(x + L_x) = \mathbf{E}(x)\,\mathrm{e}^{\mathrm{i}\alpha}. \tag{2.52}$$

This discretises the continuum of radiation modes into discrete modes, which is often called semi-radiation modes.

Another common boundary that is frequently used is the closed boundary consisting of perfectly conducting walls as shown in fig. 2.1c. The corresponding boundary condition reads

$$\mathbf{E}(0) = \mathbf{E}(L_x) = 0, \tag{2.53}$$

and reduces the computational domain to finite size of L_x leading again to a discretisation of the continuum of radiation modes.

2.4 Orthogonality

This section sets out to prove the orthogonality relation between the lateral eigenmodes. This is done by considering two solutions to Maxwell's equations $(\mathbf{E}_j, \mathbf{H}_j)$, which is generated by the corresponding free current sources $\mathbf{J}_j$, where $j \in \{1, 2\}$. These solutions need to satisfy Maxwell's equations

$$\nabla \times \mathbf{E}_j = \mathrm{i}\omega\mu_0\mu\mathbf{H}_j \tag{2.54}$$

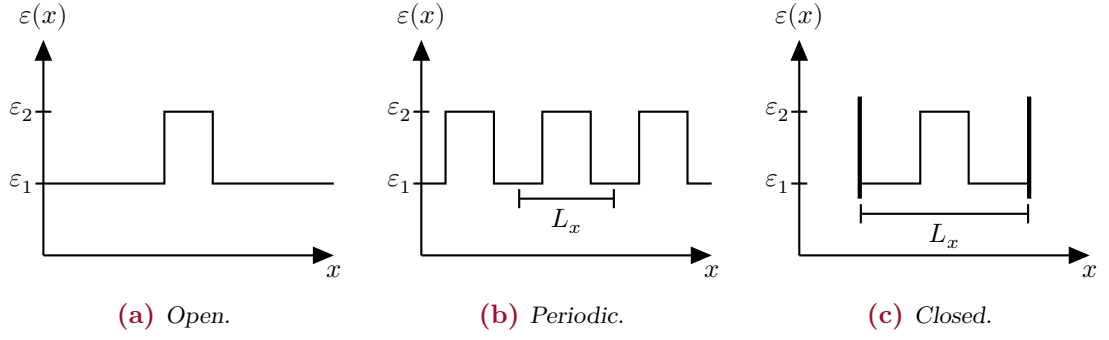(a) *Open.*   (b) *Periodic.*   (c) *Closed.*

Figure 2.1: *(a) Shows an open geometry having no boundary conditions. (b) Shows a geometry with periodic boundary conditions. (b) Shows a geometry with closed boundary conditions. The latter two leads to a discretiation of the radiation band.*

$$\nabla \times \mathbf{H}_j = -\,\mathrm{i}\omega\varepsilon_0\varepsilon\mathbf{E}_j + \mathbf{J}_j. \tag{2.55}$$

The first step is to take the dot product between $\mathbf{E}_i$ and $\nabla \times \mathbf{H}_j$ and the dot product between $\mathbf{H}_i$ and $\nabla \times \mathbf{E}_j$, where $i, j \in \{1, 2\}$ and $i \neq j$. The four dot products are then added and subtracted in the following way

$$\mathbf{H}_2 \cdot (\nabla \times \mathbf{E}_1) - \mathbf{E_1} \cdot (\nabla \times \mathbf{H}_2) + \mathbf{E}_2 \cdot (\nabla \times \mathbf{H}_1) - \mathbf{H}_1 \cdot (\nabla \times \mathbf{E}_2) = \tag{2.56}$$
$$\mathbf{H}_2 \cdot (\mathrm{i}\omega\mu_0\mu\mathbf{H}_1) - \mathbf{E}_1 \cdot (-\,\mathrm{i}\omega\varepsilon_0\varepsilon\mathbf{E}_2 + \mathbf{J}_2) + \mathbf{E}_2 \cdot (-\,\mathrm{i}\omega\varepsilon_0\varepsilon\mathbf{E}_1 + \mathbf{J}_1) - \mathbf{H}_1 \cdot (\mathrm{i}\omega\mu_0\mu\mathbf{H}_2).$$

This expression can be greatly simplified by noticing that most terms on the right hand side of eq. (2.56) cancels and applying the identity $\nabla \cdot (\mathbf{A} \times \mathbf{B}) = \mathbf{B} \cdot (\nabla \times \mathbf{A}) - \mathbf{A} \cdot (\nabla \times \mathbf{B})$ and this leaves us with

$$\nabla \cdot (\mathbf{E}_1 \times \mathbf{H}_2 - \mathbf{E}_2 \times \mathbf{H}_1) = \mathbf{J}_1 \cdot \mathbf{E}_2 - \mathbf{J}_2 \cdot \mathbf{E}_1. \tag{2.57}$$

Integrating the above equation over a volume V as shown in fig. 2.2 and applying Gauss Theorem one can obtain

$$\oint_S (\mathbf{E}_1 \times \mathbf{H}_2 - \mathbf{E}_2 \times \mathbf{H}_1) \cdot \hat{\mathbf{n}}\,\mathrm{d}A = \int_V \mathbf{J}_1 \cdot \mathbf{E}_2 - \mathbf{J}_2 \cdot \mathbf{E}_1\,\mathrm{d}V, \tag{2.58}$$

where $\hat{\mathbf{n}}$ is a unit vector normal to the surface S pointing outward. Assume the structure is uniform along the z-axis with thickness $\Delta z = z_2 - z_1$. The surface of the structure can be separated into three parts, a front surface S_1, a back surface S_2 and the side surfaces S_a, S_b, S_c and S_d as shown in fig. 2.2. The surface integral in eq. (2.58) for the sides can be expressed as a sum of surface integrals for each side hence

$$\int_{\delta S} \mathbf{F} \cdot \hat{\mathbf{n}}\,\mathrm{d}A = \int_{S_a} \mathbf{F} \cdot \hat{\mathbf{n}}_a\,\mathrm{d}A + \int_{S_b} \mathbf{F} \cdot \hat{\mathbf{n}}_b\,\mathrm{d}A + \int_{S_c} \mathbf{F} \cdot \hat{\mathbf{n}}_c\,\mathrm{d}A + \int_{S_d} \mathbf{F} \cdot \hat{\mathbf{n}}_d\,\mathrm{d}A, \tag{2.59}$$

where we have introduced the notation $\mathbf{F} = \mathbf{E}_1 \times \mathbf{H}_2 - \mathbf{E}_2 \times \mathbf{H}_1$ and $\delta S = S_a \cup S_b \cup S_c \cup S_d$ to simplify the expression.
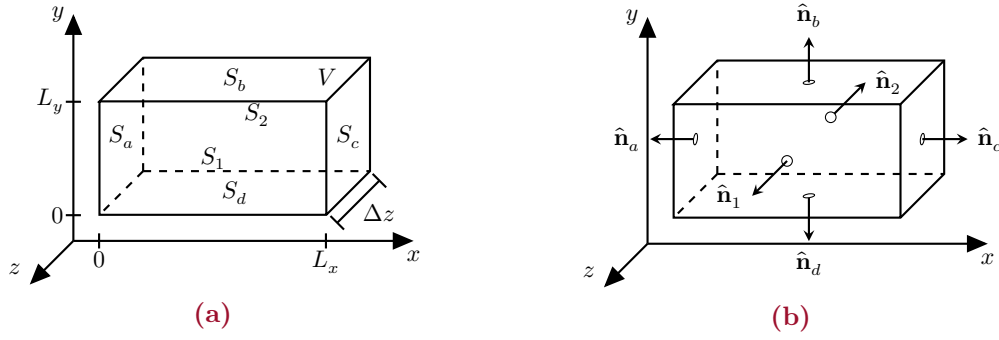
Figure 2.2: *(a) A box volume V covered by the surface top S_1, bottom S_2, the four sides S_a, S_b, S_c and S_d. (b) Shows the same box with the normal unit vectors of each surface with a similar label convention.*

In the case of a periodic boundary condition $\mathbf{F}(0, y, z) = \mathbf{F}(L_x, y, z)$ we have

$$\int_{S_a} \mathbf{F}(0, y, z) \cdot \hat{\mathbf{n}}_a \, dA = -\int_{S_c} \mathbf{F}(L_x, y, z) \cdot \hat{\mathbf{n}}_c \, dA. \tag{2.60}$$

A similar argument can be made for the surfaces S_b and S_d, hence showing that the surface integrals of the sides cancel out.

In the case where the sides are made of perfect conducting metal walls, the tangential components of the magnetic field must tend to zero at the boundary, leading to $\mathbf{F} \cdot \hat{\mathbf{n}} = 0$ at the walls, hence the boundary integral disappears. The surface integrals for the top and bottom surfaces in eq. (2.58) can be expressed as

$$\int_{S_1} \mathbf{F} \cdot \hat{\mathbf{n}}_1 \, dA + \int_{S_2} \mathbf{F} \cdot \hat{\mathbf{n}}_2 \, dA = -\int F_z(x, y, z_1) \, d\mathbf{r}_\perp + \int F_z(x, y, z_2) \, d\mathbf{r}_\perp \tag{2.61}$$

$$= \int F_z(x, y, z_2) - F_z(x, y, z_1) \, d\mathbf{r}_\perp. \tag{2.62}$$

Since we already assumed that the structure is invariant along the z-axis, the field must be continuous along z. For small Δz the field can be seen as constant hence the surface integral can be written as

$$\int_V \mathbf{J}_1 \cdot \mathbf{E}_2 - \mathbf{J}_2 \cdot \mathbf{E}_1 \, dV = \Delta z \int \mathbf{J}_1 \cdot \mathbf{E}_2 - \mathbf{J}_2 \cdot \mathbf{E}_1 \, d\mathbf{r}_\perp. \tag{2.63}$$

By dividing with Δz and taking the limit $\Delta z \to 0$ we obtain

$$\int \frac{\partial}{\partial z}(\mathbf{E}_1 \times \mathbf{H}_2 - \mathbf{E}_2 \times \mathbf{H}_1) \cdot \hat{\mathbf{z}} \, d\mathbf{r}_\perp = \int \mathbf{J}_1 \cdot \mathbf{E}_2 - \mathbf{J}_2 \cdot \mathbf{E}_1 \, d\mathbf{r}_\perp. \tag{2.64}$$

Now assume that the free currents $\mathbf{J}_1$ and $\mathbf{J_2}$ are absent i.e. $\mathbf{J}_1 = \mathbf{J_2} = \mathbf{0}$, then the right hand side of eq. (2.64) is zero. Consider the two solutions $(\mathbf{E}_1, \mathbf{H}_1)$ and $(\mathbf{E}_2, \mathbf{H}_2)$ as forward propagating modes on the form in eq. (2.46)

$$\begin{bmatrix} \mathbf{E}_j^+(\mathbf{r}) \\ \mathbf{H}_j^+(\mathbf{r}) \end{bmatrix} = \begin{bmatrix} \mathbf{e}_{\perp,j}(\mathbf{r}_\perp) + e_{z,j}(\mathbf{r}_\perp)\hat{\mathbf{z}} \\ \mathbf{h}_{\perp,j}(\mathbf{r}_\perp) + h_{z,j}(\mathbf{r}_\perp)\hat{\mathbf{z}} \end{bmatrix} e^{i\beta_j z}, \tag{2.65}$$

for $j \in \{1, 2\}$ and inserting it into eq. (2.64) gives

$$(\beta_1 + \beta_2) \int (\mathbf{e}_{\perp,1} \times \mathbf{h}_{\perp,2} - \mathbf{e}_{\perp,2} \times \mathbf{h}_{\perp,1}) \cdot \hat{\mathbf{z}} \, \mathrm{d}\mathbf{r}_\perp = 0. \qquad (2.66)$$

A similar expression can be derived by replacing the forward propagating mode to a backward propagating mode i.e. $(\mathbf{E}_2^+, \mathbf{H}_2^+) \to (\mathbf{E}_2^-, \mathbf{H}_2^-)$. The backward propagating mode is on the form in eq. (2.46)

$$\begin{bmatrix} \mathbf{E}_2^-(\mathbf{r}) \\ \mathbf{H}_2^-(\mathbf{r}) \end{bmatrix} = \begin{bmatrix} \mathbf{e}_{\perp,2}(\mathbf{r}_\perp) - e_{z,2}(\mathbf{r}_\perp)\hat{\mathbf{z}} \\ -\mathbf{h}_{\perp,2}(\mathbf{r}_\perp) + h_{z,2}(\mathbf{r}_\perp)\hat{\mathbf{z}} \end{bmatrix} \mathrm{e}^{-\mathrm{i}\beta_2 z}. \qquad (2.67)$$

Note that $\mathbf{e}_{\perp,2}$, $\mathbf{h}_{\perp,2}$, $e_{z,2}$ and $h_{z,2}$ for the forward and backward propagating modes are identical. Inserting $(\mathbf{E}_1^+, \mathbf{H}_1^+)$ and $(\mathbf{E}_2^-, \mathbf{H}_2^-)$ into eq. (2.64) gives

$$(\beta_2 - \beta_1) \int (\mathbf{e}_{\perp,1} \times \mathbf{h}_{\perp,2} + \mathbf{e}_{\perp,2} \times \mathbf{h}_{\perp,1}) \cdot \hat{\mathbf{z}} \, \mathrm{d}\mathbf{r}_\perp = 0. \qquad (2.68)$$

If $\beta_1 \neq \beta_2$, then the only way for eqs. (2.66) and (2.68) to be fulfilled is to set the integrals equal to zero. Summing eqs. (2.66) and (2.68) together gives

$$\int (\mathbf{e}_1 \times \mathbf{h}_2) \cdot \hat{\mathbf{z}} \, \mathrm{d}\mathbf{r}_\perp = 0, \qquad (2.69)$$

which is the called the orthogonality relation. If $\beta_1 = \beta_2$ then the solutions $(\mathbf{E}_1, \mathbf{H}_1)$ and $(\mathbf{E}_2, \mathbf{H}_2)$ are not necessary orthogonal and in that case cannot satisfy eq. (2.69). However, a Gram-Schmidt procedure can be used to orthogonalise the solutions.

Another orthogonality relation can be obtained by making the replacement $(\mathbf{E}_2, \mathbf{H}_2, \mathbf{J}_2)$ $\to (\mathbf{E}_2^*, \mathbf{H}_2^*, \mathbf{J}_2^*)$ and repeating the above steps leads to the power orthogonality relation given by [3]

$$\int (\mathbf{e}_1 \times \mathbf{h}_2^*) \cdot \hat{\mathbf{z}} \, \mathrm{d}\mathbf{r}_\perp = 0. \qquad (2.70)$$

The last relation can be used along with the time-averaged Poynting vector (eq. (2.93)), hence its name. Equation (2.69) is more general than eq. (2.70) as it holds for arbitrary geometries including those with complex dielectric profiles. Equation (2.70) however, only holds for real-valued dielectric profiles [3].

2.5 Poynting Vector

The Poynting vector is defined as

$$\mathbf{S}(\mathbf{r}, t) = \mathbf{E}(\mathbf{r}, t) \times \mathbf{H}(\mathbf{r}, t). \qquad (2.71)$$

The net electromagnetic power P_{out} that propagates out of the surface S surrounding a volume Ω can be found by integrating the outward flux of the Poynting vector across S.

$$P_{\mathrm{out}} = \oint_S \mathbf{S}(\mathbf{r}, t) \cdot \hat{\mathbf{n}} \, \mathrm{d}A, \qquad (2.72)$$

where $\hat{\mathbf{n}}$ is an outward pointing normal unit vector to the surface S. This surface integral can be written as a volume integral by the divergence theorem

$$\oint_S \mathbf{S}(\mathbf{r},t) \cdot \hat{\mathbf{n}} \, \mathrm{d}A = \int_\Omega \nabla \cdot \mathbf{S}(\mathbf{r},t) \, \mathrm{d}V. \tag{2.73}$$

Note that in the following equations $\mathbf{H}, \mathbf{E}, \mathbf{D}, \mathbf{J}$ and $\mathbf{P}$ are all dependent on $\mathbf{r}$ and t, but in order to shorten the notation this is made implicit. To see how the Poynting vector can describe the flow of electromagnetic power, the above expression can be expanded by adding the following on each side

$$\frac{1}{2}\frac{\mathrm{d}}{\mathrm{d}t}\int_\Omega \mathbf{B}\cdot\mathbf{H} + \mathbf{D}\cdot\mathbf{E}\,\mathrm{d}V$$

$$= \frac{1}{2}\int_\Omega \mathbf{H}\cdot\frac{\partial\mathbf{B}}{\partial t} + \mathbf{B}\cdot\frac{\partial\mathbf{H}}{\partial t} + \mathbf{E}\cdot\frac{\partial\mathbf{D}}{\partial t} + \mathbf{D}\cdot\frac{\partial\mathbf{E}}{\partial t}\,\mathrm{d}V \tag{2.74}$$

$$= \frac{1}{2}\int_\Omega 2\mathbf{H}\cdot(-\nabla\times\mathbf{E}) + \mathbf{E}\cdot(\nabla\times\mathbf{H}-\mathbf{J}) + (\varepsilon_0\mathbf{E}+\mathbf{P})\cdot\left(\frac{1}{\varepsilon_0}\frac{\partial}{\partial t}(\mathbf{D}-\mathbf{P})\right)\mathrm{d}V \tag{2.75}$$

$$= \frac{1}{2}\int_\Omega 2\mathbf{H}\cdot(-\nabla\times\mathbf{E}) + 2\mathbf{E}\cdot(\nabla\times\mathbf{H}-\mathbf{J}) - \mathbf{E}\cdot\frac{\partial}{\partial t}\mathbf{P} + \frac{\mathbf{P}}{\varepsilon_0}\cdot\frac{\partial}{\partial t}(\mathbf{D}-\mathbf{P})\,\mathrm{d}V. \tag{2.76}$$

Hence eq. (2.73) can be written as

$$\oint_S \mathbf{S}(\mathbf{r},t)\cdot\hat{\mathbf{n}}\,\mathrm{d}A + \frac{1}{2}\frac{\mathrm{d}}{\mathrm{d}t}\int_\Omega \mathbf{B}\cdot\mathbf{H}+\mathbf{D}\cdot\mathbf{E}\,\mathrm{d}V \tag{2.77}$$

$$= \int_\Omega \nabla\cdot\mathbf{S}\,\mathrm{d}V + \frac{1}{2}\int_\Omega 2\mathbf{E}\cdot(\nabla\times\mathbf{H}-2\mathbf{H}\cdot(\nabla\times\mathbf{E})+-\mathbf{J}) - \mathbf{E}\cdot\frac{\partial}{\partial t}\mathbf{P} + \frac{\mathbf{P}}{\varepsilon_0}\cdot\frac{\partial}{\partial t}(\mathbf{D}-\mathbf{P})\,\mathrm{d}V,$$

where we have used the approximation $\mathbf{B}(\mathbf{r},t) = \mu_0\mathbf{H}(\mathbf{r},t)$. By using the identity

$$\nabla\cdot\mathbf{S} = \nabla\cdot(\mathbf{E}\times\mathbf{H}) = \mathbf{H}\cdot(\nabla\times\mathbf{E}) - \mathbf{E}\cdot(\nabla\times\mathbf{H}), \tag{2.78}$$

eq. (2.77) can be written as

$$\oint_S \mathbf{S}\cdot\hat{\mathbf{n}}\,\mathrm{d}A + \frac{1}{2}\frac{\mathrm{d}}{\mathrm{d}t}\int_\Omega \mathbf{B}\cdot\mathbf{H}+\mathbf{D}\cdot\mathbf{E}\,\mathrm{d}V \tag{2.79}$$

$$= -\int_\Omega \mathbf{E}\cdot\mathbf{J}\,\mathrm{d}V - \frac{1}{2}\int_\Omega \mathbf{E}\cdot\frac{\partial\mathbf{P}}{\partial t} - \mathbf{P}\cdot\frac{\partial\mathbf{E}}{\partial t}\,\mathrm{d}V. \tag{2.80}$$

In the case of a linear and non-dispersive material, the polarisation can be expressed as

$$\mathbf{P}(\mathbf{r},t) = \chi_e(\mathbf{r})\mathbf{E}(\mathbf{r},t), \tag{2.81}$$

and since χ_e does not depend on time, then the last term on the right-hand side of eq. (2.80) cancels out and Poynting theorem is obtained

$$\oint_S \mathbf{S}(\mathbf{r},t)\cdot\hat{\mathbf{n}}\,\mathrm{d}A + \frac{\mathrm{d}U}{\mathrm{d}t} = -\int_\Omega \mathbf{E}(\mathbf{r},t)\cdot\mathbf{J}(\mathbf{r},t)\,\mathrm{d}V \tag{2.82}$$

$$U = \frac{1}{2} \int_{\Omega} \mathbf{B}(\mathbf{r}, t) \cdot \mathbf{H}(\mathbf{r}, t) + \mathbf{D}(\mathbf{r}, t) \cdot \mathbf{E}(\mathbf{r}, t) \, \mathrm{d}V. \tag{2.83}$$

Here U represent the energy stored in the built-up electric and magnetic fields whereas $\oint_S \mathbf{S}(\mathbf{r}, t) \cdot \hat{\mathbf{n}} \, \mathrm{d}A$ evidently represents the electromagnetic power that is propagating out of the volume Ω, across its boundary S. The integral $\int_{\Omega} \mathbf{E}(\mathbf{r}, t) \cdot \mathbf{J}(\mathbf{r}, t) \, \mathrm{d}V$ describes the dissipation inside Ω [2, 4].

In the case where the material is linear and dispersive, then for a narrow spectral width around $\omega = \omega_0$ the Poynting theorem can instead be expressed as [2]

$$\int_S \langle \mathbf{S}(\mathbf{r}, t) \rangle \cdot \hat{\mathbf{n}} \, \mathrm{d}A + \frac{\mathrm{d}}{\mathrm{d}t} U_{\text{eff}} \tag{2.84}$$

$$= \int_{\Omega} \langle \mathbf{E}(\mathbf{r}, t) \cdot \mathbf{J}_s(\mathbf{r}, t) \rangle \, \mathrm{d}V - \omega_0 \varepsilon_0 \int_{\omega} \text{Im}(\varepsilon(\mathbf{r}, \omega_0)) \langle \mathbf{E}(\mathbf{r}, t) \cdot \mathbf{E}(\mathbf{r}, t) \rangle \, \mathrm{d}V. \tag{2.85}$$

The effective electromagnetic energy built up is now given by

$$U_{\text{eff}} = \frac{1}{2} \varepsilon_0 \int_{\Omega} \text{Re} \left(\frac{\mathrm{d}\omega \varepsilon(\mathbf{r}, \omega)}{\mathrm{d}\omega} \right)_{\omega = \omega_0} \langle \mathbf{E}(\mathbf{r}, t) \cdot \mathbf{E}(\mathbf{r}, t) \rangle \, \mathrm{d}V. \tag{2.86}$$

Note that the brackets $\langle \cdots \rangle$ denote the time average over one cycle of the frequency ω_0.

In the case where the spectral width of the fields is small enough to be treated as a monochromatic field, it is then convenient to express the electric field on the form

$$\mathbf{E}(\mathbf{r}, t) = \text{Re}\big(\mathbf{E}(\mathbf{r}, \omega) \, \mathrm{e}^{-\mathrm{i}\omega t}\big) = \frac{1}{2}\big(\mathbf{E}(\mathbf{r}, \omega) \, \mathrm{e}^{-\mathrm{i}\omega t} + \mathbf{E}^*(\mathbf{r}, \omega) \, \mathrm{e}^{+\mathrm{i}\omega t}\big). \tag{2.87}$$

The fields $\mathbf{H}$, $\mathbf{D}$, $\mathbf{B}$ and $\mathbf{J}$ can be written on a similar form. The time average of the Poynting vector can be found by integrating over a time period $T = 2\pi/\omega$ such that

$$\mathbf{S}_{\text{av}}(\mathbf{r}) = \frac{1}{T} \int_0^T \mathbf{S}(\mathbf{r}, t) \, \mathrm{d}t. \tag{2.88}$$

The Poynting vector in eq. (2.71) for the monochromatic field in eq. (2.87) reads

$$\mathbf{S}(\mathbf{r}, t) = \mathbf{E}(\mathbf{r}, t) \times \mathbf{H}(\mathbf{r}, t) \tag{2.89}$$

$$= \frac{1}{2}\big(\mathbf{E}(\mathbf{r}, \omega) \, \mathrm{e}^{-\mathrm{i}\omega t} + \mathbf{E}^*(\mathbf{r}, \omega) \, \mathrm{e}^{+\mathrm{i}\omega t}\big) \times \frac{1}{2}\big(\mathbf{H}(\mathbf{r}, \omega) \, \mathrm{e}^{-\mathrm{i}\omega t} + \mathbf{H}^*(\mathbf{r}, \omega) \, \mathrm{e}^{+\mathrm{i}\omega t}\big) \tag{2.90}$$

$$= \frac{1}{4}\Big\{ (\mathbf{E}(\mathbf{r}, \omega) \times \mathbf{H}(\mathbf{r}, \omega)) \, \mathrm{e}^{-2\,\mathrm{i}\omega t} + (\mathbf{E}^*(\mathbf{r}, \omega) \times \mathbf{H}^*(\mathbf{r}, \omega)) \, \mathrm{e}^{2\,\mathrm{i}\omega t}$$

$$+ \mathbf{E}(\mathbf{r}, \omega) \times \mathbf{H}^*(\mathbf{r}, \omega) + \mathbf{E}^*(\mathbf{r}, \omega) \times \mathbf{H}(\mathbf{r}, \omega) \Big\} \tag{2.91}$$

$$= \frac{1}{2} \text{Re}(\mathbf{E}(\mathbf{r}, \omega) \times \mathbf{H}^*(\mathbf{r}, \omega)) + \frac{1}{2} \text{Re}(\mathbf{E}(\mathbf{r}, \omega) \times \mathbf{H}(\mathbf{r}, \omega) \, \mathrm{e}^{-2\,\mathrm{i}\omega t}). \tag{2.92}$$

By inserting this expression into eq. (2.88) and noting that the last term vanishes when integrating over time, the average Poynting vector reads

$$\mathbf{S}_{\text{av}}(\mathbf{r}) = \frac{1}{2} \text{Re}(\mathbf{E}(\mathbf{r}, \omega) \times \mathbf{H}^*(\mathbf{r}, \omega)). \tag{2.93}$$

2.6 The step-index optical fiber

This section discusses a method for calculating the mode profile for an electric field in a step index fiber consisting of two layers, with the inner layer having a radius of length a. By assuming that the refractive index is constant in each layer it can be written as the following step-function

$$n = \begin{cases} n_1, & \rho \leq a, \\ n_2, & \rho > a \end{cases} \tag{2.94}$$

where we require that $n_1 > n_2$. We will then search for solution on the form

$$\mathbf{E}(\mathbf{r}) = \left(\hat{\mathbf{z}} E_z(\rho) + \hat{\boldsymbol{\rho}} E_\rho(\rho) + \hat{\boldsymbol{\phi}} E_\phi(\rho) \right) \mathrm{e}^{\mathrm{i}m\phi} \, \mathrm{e}^{\mathrm{i}\beta z} \tag{2.95}$$

$$\mathbf{H}(\mathbf{r}) = \left(\hat{\mathbf{z}} H_z(\rho) + \hat{\boldsymbol{\rho}} H_\rho(\rho) + \hat{\boldsymbol{\phi}} H_\phi(\rho) \right) \mathrm{e}^{\mathrm{i}m\phi} \, \mathrm{e}^{\mathrm{i}\beta z}, \tag{2.96}$$

where $m \in \mathbb{N}_0$ is the azimuthal index and β is the propagation constant [5]. Within each layer the refractive index n does not depend on the position hence we can use the Helmholtz equation introduced in eq. (2.32) and by writing them in cylindrical coordinates the following equation emerges

$$\left(\frac{\partial^2}{\partial \rho^2} + \frac{1}{\rho} \frac{\partial}{\partial \rho} + \frac{1}{\rho^2} \frac{\partial^2}{\partial \phi^2} + \frac{\partial^2}{\partial z^2} + k_0^2 n^2 \right) \mathbf{E}(\mathbf{r}) = \mathbf{0} \tag{2.97}$$

$$\left(\frac{\partial^2}{\partial \rho^2} + \frac{1}{\rho} \frac{\partial}{\partial \rho} + \frac{1}{\rho^2} \frac{\partial^2}{\partial \phi^2} + \frac{\partial^2}{\partial z^2} + k_0^2 n^2 \right) \mathbf{H}(\mathbf{r}) = \mathbf{0}. \tag{2.98}$$

These equation can be written into a Bessel differential equation by multiplying the equation with ρ^2 on each side and introducing the notation $\kappa_i = \sqrt{k_0^2 n_i^2 - \beta^2}$, where $i \in \{1, 2\}$ such that

$$\left(\rho^2 \frac{\partial^2}{\partial \rho^2} + \rho \frac{\partial}{\partial \rho} + (\rho^2 \kappa_i^2 - m^2) \right) \mathbf{E}(\mathbf{r}) = \mathbf{0} \tag{2.99}$$

$$\left(\rho^2 \frac{\partial^2}{\partial \rho^2} + \rho \frac{\partial}{\partial \rho} + (\rho^2 \kappa_i^2 - m^2) \right) \mathbf{H}(\mathbf{r}) = \mathbf{0}. \tag{2.100}$$

For the case where the modes are bounded to the waveguide, $k_0 n_1 < \beta < k_0 n_2$ the z-component will have the solution on the form

$$E_z(\rho) = \begin{cases} A J_m(\kappa_1 \rho) + A' Y_m(\kappa_1 \rho), & \rho \leq a \\ B K_m(\gamma_2 \rho) + B' I_m(\gamma_2 \rho), & \rho > a \end{cases} \tag{2.101}$$

$$H_z(\rho) = \begin{cases} C J_m(\kappa_1 \rho) + C' Y_m(\kappa_1 \rho), & \rho \leq a \\ D K_m(\gamma_2 \rho) + D' I_m(\gamma_2 \rho), & \rho > a \end{cases} \tag{2.102}$$

where $\gamma_2 = \sqrt{\beta^2 - k_0^2 n_2^2}$, J_m and Y_m are the Bessel functions of the first and second kind, respectively, and I_m and K_m are the modified Bessel functions of the first and second kind, respectively. Furthermore, A, B, C and D with and without primes are

constants. We can discard the solution Y_m because $Y_m(x) \to -\infty$ as $x \to 0$ for all m which is non-physical. Therefore we can set $A' = C' = 0$. Outside the core we seek a decaying solution, but $I_m(x) \to \infty$ and $K_m(x) \to 0$ as $x \to \infty$ for all m, meaning that I_m is not a decaying solution. Therefore we can set $B' = D' = 0$.

It is now possible to relate the electric field and the magnetic field through Maxwell's equation given in eqs. (2.24a) and (2.24b), which will then yield

$$i\omega\mu_0 H_z = \frac{\mathrm{d}E_\phi}{\mathrm{d}\rho} - \frac{im}{\rho}E_\rho + \frac{1}{\rho}E_\phi, \qquad -i\omega\varepsilon_0 n^2 E_z = \frac{\mathrm{d}H_\phi}{\mathrm{d}\rho} - \frac{im}{\rho}H_\rho + \frac{1}{\rho}H_\phi \qquad (2.103)$$

$$i\omega\mu_0 H_\rho = -i\beta E_\phi + \frac{im}{\rho}E_z, \qquad -i\omega\varepsilon_0 n^2 E_\rho = -i\beta H_\phi + \frac{im}{\rho}H_z \qquad (2.104)$$

$$i\omega\mu_0 H_\phi = i\beta E_\rho - \frac{\mathrm{d}E_z}{\mathrm{d}\rho}, \qquad -i\omega\varepsilon_0 n^2 E_\phi = i\beta H_\rho - \frac{\mathrm{d}H_z}{\mathrm{d}\rho}. \qquad (2.105)$$

It possible to combine these equation to express the ρ and ϕ component of the electric and magnetic field through the z components such that

$$E_\rho = \frac{i}{\kappa^2}\left(\beta\frac{\mathrm{d}E_z}{\mathrm{d}\rho} + \frac{im\mu_0\omega}{\rho}H_z\right), \qquad H_\rho = \frac{i}{\kappa^2}\left(\beta\frac{\mathrm{d}H_z}{\mathrm{d}\rho} - \frac{im\varepsilon_0 n^2\omega}{\rho}E_z\right) \qquad (2.106)$$

$$E_\phi = \frac{i}{\kappa^2}\left(\frac{im\beta}{\rho}E_z - \mu_0\omega\frac{\mathrm{d}H_z}{\mathrm{d}\rho}\right), \qquad H_\phi = \frac{i}{\kappa^2}\left(\frac{im\beta}{\rho}H_z + \varepsilon_0 n^2\omega\frac{\mathrm{d}E_z}{\mathrm{d}\rho}\right). \qquad (2.107)$$

Furthermore we require that H_z, E_z, H_ϕ and E_ϕ are continuous across the interface which gives the follow four equation (the radius of the core is $\rho = a$)

$$\frac{m\beta}{\kappa_1^2 a}AJ_m(\kappa_1 a) + \frac{i\omega\mu_0}{\kappa_1}CJ'_m(\kappa_1 a) = \frac{m\beta}{\kappa_2^2 a}BK_m(\gamma_2 a) + \frac{i\omega\mu_0}{\kappa_2^2}DK'_m(\gamma_2 a)\gamma_2 \qquad (2.108)$$

$$\frac{m\beta}{\kappa_1^2 a}CJ_m(\kappa_1 a) - \frac{i\omega\varepsilon_0 n^2}{\kappa_1}AJ'_m(\kappa_1 a) = \frac{m\beta}{\kappa_2^2 a}DJ_m(\gamma_2 a) - \frac{i\omega\varepsilon_0 n^2}{\kappa_2^2}BK'_m(\gamma_2 a)\gamma_2 \qquad (2.109)$$

$$AJ_m(\kappa_1 a) = BK_m(\gamma_2 a) \qquad (2.110)$$

$$CJ_m(\kappa_1 a) = DK_m(\gamma_2 a). \qquad (2.111)$$

By combining the above equation one can obtain

$$\begin{bmatrix} \omega\varepsilon_0\left(\frac{n_1^2}{\kappa_1}\frac{J'_m(\kappa_1 a)}{J_m(\kappa_1 a)} + \frac{n_2^2}{\gamma_2}\frac{K'_m(\gamma_2 a)}{K_m(\gamma_2 a)}\right) & i\frac{m\beta}{a}\left(\frac{1}{\kappa_1^2} + \frac{1}{\gamma_2^2}\right) \\ \frac{m\beta}{a}\left(\frac{1}{\kappa_1^2} + \frac{1}{\gamma_2^2}\right) & i\omega\mu_0\left(\frac{1}{\kappa_1}\frac{J'_m(\kappa_1 a)}{J_m(\kappa_1 a)} + \frac{1}{\gamma_2}\frac{K'_m(\gamma_2 a)}{K_m(\gamma_2 a)}\right) \end{bmatrix}\begin{bmatrix} A \\ C \end{bmatrix} = \mathbf{0} \qquad (2.112)$$

This system of equations only contains non-trivial solution for β when its determinant is zero, hence the following equation of β can be derived

$$F(\beta) = \left[\frac{n_1^2}{\kappa_1}\frac{J'_m(\kappa_1 a)}{J_m(\kappa_1 a)} + \frac{n_2^2}{\gamma_2}\frac{K'_m(\gamma_2 a)}{K_m(\gamma_2 a)}\right]\left[\frac{1}{\kappa_1}\frac{J'_m(\kappa_1 a)}{J_m(\kappa_1 a)} + \frac{1}{\gamma_2}\frac{K'_m(\gamma_2 a)}{K_m(\gamma_2 a)}\right] - \left[\frac{m\beta}{k_0 a}\right]^2\left[\frac{1}{\kappa_1^2} + \frac{1}{\gamma_2^2}\right]^2.$$
$$(2.113)$$

For each index m there can exist multiple solutions β denoted $\beta_{m,n}$.

2.7 Gaussian Beam

In this section, we will expand a Gaussian beam in plane waves and derive an expression for the expansion coefficients. The result will be used in connection with a two-dimensional geometry that is periodic along the x axis with period Λ.

Consider a fundamental laser beam with a Gaussian field distribution in the beam waist centred around $x = x_c$ [6]

$$E(x; z = 0) = E_0 \, e^{-(x-x_c)^2/w^2}, \qquad x \in [-\Lambda/2 + x_c; \Lambda/2 + x_c], \tag{2.114}$$

where E_0 is a constant. The beam waist, with radius w, have been choses to be located at $z = 0$. By expanding the field in an infinite series of plane waves, the field can be written as

$$E(x, z) = \sum_{n=-\infty}^{\infty} E_{0,n} \, e^{inGx} \, e^{-i\beta_n z}, \tag{2.115}$$

where $G = 2\pi/\Lambda$. In order to find $E_{0,n}$ we can use a Fourier transformation

$$E_{0,n} = \frac{1}{\Lambda} \int_{x=-\frac{\Lambda}{2}+x_c}^{x=\frac{\Lambda}{2}+x_c} E(x; z = 0) \, e^{-inGx} \, \mathrm{d}x \tag{2.116}$$

$$= \frac{1}{\Lambda} \int_{x=-\frac{\Lambda}{2}+x_c}^{x=\frac{\Lambda}{2}+x_c} E_0 \, e^{-(x-x_c)^2/w^2} \, e^{-inGx} \, \mathrm{d}x. \tag{2.117}$$

This integral can be simplified with the substitution $x' = x - x_c$ which leads to

$$E_{0,n} = \frac{e^{-inGx_c}}{\Lambda} \int_{x'=-\Lambda/2}^{x'=\Lambda/2} E_0 \, e^{-(x')^2/w^2} \, e^{-inGx'} \, \mathrm{d}x'. \tag{2.118}$$

Assuming the period of the structure is much larger than the width of the Gaussian beam i.e. $w \ll \Lambda$, the limits of the above integral can be changed to $x' = \infty$ and $x' = -\infty$ for the upper and lower limit, respectively

$$E_{0,n} \approx E_0 \frac{e^{-inGx_c}}{\Lambda} w\sqrt{\pi} \, e^{-\frac{(nGw)^2}{4}}. \tag{2.119}$$

3 Finite difference Frequency Domain

3.1 Finite difference

Most of the methods in electrodynamic and optic require knowledge of a function's derivatives, usually the first and second order. Sometimes analytical expressions can be derived for derivatives, however when functions (or their derivatives) becomes too complicated or no analytical expressions are available, then numerical derivatives must be used. In this section, we will discuss the finite difference method to obtain first-order derivatives.

There are three common finite difference operators; forward, backward and central finite difference, which are defined as

$$\text{Forward:} \qquad \frac{\mathrm{d}f}{\mathrm{d}x} \approx \frac{f(x+h) - f(x)}{h} \tag{3.1}$$

$$\text{Backward:} \qquad \frac{\mathrm{d}f}{\mathrm{d}x} \approx \frac{f(x) - f(x-h)}{h} \tag{3.2}$$

$$\text{Central:} \qquad \frac{\mathrm{d}f}{\mathrm{d}x} \approx \frac{f(x+h) - f(x-h)}{2h} \tag{3.3}$$

where $h > 0$ [3, 7]. The forward difference uses the function-values at the point of interest x and a step forward point $x + h$, whereas backward difference uses backwards step $x - h$ instead. Central difference 'skips' the point of interest, and only look at the forward and backward points.

Finite difference has its roots in Taylor's theorem. Consider a smooth function $f\colon \mathbb{R} \to \mathbb{R}$ which is differential at some point $a \in \mathbb{R}$. The derivative of f is

$$\frac{\mathrm{d}f}{\mathrm{d}x}\bigg|_a = \lim_{h \to 0} \frac{f(a+h) + f(a)}{h} \tag{3.4}$$

and the function can be written as the Taylor expansion

$$f(x) = \sum_{n=0}^{\infty} \frac{1}{n!} \frac{\mathrm{d}^n f}{\mathrm{d}x^n}\bigg|_a (x - a)^n. \tag{3.5}$$

Setting $h = x - a$ then the forward difference is obtained by neglecting the second and higher-order terms in

$$f(a+h) = f(a) + \frac{\mathrm{d}f}{\mathrm{d}x}\bigg|_a h + \frac{1}{2} \frac{\mathrm{d}^2 f}{\mathrm{d}x^2}\bigg|_a h^2 + \cdots \tag{3.6}$$

$$\implies \frac{\mathrm{d}f}{\mathrm{d}x}\bigg|_a = \frac{f(a+h) - f(a)}{h} + \frac{1}{2} \frac{\mathrm{d}^2 f}{\mathrm{d}x^2}\bigg|_a h + \cdots, \tag{3.7}$$

which have the truncation error as a function of h as $c_1 h + c_2 h^2 + \cdots$ and decreases with smaller h.

Before continuing, we introduce the big-O notation. Say we have two functions h, g where $g(x)$ is strictly positive. The Big O notation is used to describe the limiting behaviour of $h(x)$ as $x \to a$, where a is a constant and are allowed to be infinity, however we describe *only* the case where a is finite. To describe the behaviour of h near some real number a, then we write $h(x) = O(g(x))$ as $x \to a$, if and only if there exist two constants $M, \delta > 0$, such that $|h(x)| < M g(x)$ for all $|x - a| \leq \delta$ [7]. It means that the absolute value of $h(x)$ is at most a constant multiple of $g(x)$. For a Taylor series of the form eq. (3.5), we look at the limiting behaviour of $h(x)$ as $x \to 0$ [7].

For the case in eq. (3.7), we are interested in $h \to 0^+$, specifically for $0 < h < 1$ such that $h > h^2 > h^3 > \cdots$. Let $h = 1/k$, for $k \to \infty$ then the truncation error of the forward difference

$$c_1 h + c_2 h^2 + \cdots = c_1/k + c_2/k^2 + \cdots \tag{3.8}$$

is $O(1/k) = O(h)$ as $h \to 0$.

Repeating the above steps with a negative step length $-h$ then the Taylor expansion reads

$$f(a - h) = f(a) - \frac{\mathrm{d}f}{\mathrm{d}x}\bigg|_a h + \frac{1}{2}\frac{\mathrm{d}^2 f}{\mathrm{d}x^2}\bigg|_a h^2 - \cdots \tag{3.9}$$

and the backward difference is obtained

$$\frac{\mathrm{d}f}{\mathrm{d}x}\bigg|_a = \frac{f(a) - f(a - h)}{h} + O(h), \tag{3.10}$$

which have the same order of truncation error as the forward difference.

The central difference may be obtained by taking the difference of eqs. (3.6) and (3.9) and dividing with two

$$f(a + h) - f(a - h) = 2\frac{\mathrm{d}f}{\mathrm{d}x}\bigg|_a h + 2\frac{1}{3!}\frac{\mathrm{d}^3 f}{\mathrm{d}x^3}\bigg|_a h^3 + \cdots \tag{3.11}$$

leading to

$$\frac{\mathrm{d}f}{\mathrm{d}x}\bigg|_a = \frac{f(a + h) - f(a - h)}{2h} + O(h^2). \tag{3.12}$$

Since the truncation error for the central difference is $O(h^2)$, then it leads to significantly improved accuracy over the forward (and backward) difference, which have the truncation error $O(h)$. Generally, the truncation error decreases with smaller h. Ideally, we would choose h as small as possible to achieve the smallest truncation error. However, in numerical calculations, the floating points arithmetic on a computer leads to round-off errors which are of order $O(\epsilon_M/h)$ and *increases* with smaller h, where ϵ_M is machine epsilon [7]. The best accuracy is found when the truncation and round-off errors are approximately equal and the optimal h can be roughly estimated from this [7].

In fig. 3.1 a comparison of the total error between the discussed methods is shown. It is seen that the error of each method decreases with smaller h until the optimal solution is roughly reached. After that point, the round-off error becomes significant and grows large.
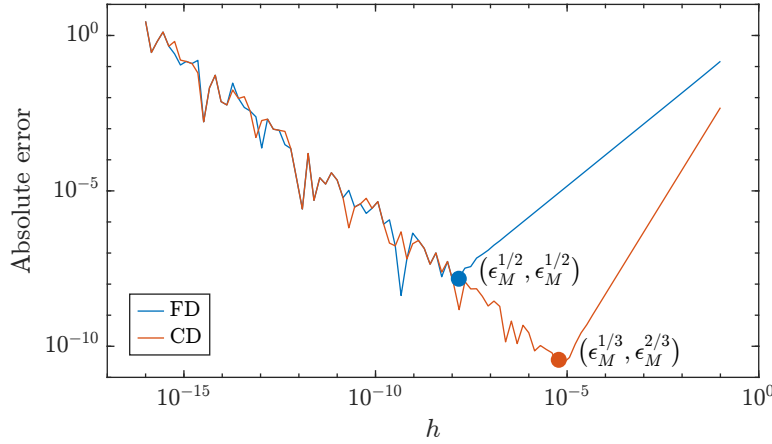
Figure 3.1: *A comparison of forward difference and central difference approximations absolute error using $f(x) = \sin(\sin(x)\cos(x))$ at $x = \pi/3$. The points are rough estimates of the optimal accuracy.*

3.2 Yee Mesh

To understand the idea behind a Yee Mesh, it will be introduced with an example and Maxwell's equations eqs. (2.24a) and (2.24b). Writing out each vector component yields

$$\begin{bmatrix} H_x \\ H_y \\ H_z \end{bmatrix} = \frac{1}{\mathrm{i}\omega\mu_0} \begin{bmatrix} \frac{\partial}{\partial y}E_z - \frac{\partial}{\partial z}E_y \\ \frac{\partial}{\partial z}E_x - \frac{\partial}{\partial x}E_z \\ \frac{\partial}{\partial x}E_y - \frac{\partial}{\partial y}E_x \end{bmatrix} \tag{3.13}$$

$$\begin{bmatrix} E_x \\ E_y \\ E_z \end{bmatrix} = -\frac{1}{\mathrm{i}\omega\varepsilon_0\varepsilon} \begin{bmatrix} \frac{\partial}{\partial y}H_z - \frac{\partial}{\partial z}H_y \\ \frac{\partial}{\partial z}H_x - \frac{\partial}{\partial x}H_z \\ \frac{\partial}{\partial x}H_y - \frac{\partial}{\partial y}H_x \end{bmatrix}. \tag{3.14}$$

The idea is to use the central difference formula eq. (3.12) to calculate the derivatives. For the discussion below, we define the x-axis to be horizontal and the y-axis is the vertical as illustrated in fig. 3.2.

Looking at the above expression for E_z, the derivative $\frac{\partial}{\partial x}H_y$ and $\frac{\partial}{\partial y}H_x$ must be evaluated. With central difference, it is required to determine H_y to the left and right of E_z and determine H_x above and below E_z (using the terminology from fig. 3.2). It is not needed to evaluate H_x and H_y at the same point as E_z. Similar arguments can be made for all other field components. This is essentially the idea behind how to construct a Yee grid.

Since it was assumed that the waveguide is uniform along the z-axis in section 2.3, the electric and magnetic field can be written

$$\mathbf{E}(\mathbf{r}) = \mathbf{E}(x,y)\,\mathrm{e}^{\mathrm{i}\beta z} \tag{3.15}$$

$$\mathbf{H}(\mathbf{r}) = \mathbf{H}(x,y)\,\mathrm{e}^{\mathrm{i}\beta z}, \tag{3.16}$$
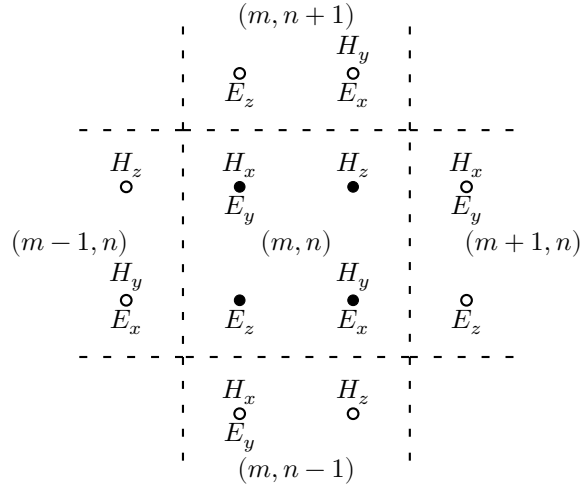
Figure 3.2: *A two dimensional Yee mesh. Each box illustrate a fundamental cell with four interior points in which the field components are evaluated by a central difference scheme.*

which means that the derivatives of the field components with respect to z gives the field itself multiplied by a factor of $i\beta$. For example, consider the E_x component. Then H_z must be determined above and below of E_x, whereas the z-derivative of H_y must be evaluated at the same point as E_x and simply becomes $i\beta H_y$. The rest of the equations can be discretised in a similar manner and the Yee grid is formed. The grid that will be considered consist of cells with side length Δx and Δy, where each cell contains four points in which the magnetic and electric field components are calculated as illustrated in fig. 3.2.

Before proceeding with the calculations, we need to determine at which points to calculate the dielectric function ε. We could restrict the discontinuities of ε to lie on lines running through the grid points where the electric fields are represented. But this is inconveniently when modelling curved boundaries because the boundaries must be approximated by right-angled steps, which is also called the staircase approximation [3] and is illustrated in fig. 3.4b. Furthermore the discretisation of ε would also be tied to the grid size and shape, which for example means that small changes of the structure cannot be studied [3]. A better method is to use the dielectric averaging scheme and the discussion of it is postponed to section 3.3. However, it implies that different ε values for each electric field components should be used i.e. ε_x is calculated at E_x, ε_y is calculated at E_y and ε_z is calculated at E_z [3].

Discretising eqs. (3.13) and (3.14) (with different ε values as mentioned above) using the central difference scheme leads to

$$i\omega\mu_0 H_x(m,n) = \frac{E_z(m,n+1) - E_z(m,n)}{\Delta y} - i\beta E_y(m,n) \tag{3.17}$$

$$i\omega\varepsilon_0\varepsilon_x(m,n)E_x(m,n) = -\frac{H_z(m,n) - H_z(m,n-1)}{\Delta y} + i\beta H_y(m,n) \tag{3.18}$$

$$i\omega\mu_0 H_y(m,n) = i\beta E_x(m,n) - \frac{E_z(m+1,n) - E_z(m,n)}{\Delta x} \tag{3.19}$$

$$i\omega\varepsilon_0\varepsilon_y(m,n)E_y(m,n) = -i\beta H_x(m,n) + \frac{H_z(m,n) - H_z(m-1,n)}{\Delta x} \tag{3.20}$$

$$i\omega\mu_0 H_z(m,n) = \frac{E_y(m+1,n) - E_y(m,n)}{\Delta x} - \frac{E_x(m,n+1) - E_x(m,n)}{\Delta y} \tag{3.21}$$

$$i\omega\varepsilon_0\varepsilon_z(m,n)E_z(m,n) = -\frac{H_y(m,n) - H_y(m-1,n)}{\Delta x} + \frac{H_x(m,n) - H_x(m,n-1)}{\Delta y}. \tag{3.22}$$

where each box in fig. 3.2 have been given an index. If we have a $M \times N$ grid, then the m index refer to the column and takes on the values $m \in \{1, 2, ..., M\}$, and the n index refers to the row and takes on the values $n \in \{1, 2, ..., N\}$.

From the above equations it is possible to derive an eigenvalue equation for β^2. Starting off with inserting eqs. (3.20) and (3.22) into eq. (3.17), one obtains the following equation

$$\left(k_0^2 - \frac{\beta^2}{\varepsilon_y(m,n)} - \frac{1}{\Delta y^2 \varepsilon_z(m,n+1)} - \frac{1}{\Delta y^2 \varepsilon_z(m,n)}\right) H_x(m,n) \tag{3.23}$$

$$= \frac{1}{\Delta x \Delta y \varepsilon_z(m,n)}\left[H_y(m-1,n) - H_y(m,n)\right]$$

$$+ \frac{1}{\Delta x \Delta y \varepsilon_z(m,n+1)}\left[H_y(m,n+1) - H_y(m-1,n+1)\right]$$

$$+ \frac{1}{\Delta y^2 \varepsilon_z(m,n+1)}H_x(m,n+1) - \frac{1}{\Delta y^2 \varepsilon_z(m,n)}H_x(m,n-1)$$

$$+ \frac{i\beta}{\Delta x \varepsilon_y(m,n)}\left[H_z(m,n) - H_z(m-1,n)\right]. \tag{3.24}$$

It was found in eq. (2.41) that the z-component of the magnetic field can be decoupled from the two remaining components as

$$H_z = \frac{i}{\beta}\nabla_\perp \cdot \mathbf{H}_\perp. \tag{3.25}$$

Proceeding to discretise eq. (3.25) with the central difference scheme gives

$$H_z(m,n) = \frac{i}{\beta}\left(\frac{H_x(m+1,n) - H_x(m,n)}{\Delta x} + \frac{H_x(m,n+1) - H_x(m,n)}{\Delta y}\right), \tag{3.26}$$

which is inserted into eq. (3.24) so that it only depends on the x and y components of the magnetic field

$$\beta^2 H_x(m,n) = \left[k_0^2\varepsilon_y(m,n) - \frac{1}{\Delta y^2}\left(\frac{\varepsilon_y(m,n)}{\varepsilon_z(m,n)} + \frac{\varepsilon_y(m,n)}{\varepsilon_z(m,n+1)}\right) - \frac{2}{\Delta x}\right] H_x(m,n)$$

$$- \frac{1}{\Delta x \Delta y}\left[1 - \frac{\varepsilon_y(m,n)}{\varepsilon_z(m,n)}\right] H_y(m,n) + \frac{1}{\Delta x^2}\left[H_x(m+1,n) + H_x(m-1,n)\right]$$

$$+ \frac{\varepsilon_y(m,n)}{\Delta y^2} \left[\frac{1}{\varepsilon_z(m,n)} H_x(m,n-1) + \frac{1}{\varepsilon_z(m,n+1)} H_x(m,n+1) \right] \tag{3.27}$$

$$+ \frac{1}{\Delta x \Delta y} \left[1 - \frac{\varepsilon_y(m,n)}{\varepsilon_z(m,n)} \right] H_y(m-1,n)$$

$$+ \frac{1}{\Delta x \Delta y} \left[1 - \frac{\varepsilon_y(m,n)}{\varepsilon_z(m,n+1)} \right] [H_y(m,n+1) - H_y(m-1,n+1)].$$

Similarly one can obtain the following eigenvalue equation by inserting eqs. (3.18) and (3.22) into eq. (3.19) and use eq. (3.26) to eliminate the z component of the magnetic field

$$\beta^2 H_y(m,n) = \left[k_0^2 \varepsilon_x(m,n) - \frac{1}{\Delta x^2} \left(\frac{\varepsilon_x(m,n)}{\varepsilon_x(m,n)} + \frac{\varepsilon_x(m,n)}{\varepsilon_z(m+1,n)} \right) - \frac{2}{\Delta y^2} \right] H_y(m,n)$$

$$- \frac{1}{\Delta x \Delta y} \left[1 - \frac{\varepsilon_x(m,n)}{\varepsilon_z(m,n)} \right] H_x(m,n) + \frac{1}{\Delta y^2} [H_y(m,n+1) + H_y(m,n-1)]$$

$$+ \frac{\varepsilon_x(m,n)}{\Delta x^2} \left[\frac{1}{\varepsilon_z(m,n)} H_y(m-1,n) + \frac{1}{\varepsilon_z(m+1,n)} H_y(m+1,n) \right] \tag{3.28}$$

$$+ \frac{1}{\Delta x \Delta y} \left[1 - \frac{\varepsilon_x(m,n)}{\varepsilon_z(m,n)} \right] H_x(m,n-1)$$

$$+ \frac{1}{\Delta x \Delta y} \left[1 - \frac{\varepsilon_x(m,n)}{\varepsilon_z(m+1,n)} \right] [H_x(m+1,n) - H_x(m+1,n-1)].$$

From eqs. (3.27) and (3.28) a large matrix can be constructed of size $(2MN) \times (2MN)$ and one can quickly run into memory issues. Since only neighbouring boxes to the (m,n)'th box is used, then most of the entrances in the matrix are zero, and therefore can be treated as a sparse matrix. This solves the memory issue. The indices $m = 0$, $m = M + 1$, $n = 0$ and $n = N + 1$ should be ignored due to them being outside of the grid [3].

3.3 Tensor averaging

In more general electromagnetic theory, the dielectric function ε is written as a second rank tensor $\bar{\bar{\varepsilon}}$. Consider a box with a grid point in the centre and with a boundary crosses through it. On each side of the boundary there are different dielectric constants ε_1 and ε_2 as in fig. 3.3. Let $\mathbf{n} = (n_x, n_y, 0)$ be a unit normal vector to the boundary at the grid point, then $\bar{\bar{\varepsilon}}$ can be split into a parallel and perpendicular components as

$$\bar{\bar{\varepsilon}} = \hat{\mathbf{n}}\hat{\mathbf{n}}\varepsilon_\perp + \left(\bar{\bar{I}} - \hat{\mathbf{n}}\hat{\mathbf{n}} \right) \varepsilon_\parallel, \tag{3.29}$$

where $\hat{\mathbf{n}}\hat{\mathbf{n}}$ is a dyadic product. For $\hat{\mathbf{n}}$ lying in the xy-plane, then $\bar{\bar{\varepsilon}}$ components can be written as

$$\bar{\bar{\varepsilon}} = \begin{bmatrix} \varepsilon_{xx} & \varepsilon_{xy} & \varepsilon_{xz} \\ \varepsilon_{yx} & \varepsilon_{yy} & \varepsilon_{yz} \\ \varepsilon_{zx} & \varepsilon_{zy} & \varepsilon_{zz} \end{bmatrix} = \begin{bmatrix} n_x^2 \varepsilon_\perp + (1-n_x^2)\varepsilon_\parallel & n_x n_y \varepsilon_\perp - n_x n_y \varepsilon_\parallel & 0 \\ n_y n_x \varepsilon_\perp - n_y n_x \varepsilon_\parallel & n_y^2 \varepsilon_\perp + (1-n_y^2)\varepsilon_\parallel & 0 \\ 0 & 0 & \varepsilon_\parallel \end{bmatrix}. \tag{3.30}$$
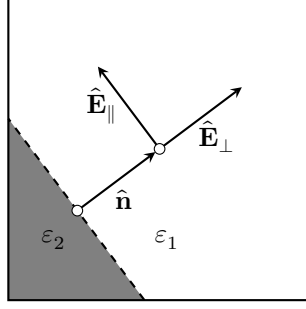
Figure 3.3: *A single gridpoint and its surrounding box. A boundary crosses through the box with different dielectric on each side. The boundary defines the parallel and perpendicular direction through $\hat{\mathbf{n}}$.*

What is left, is a way to determine $\varepsilon_\perp$ and $\varepsilon_\parallel$. To do so, we consider an example with a scalar dielectric function ε, then $\varepsilon_\perp = \varepsilon_\parallel = \varepsilon$. We could determine the values of ε at the grid points. This corresponds to the staircase approximation illustrated in fig. 3.4b. However, there is no reason for the ε value at grid points to be more significant over the ε value at any other point in the surrounding boxes of the grid points. Averaging the values of ε over the boxes turns out to significantly improve convergence [3]. It also let us study small changes to the structure.

Let $\langle \cdots \rangle$ denote the average value over a box of area A. Then the average value of some function $f(x, y)$ can be calculated as

$$\langle f(x, y) \rangle = \frac{1}{A} \int_A f(x, y) \, \mathrm{d}x \, \mathrm{d}y. \tag{3.31}$$

Let $\mathbf{E}_i \cdot \mathbf{D}_i$ denote the electric field energy density at the i'th grid point. If we assume that $\mathbf{E}_i \cdot \mathbf{D}_i$ represents the average value $\langle \mathbf{E} \cdot \mathbf{D} \rangle$ of the i'th box that surrounds the i'th grid point. Then

$$\mathbf{E}_i \cdot \mathbf{D}_i = \mathbf{E}_i \cdot (\varepsilon_i \mathbf{E}_i) = \frac{1}{\varepsilon_i} \mathbf{D}_i \cdot \mathbf{D}_i = \langle \mathbf{E} \cdot \mathbf{D} \rangle. \tag{3.32}$$

If we further assume this also holds independently for the parallel and perpendicular components of $\mathbf{E}_i$ and $\mathbf{D}_i$ to the refractive index boundary, then

$$\mathbf{E}_{i,\parallel} \cdot \mathbf{D}_{i,\parallel} = \mathbf{E}_{i,\parallel} \cdot (\varepsilon_{i,\parallel} \mathbf{E}_{i,\parallel}) = \left\langle \mathbf{E}_\parallel \cdot \mathbf{D}_\parallel \right\rangle \tag{3.33}$$

$$\mathbf{E}_{i,\perp} \cdot \mathbf{D}_{i,\perp} = \frac{1}{\varepsilon_{i,\perp}} \mathbf{D}_{i,\perp} \cdot \mathbf{D}_{i,\perp} = \langle \mathbf{E}_\perp \cdot \mathbf{D}_\perp \rangle. \tag{3.34}$$

Note that we wrote dielectric function ε_i with an additional subscript $\perp$ or $\parallel$ to make it compatible with the tensor averaging notation above, but for now they are equal i.e. $\varepsilon_{i,\perp} = \varepsilon_{i,\parallel} = \varepsilon_i$.

Since $\mathbf{E}_\parallel$ and $\mathbf{D}_\perp$ are both continuous across the boundary, then they should be approximately constant over the box e.g. we can write

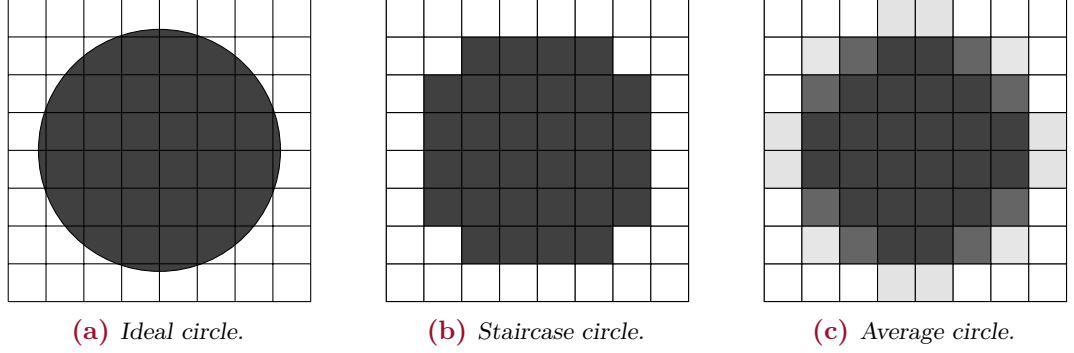$$\mathbf{E}_\parallel \approx \mathbf{E}_{i,\parallel} \tag{3.35}$$

(a) *Ideal circle.*   **(b)** *Staircase circle.*   **(c)** *Average circle.*

Figure 3.4: *(a) Represents a circle in a square grid. (b) The staircase approximation, where a box's ε value is determined from its centre. (c) An average scheme is used to smear out the circle.*

$$\mathbf{D}_\perp \approx \mathbf{D}_{i,\perp}. \tag{3.36}$$

Rewriting eq. (3.33) into

$$\left\|\mathbf{E}_{i,\|}\right\|^2 \varepsilon_{i,\|} = \left\langle \mathbf{E}_\| \cdot (\varepsilon \mathbf{E}_\|) \right\rangle \approx \left\|\mathbf{E}_{i,\|}\right\|^2 \langle\varepsilon\rangle, \tag{3.37}$$

which suggest us to use $\varepsilon_{i,\|} = \langle\varepsilon\rangle$. However, if we rewrite eq. (3.34)

$$\frac{1}{\varepsilon_{i,\perp}}\left\|\mathbf{D}_{i,\perp}\right\|^2 = \left\langle \frac{1}{\varepsilon}\mathbf{D}_\perp \cdot \mathbf{D}_\perp \right\rangle \approx \left\|\mathbf{D}_{i,\perp}\right\|^2 \left\langle\frac{1}{\varepsilon}\right\rangle, \tag{3.38}$$

which suggest us to use $\varepsilon_{i,\perp} = \langle 1/\varepsilon\rangle^{-1}$. Generally $\langle\varepsilon\rangle$ and $\langle 1/\varepsilon\rangle^{-1}$ are not equal and for a scalar ε we have the relation $\varepsilon_{i,\perp} = \varepsilon_{i,\|} = \varepsilon_i$. This means that $\varepsilon_i = \langle\varepsilon\rangle$ and $\varepsilon_i = \langle 1/\varepsilon\rangle^{-1}$ cannot satisfied simultaneously. This is the reason we cannot use a scalar ε if we want to average ε over a box, however the tensor version $\bar{\bar{\varepsilon}}$ given in eq. (3.30) allows that $\varepsilon_{i,\perp}$ and $\varepsilon_{i,\|}$ are different when averaging.

The off-diagonal elements in eq. (3.30) becomes problematic for a Yee grid and it is suggested in [3] that these are ignored and only the diagonal elements are used. Setting $\varepsilon_x := \varepsilon_{xx}$, $\varepsilon_y := \varepsilon_{yy}$ and $\varepsilon_z := \varepsilon_{zz}$. It was mentioned in the previous section that ε_x, ε_y and ε_z should be calculated at E_x, E_y and E_z, respectively. For example, ε_x is calculated from $\varepsilon_\| = \langle\varepsilon\rangle$ and $\varepsilon_\perp = \langle 1/\varepsilon\rangle^{-1}$, which themselves are found by averaging over a box around the grid point, where E_x is calculated. This averaging scheme is sketched in fig. 3.4c.

4 Modal Method

The modal method is a family of eigenmode expansion techniques for the frequency domain. It relies on decomposing the optical field into a basis set of transverse eigenmodes for each layer of the modelled device [3]. The device's geometry is divided into layers of uniform permittivity along the propagation axis, taken to be the z-axis, while the permittivity profile along the lateral coordinates may depend on $\mathbf{r}_\perp$, depending on the dimensions of the geometry [3]. The transverse eigenmodes are determined by solving Maxwell's equations or the wave equation for each layer of the geometry. In each layer, the optical field is expanded on the corresponding eigenmodes and the fields are connected at the interfaces using mode-matching techniques, e.g. the T-matrix or S-matrix formalisms can be used [3].

As mentioned above, the optical field can be expanded in a set of eigenmodes that are obtained by solving eq. (2.38), and the field can be described by

$$\mathbf{E}_\perp(\mathbf{r}) = \sum_{m=1}^{\infty} a'_m \mathbf{e}_{\perp m}(\mathbf{r}_{\perp m}) \, \mathrm{e}^{\mathrm{i}\beta_m z} + \sum_{m=1}^{\infty} b_m \mathbf{e}_{\perp m}(\mathbf{r}_{\perp m}) \, \mathrm{e}^{-\mathrm{i}\beta_m z}, \tag{4.1}$$

where we have used the time convention $\mathrm{e}^{-\mathrm{i}\omega t}$ so that the a and b coefficients are describing the forward and backward modes, respectively. Here a'_m and b_m are the expansion coefficients which refers to the m'th forward and backward travelling eigenmodes, respectively. In practice, the infinite sums are limited to include N finite number of modes. While eqs. (2.38) and (4.1) only gives the transverse field components, the remaining four components of the electromagnetic field can be found using the equations in section 2.3.

The next sections will consider 1D and 2D geometries. For the latter geometry, Fourier modal method will be introduced.

4.1 1D Geometry

In the one dimensional case, we assume that the propagation axis is along the z-axis. The dielectric function $\varepsilon(z)$ is independent of the lateral coordinates $(\mathbf{r}_\perp) = (x, y)$, however it vary along the propagation axis z. We divide the geometry along the z axis into N layers of constant permittivity with ε_q being the permittivity in layer q.

Consider layer q. Since $\varepsilon(z)$ is independent of $(\mathbf{r}_\perp)$ then $\nabla \varepsilon_q(\mathbf{r}_\perp) = 0$ and eq. (2.38) reduces to

$$\nabla_\perp^2 \mathbf{e}_q + \varepsilon_q k_0^2 \mathbf{e}_q = \beta_q^2 \mathbf{e}_q. \tag{4.2}$$

This is a linear partial differential equation of second order which solutions depend on the field of interest. If one seeks a solution independent on the lateral coordinates $\mathbf{r}_\perp$
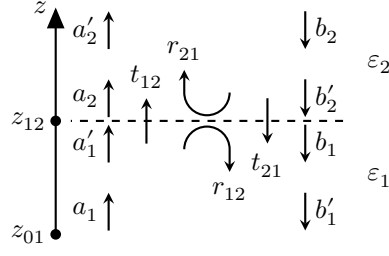
Figure 4.1: *A two-layer structure showing how the fields are travelling through the structure i.e. reflection and transmission.*

then there exist only one eigenmode given by $\mathbf{e}_q = C\mathbf{u}$ with the dispersion $\varepsilon_q k_0^2 = \beta_q^2$, where C is a constant and $\mathbf{u}$ is a vector in the xy-plane.

The field can then be calculated from eq. (4.1) with the sum limited to $m = 1$ once the unknown expansion coefficients $a'_{1,q}$ and $b_{1,q}$ have been determined. The coefficients $a'_{1,1}$ and $a'_{1,N}$ are found from boundary conditions at the interfaces between the layers, by requiring the tangential components of $\mathbf{E}$ and $\mathbf{H}$ are continuous across the boundary.

4.1.1 Single interface and propagation

To make the calculations on a general *N*-layer structure, two core concepts must be addressed: mode-matching and propagation. The former deals with how the fields are matched at the interface between two layers, that is reflection and transmission. The latter deals with how the fields propagate inside a layer.

Continuing on the previous example with a constant field, then the field for a two-layer structure can be described by

$$E(z) = \begin{cases} a_1\,\mathrm{e}^{\mathrm{i}n_1 k_0(z-z_{01})} + b'_1\,\mathrm{e}^{-\mathrm{i}n_1 k_0(z-z_{01})} & \infty < z \leq z_{12} \\ a_2\,\mathrm{e}^{\mathrm{i}n_2 k_0(z-z_{12})} + b'_2\,\mathrm{e}^{-\mathrm{i}n_2 k_0(z-z_{12})} & z_{12} < z < \infty \end{cases}. \tag{4.3}$$

Here we have used the notation in fig. 4.1. Before looking at the boundary condition at the interface, the field in layer 1 at z_{12} must be determined. We construct a propagation matrix relating the coefficients at z_{01} and z_{12} by

$$\begin{bmatrix} a'_1 \\ b_1 \end{bmatrix} = \bar{P}_1 \begin{bmatrix} a_1 \\ b'_1 \end{bmatrix}. \tag{4.4}$$

Its entries can be found by describing the field with z_{12} as its reference point, which is equal to eq. (4.3) at the same point z

$$E_1(z) = a_1\,\mathrm{e}^{\mathrm{i}n_1 k_0(z-z_{01})} + b'_1\,\mathrm{e}^{-\mathrm{i}n_1 k_0(z-z_{01})} = a'_1\,\mathrm{e}^{\mathrm{i}n_1 k_0(z-z_{12})} + b_1\,\mathrm{e}^{-\mathrm{i}n_1 k_0(z-z_{12})}. \tag{4.5}$$

Since the forward and backward travelling waves are independent, then b'_1 does not contribute to a'_1 through the propagation matrix. A similar argument can be applied to a_1 and b_1, hence

$$\bar{P}_1 = \begin{bmatrix} \mathrm{e}^{\mathrm{i}n_1 k_0 \Delta z} & 0 \\ 0 & \mathrm{e}^{-\mathrm{i}n_1 k_0 \Delta z} \end{bmatrix}, \tag{4.6}$$

where $\Delta z = z_{12} - z_{01}$. For every layer, a propagation matrix can be constructed as the above but with their corresponding propagation constants.

Consider the case where the field is incident form region 1. It should be noted that since there is no interface at the end of region 2 there cannot be any backward travelling waves hence b_2' must be equal to 0. In order to determine the rest of the coefficients, the Fresnel reflection and transmission coefficients can be used to link a_1' to b_1 and a_2, such that $b_1 = r_{12}a_1'$ and $a_2 = t_{12}a_1'$. The Fresnel coefficients can be determined with the criteria that the transverse part of the electric and magnetic fields needs to be continuous across the interface at $z =_{12}$, giving

$$a_1' + b_1 = a_2 \tag{4.7}$$

$$n_1(a_1' - b_1) = a_2 n_2, \tag{4.8}$$

where the first condition arises from the continuity of the electric field and the second comes from the continuity of the magnetic field. The above two equations can be solved for which we get the reflection and transmission coefficients

$$r_{12} = \frac{n_1 - n_2}{n_1 + n_2} \tag{4.9}$$

$$t_{12} = \frac{2n_1}{n_1 + n_2}. \tag{4.10}$$

In the case where the field is incident from the other side (region 2) the calculation can be performed similarly, yielding

$$r_{21} = \frac{n_2 - n_1}{n_1 + n_2} \tag{4.11}$$

$$t_{21} = \frac{2n_2}{n_1 + n_2}. \tag{4.12}$$

If the fields are incident from both sides then the full relation becomes

$$\begin{bmatrix} a_2 \\ b_1 \end{bmatrix} = \begin{bmatrix} t_{12} & r_{21} \\ r_{12} & t_{21} \end{bmatrix} \begin{bmatrix} a_1' \\ b_2' \end{bmatrix}. \tag{4.13}$$

This matrix relates the incident fields with the outgoing fields. This is known as the *S*-matrix formalism which will be discussed later. Another common approach is to relate the fields in one region with the fields in another region. For example, the above case would correspond to

$$\begin{bmatrix} a_2 \\ b_2' \end{bmatrix} = \frac{1}{t_{21}} \begin{bmatrix} t_{12}t_{21} - r_{12}r_{21} & r_{21} \\ -r_{12} & 1 \end{bmatrix} \begin{bmatrix} a_1' \\ b_1 \end{bmatrix}, \tag{4.14}$$
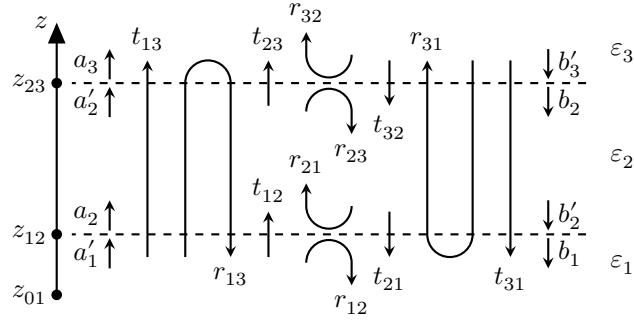
which is called the *T*-matrix formalism.

Figure 4.2: *The reflection and transmission illustrated for a 3-layer geometry.*

4.2 S Matrix Theory

The first focus point of this section will be on a three-layer structure as illustrated in seen in fig. 4.2. Thereafter we will use the three-layer structure to generalise to a *N*-layer structure in a recursive scheme.

We consider a single mode m incident from region 1 propagating along the z-axis. When the incoming field reached the first interface at z_{12}, multiple modes can be reflected and transmitted at the interface. The transmitted field will similarly be reflected and transmitted at the other region, hence the field can be written on the form

$$\mathbf{E}_1(\mathbf{r}) = a'_{1m}\mathbf{e}^+_{1m}(\mathbf{r}_\perp)\,\mathrm{e}^{\mathrm{i}\beta_{1m}(z-z_{12})} + \sum_{j=1}^{N} b_{1j}\mathbf{e}^-_{1j}(\mathbf{r}_\perp)\,\mathrm{e}^{-\mathrm{i}\beta_{1j}(z-z_{12})} \tag{4.15}$$

$$\mathbf{E}_2(\mathbf{r}) = \sum_{j=1}^{N} a_{2j}\mathbf{e}^+_{2j}(\mathbf{r}_\perp)\,\mathrm{e}^{\mathrm{i}\beta_{2j}(z-z_{12})} + \sum_{j=1}^{N} b'_{2j}\mathbf{e}^-_{2j}(\mathbf{r}_\perp)\,\mathrm{e}^{-\mathrm{i}\beta_{2j}(z-z_{23})} \tag{4.16}$$

$$\mathbf{E}_3(\mathbf{r}) = \sum_{j=1}^{N} a_{3j}\mathbf{e}^+_{3j}(\mathbf{r}_\perp)\,\mathrm{e}^{\mathrm{i}\beta_{3j}(z-z_{23})}. \tag{4.17}$$

It should be noted that some of the coefficients are marked with a prime, which indicates that those coefficients are facing the interface and the coefficient without is having their back towards an interface. Therefore in region 2 we can describe the propagation as $a'_{2j} = \mathrm{e}^{\mathrm{i}\beta L_2}a_{2j}$ and $b_{2j} = \mathrm{e}^{-\mathrm{i}\beta L_2}b'_{2j}$, where L_2 is the width of region 2.

The field is incident from region 1 and will be partially reflected and transmitted once it reaches the interface at z_{12}. The reflected part will be described by $\bar{r}_{12}$ and the transmitted part will be described by $\bar{t}_{12}$. The transmitted part can then propagate through region 2 and will then be partially reflected and transmitted at the next interface z_{23}. Hence the field in region 2 can bounce back and forth. One cycle of this can be described by $\bar{t}_{21}\bar{p}_2\bar{r}_{23}\bar{p}_2$ with $\bar{p}_2$ being the propagation matrix in region 2. The total reflected field in region 1 is partially described by the initial reflection $\bar{r}_{12}$ but will also consist of the reflected field from z_{23} that is transmitted through z_{12}. It may be described

by the reflection matrix

$$\bar{r}_{13} = \bar{r}_{12} + \bar{t}_{21}\bar{p}_2\bar{r}_{23}\bar{p}_2 \sum_{n=0}^{\infty} (\bar{r}_{21}\bar{p}_2\bar{r}_{23}\bar{p}_2)^n \bar{t}_{12}, \tag{4.18}$$

where each term in the sum represents the field that has propagated back and fourth $n+1$ times. It should be noted that the form of r_{13} and all following coefficients have been chosen such that as few different matrices as possible are inverted.

Similarly, the transmission matrix $\bar{t}_{13}$ can be used to describe the total transmitted field to region 3 as

$$\bar{t}_{13} = \bar{t}_{23}\bar{p}_2 \sum_{n=0}^{\infty} (\bar{r}_{21}\bar{p}_2\bar{r}_{23}\bar{p}_2)^n \bar{t}_{12}. \tag{4.19}$$

The sum in the above two equations can be greatly simplified by applying the geometric series $\sum_{n=0}^{\infty} \bar{a}^n = (\bar{I} - \bar{a})^{-1}$, which is only valid when the matrix $\bar{a}$ have absolute eigenvalues below unity [3]. With this, the equations becomes

$$\bar{r}_{13} = \bar{r}_{12} + \bar{t}_{21}\bar{p}_2\bar{r}_{23}\bar{p}_2(\bar{I} - \bar{r}_{21}\bar{p}_2\bar{r}_{23}\bar{p}_2)^{-1}\bar{t}_{12} \tag{4.20}$$

$$\bar{t}_{13} = \bar{t}_{23}\bar{p}_2(\bar{I} - \bar{r}_{21}\bar{p}_2\bar{r}_{23}\bar{p}_2)^{-1}\bar{t}_{12}. \tag{4.21}$$

If the field is incident from region 3 then the $\bar{r}_{31}$ and $\bar{t}_{31}$ coefficients are needed and can be found similarly as the $\bar{r}_{13}$ and $\bar{t}_{13}$ coefficients. This will yield

$$\bar{r}_{31} = \bar{r}_{32} + \bar{t}_{23}\bar{p}_2(\bar{I} - \bar{r}_{21}\bar{p}_2\bar{r}_{23}\bar{p}_2)^{-1}\bar{r}_{21}\bar{p}_2\bar{t}_{32} \tag{4.22}$$

$$\bar{t}_{31} = \bar{t}_{21}\bar{p}_2\bar{t}_{32} + \bar{t}_{21}\bar{p}_2\bar{r}_{23}\bar{p}_2(\bar{I} - \bar{r}_{21}\bar{p}_2\bar{r}_{23}\bar{p}_2)^{-1}\bar{r}_{21}\bar{p}_2\bar{t}_{32}. \tag{4.23}$$

The remaining field coefficients in region 1 and 3 can now be calculated by eq. (4.13) with index 2 replaced by 3

$$\mathbf{a}_3 = \bar{t}_{13}\mathbf{a}_1' + \bar{r}_{31}\mathbf{b}_3' \tag{4.24}$$

$$\mathbf{b}_1 = \bar{r}_{13}\mathbf{a}_1' + \bar{t}_{31}\mathbf{b}_3'. \tag{4.25}$$

The coefficients $\mathbf{a}_2$ and $\mathbf{b}_2$ should likewise take into account of the fields bouncing back and forth in region 2. If the field is incident from region 1, then the contribution to $\mathbf{a}_2$ comes from $\bar{t}_{12}$ and a infinite sum of multiples of $\bar{r}_{21}\bar{p}_2\bar{r}_{23}\bar{p}_2$. While the contribution to $\mathbf{b}_2$ comes from $\bar{r}_{23}\bar{p}_2\bar{t}_{12}$ and a infinite sum of multiples of $\bar{r}_{23}\bar{p}_2\bar{r}_{12}\bar{p}_2$. A similar analysis can be made if the field is incident from region 3 instead and gives

$$\mathbf{a}_2 = (\bar{I} - \bar{r}_{21}\bar{p}_2\bar{r}_{23}\bar{p}_2)^{-1}(\bar{t}_{12}\mathbf{a}_1' + \bar{r}_{21}\bar{p}_2\bar{t}_{32}\mathbf{b}_3') \tag{4.26}$$

$$\mathbf{b}_2 = (\bar{I} - \bar{r}_{23}\bar{p}_2\bar{r}_{21}\bar{p}_2)^{-1}(\bar{r}_{23}\bar{p}_2\bar{t}_{12}\mathbf{a}_1' + \bar{t}_{32}\mathbf{b}_3'), \tag{4.27}$$

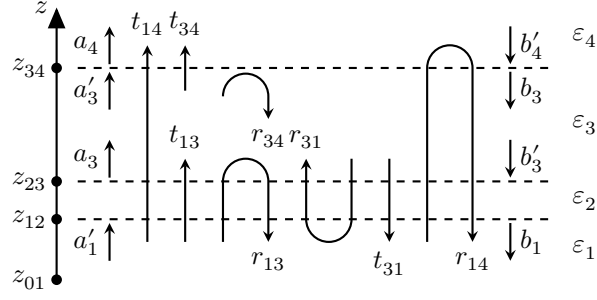where the first factors of each expression take care of the multiple reflections inside region 2.

Figure 4.3: *The reflection and transmission of field inside a 4-layer geometry.*

4.2.1 Multi-layer Structure

The next part of the section will be focusing on expanding the structure to a *N*-layer geometry, which is illustrated in fig. 4.4. This will firstly be done by giving a rough idea of what happens when the geometry contains 4 layers. The four-layer structure is illustrated in fig. 4.3. In this case, the reflection and transmission coefficients between layer 1 and 3 can be calculated as before. These matrices take into account of the modes that are reflected and transmitted from/into layer 3. Hence everything that happens in layer 2 has already been calculated into $\bar{r}_{13}$ and $\bar{t}_{13}$, therefore the four-layer structure can be thought as a 3-layer structure. The problem is then similar to the one already solved, hence we can reuse eq. (4.18) by doing some replacements

$$\bar{r}_{14} = \bar{r}_{13} + \bar{t}_{31}\bar{p}_3\bar{r}_{34}\bar{p}_3\big(\bar{I} - \bar{r}_{31}\bar{p}_3\bar{r}_{34}\bar{p}_3\big)^{-1}\bar{t}_{13}. \tag{4.28}$$

Generally, when knowing the reflection and transmission coefficients for a *q*-layer structure one can calculate $\bar{r}_{1,q+1}$, $\bar{t}_{1,q+1}$, $\bar{r}_{q+1,1}$ and $\bar{t}_{q+1,1}$ by reducing the structure to a three-layer geometry [3]. Let the structure in question contain *n* layers in total, then the recursive procedure is similar but here we solve the three-layer geometry consistent of layer $n-2$, $n-1$ and n. In this structure we can then calculate $\bar{r}_{n-2}$, $\bar{t}_{n-2,n}$, $\bar{r}_{n,n-2}$ and $\bar{t}_{n,n-2}$, and when including the fourth layer we can collapse the structure into a three-layer geometry as before. When considering the *q*'th layer in the recursive process the matrices $\bar{r}_{q-1,n}$, $\bar{t}_{q-1,n}$, $\bar{r}_{n,q-1}$ and $\bar{t}_{n,q-1}$ can then be calculated from $\bar{r}_{q,n}$, $\bar{t}_{q,n}$, $\bar{r}_{n,q}$ and $\bar{t}_{n,q}$. Below we have given all the recursive relations [3]

$$\bar{r}_{1,q+1} = \bar{r}_{1,q} + \bar{t}_{q,1}\bar{p}_q\bar{r}_{q,q+1}\bar{p}_q\big(\bar{I} - \bar{r}_{q,1}\bar{p}_q\bar{r}_{q,q+1}\bar{p}_q\big)^{-1}\bar{t}_{1,q} \tag{4.29}$$

$$\bar{t}_{1,q+1} = \bar{t}_{q,q+1}\bar{p}_q\big(\bar{I} - \bar{r}_{q,1}\bar{p}_q\bar{r}_{q,q+1}\bar{p}_q\big)^{-1}\bar{t}_{1,q} \tag{4.30}$$

$$\bar{r}_{q+1,1} = \bar{r}_{q+1,q} + \bar{t}_{q,q+1}\bar{p}_q\big(\bar{I} - \bar{r}_{q,1}\bar{p}_q\bar{r}_{q,q+1}\bar{p}_q\big)^{-1}\bar{r}_{q,1}\bar{p}_q\bar{t}_{q+1,q} \tag{4.31}$$

$$\bar{t}_{q+1,1} = \bar{t}_{q,1}\bar{p}_q\bar{t}_{q+1,q} + \bar{t}_{q,1}\bar{p}_q\bar{r}_{q,q+1}\bar{p}_q\big(\bar{I} - \bar{r}_{q,1}\bar{p}_q\bar{r}_{q,q+1}\bar{p}_q\big)^{-1}\bar{r}_{q,1}\bar{p}_q\bar{t}_{q+1,q} \tag{4.32}$$

$$\bar{r}_{q-1,n} = \bar{r}_{q-1,q} + \bar{t}_{q,q-1}\bar{p}_q\bar{r}_{q,n}\bar{p}_q\big(\bar{I} - \bar{r}_{q,q-1}\bar{p}_q\bar{r}_{q,n}\bar{p}_q\big)^{-1}\bar{t}_{q-1,q} \tag{4.33}$$

$$\bar{t}_{q-1,n} = \bar{t}_{q,n}\bar{p}_q\big(\bar{I} - \bar{r}_{q,q-1}\bar{p}_q\bar{r}_{q,n}\bar{p}_q\big)^{-1}\bar{t}_{q-1,q} \tag{4.34}$$

$$\bar{r}_{n,q-1} = \bar{r}_{n,q} + \bar{t}_{q,n}\bar{p}_q\big(\bar{I} - \bar{r}_{q,q-1}\bar{p}_q\bar{r}_{q,n}\bar{p}_q\big)^{-1}\bar{r}_{q,q-1}\bar{p}_q\bar{t}_{n,q} \tag{4.35}$$
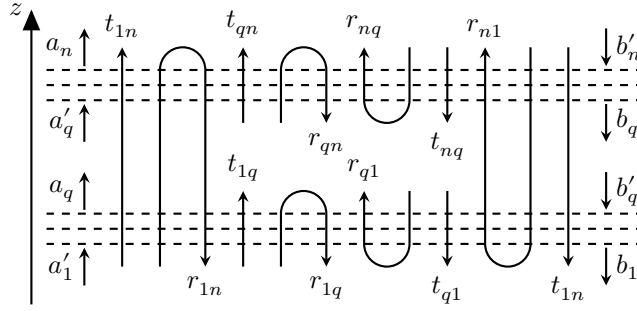
Figure 4.4: *The reflection and transmission of field inside a N layer geometry.*

$$\bar{t}_{n,q-1} = \bar{t}_{q,q-1}\bar{p}_q\bar{t}_{n,q} + \bar{t}_{q,q-1}\bar{p}_q\bar{r}_{q,n}\bar{p}_q\big(\bar{I} - \bar{r}_{q,q-1}\bar{p}_q\bar{r}_{q,n}\bar{p}_q\big)^{-1}\bar{r}_{q,q-1}\bar{p}_q\bar{t}_{n,q}. \tag{4.36}$$

The field expansion vectors for the q'th layer may be calculated by [3]

$$\mathbf{a}_q = \big(\bar{I} - \bar{r}_{q,1}\bar{p}_q\bar{r}_{q,n}\bar{p}_q\big)^{-1}\big(\bar{t}_{1,q}\mathbf{a}_1' + \bar{r}_{q,1}\bar{p}_q\bar{t}_{n,q}\mathbf{b}_n'\big) \tag{4.37}$$

$$\mathbf{b}_q = \big(\bar{I} - \bar{r}_{q,n}\bar{p}_q\bar{r}_{q,1}\bar{p}_q\big)^{-1}\big(\bar{r}_{q,n}\bar{p}_q\bar{t}_{1,q}\mathbf{a}_1' + \bar{t}_{n,q}\mathbf{b}_n'\big), \tag{4.38}$$

and the electric and magnetic fields in the q layer may be calculated by [3]

$$\mathbf{E}_q(\mathbf{r}) = \sum_j^N \Big(a_{q,j}\,\mathrm{e}^{\mathrm{i}\beta(z-z_{q-1,q})}\mathbf{e}_{q,j}^+(\mathbf{r}_\perp) + b_{q,j}\,\mathrm{e}^{-\mathrm{i}\beta(z-z_{q,q+1})}\mathbf{e}_{q,j}^-(\mathbf{r}_\perp)\Big) \tag{4.39}$$

$$\mathbf{H}_q(\mathbf{r}) = \sum_j^N \Big(a_{q,j}\,\mathrm{e}^{\mathrm{i}\beta(z-z_{q-1,q})}\mathbf{h}_{q,j}^+(\mathbf{r}_\perp) + b_{q,j}\,\mathrm{e}^{-\mathrm{i}\beta(z-z_{q,q+1})}\mathbf{h}_{q,j}^-(\mathbf{r}_\perp)\Big). \tag{4.40}$$

4.3 Fourier Modal Method

This section will contain the theory for calculating the electric field in a two-dimensional geometry that can be divided into regions that are invariant along the propagation axis and periodic along the other axis. To match the electric fields at the interfaces between the regions, one needs to use the boundary conditions such that the transverse fields are continuous across each interface. From these boundary conditions, one can create a scattering matrix which describes the modes propagating through an interface. The first case of interest is a rather simple case with only one interface. This example will then be expanded into a more complicated problem with multiple layers.

4.3.1 Single Interface

This section will look into a two-layer structure, where the first region consists of air and the other consists of a semi-infinite periodic array of infinitely long rods. This is illustrated in fig. 4.5. An s-polarised plane wave is incident from region 1, hence the electric field can be described as

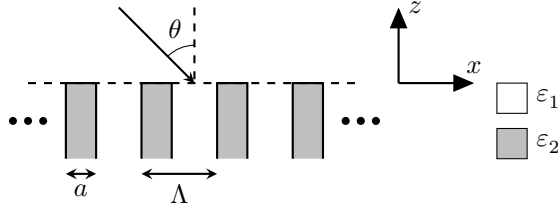$$\mathbf{E}(\mathbf{r}) = \hat{\mathbf{y}}E(x,z). \tag{4.41}$$

Figure 4.5: *An illustration of field incident from above upon a single interface. Each layer is invariant along the z axis and periodic along x.*

Since the structure is periodic along the x-axis in region two with a period of Λ, it can be assumed that the electric field is periodic as well, hence it can be divided into Bloch waves [8]

$$E(x + \Lambda, z) = E(x, z)\, \mathrm{e}^{\mathrm{i}k_x\Lambda}, \tag{4.42}$$

where $k_x = k_0 \sin(\theta)$ is the Bloch wave number. In region 1 the field is incident from above and due to the reflection at the interface there can be waves which can propagate either along the positive and negative z-axis hence the field can be written as

$$E^{(1)}(x, z) = \sum_{n=-\infty}^{\infty} \left(a_n^{(1)}\, \mathrm{e}^{-\mathrm{i}k_{z,n}^{(1)}z} + b_n^{(1)}\, \mathrm{e}^{\mathrm{i}k_{z,n}^{(1)}z} \right) \mathrm{e}^{\mathrm{i}k_{x,n}x}. \tag{4.43}$$

Note that we have used a different convention for the forward and backward propagating fields compared to previous sections. Here we have used a_n to represent the backward propagating modes and b_n represents the forward propagating modes.

The electric field needs to satisfy both the wave equation and the Bloch condition, which means that [8]

$$k_{x,n} = k_x + nG, \quad \text{where } G = 2\pi/\Lambda \tag{4.44}$$

$$k_{z,n}^{(1)} = \sqrt{k_0^2 - k_{x,n}^2}. \tag{4.45}$$

In region 2 the field can no longer be described with simple plane waves or evanescent waves, here the field will be on the form of

$$E^{(2)}(x, z) = \sum_{n=-\infty}^{\infty} \left(\mathrm{e}^{\mathrm{i}k_{x,n}x} \sum_m E_m^{(n,2)} \left(a_m^{(2)}\, \mathrm{e}^{-\mathrm{i}k_{z,m}^{(2)}z} + b_m^{(2)}\, \mathrm{e}^{\mathrm{i}k_{z,m}^{(2)}z} \right) \right), \tag{4.46}$$

since there, in general, are multiple modes in region 2, where each mode is expanded with plane waves. We will approximate the field in region 1 so that it is expanded in a finite number of plane waves, such that n varies from $-N$ to N. Furthermore, it will be assumed that there will be the same amount of modes in region 2 so $m \in \{1, 2, \dots, 2N + 1\}$.

To calculate the mode coefficients for each region, one can use the boundary conditions which require that the y-component of the electric field is continuous across the interface

$$\sum_{m=1}^{2N+1} E_m^{(n,1)} \left(a_m^{(1)} + b_m^{(1)} \right) = \sum_m^{(n,2)} E_m^{(n,2)} \left(a_m^{(2)} + b_m^{(2)} \right). \tag{4.47}$$

A similar argument can be made for x-component of the magnetic field, which can be expressed through the electric field as $H_x = -\frac{1}{\mathrm{i}\omega\mu}\frac{\partial}{\partial z}E_y$, hence the boundary conditions reads

$$\sum_{m=1}^{2N+1} k_{z,m}^{(1)} E_m^{(n,1)}\left(a_m^{(1)} - b_m^{(1)}\right) = \sum_{m=1}^{2N+1} k_{z,m}^{(2)} E_m^{(n,2)}\left(a_m^{(2)} - b_m^{(2)}\right). \tag{4.48}$$

The equation for the boundary condition can be written on matrix form

$$\bar{M}_1^{(E)}\left(\mathbf{a}^{(1)} + \mathbf{b}^{(1)}\right) = \bar{M}_2^{(E)}\left(\mathbf{a}^{(2)} + \mathbf{b}^{(2)}\right) \tag{4.49}$$

$$\bar{M}_1^{(H)}\left(\mathbf{a}^{(1)} - \mathbf{b}^{(1)}\right) = \bar{M}_2^{(H)}\left(\mathbf{a}^{(2)} - \mathbf{b}^{(2)}\right), \tag{4.50}$$

where

$$\mathbf{a}^{(i)} = \left(a_1^{(i)}, a_2^{(i)}, \dots, a_{2N+1}^{(i)}\right) \tag{4.51}$$

$$\mathbf{b}^{(i)} = \left(b_1^{(i)}, b_2^{(i)}, \dots, b_{2N+1}^{(i)}\right) \tag{4.52}$$

$$\bar{M}_i^{(E)} = \begin{bmatrix} \mathbf{E}_1^{(i)} & \mathbf{E}_2^{(i)} & \cdots & \mathbf{E}_{2N+1}^{(i)} \end{bmatrix} \tag{4.53}$$

$$\bar{M}_i^{(H)} = \begin{bmatrix} k_{z,1}^{(i)}\mathbf{E}_1^{(i)} & k_{z,2}^{(i)}\mathbf{E}_2^{(i)} & \cdots & k_{z,2N+1}^{(i)}\mathbf{E}_{2N+1}^{(i)} \end{bmatrix} \tag{4.54}$$

$$\mathbf{E}_m^{(i)} = \left(E_m^{(-N,i)}, E_m^{(-N+1,i)}, \dots, E_m^{(N,i)}\right). \tag{4.55}$$

We will later show how the matrices $\bar{M}_i^{(E)}$ and $\bar{M}_i^{(H)}$ are calculated.

Assuming that the field is incident from region 1 then there are no waves propagating along the positive z-axis in region 2, hence $\mathbf{b}^{(2)} = 0$. From eqs. (4.49) and (4.50) one can derive the two following equations for the mode coefficients

$$\mathbf{b}^{(1)} = \bar{R}_{12}\mathbf{a}^{(1)} \tag{4.56}$$

$$\mathbf{a}^{(2)} = \bar{T}_{12}\mathbf{a}^{(1)}, \tag{4.57}$$

where the $\bar{R}_{12}$ and $\bar{T}_{12}$ are the reflection and transmission matrices between region 1 and 2, respectively and they are given by

$$\bar{R}_{12} = \left(\left(\bar{M}_2^{(E)}\right)^{-1}\bar{M}_1^{(E)} + \left(\bar{M}_2^{(H)}\right)^{-1}\bar{M}_1^{(H)}\right)^{-1}\left(\left(\bar{M}_2^{(H)}\right)^{-1}\bar{M}_1^{(H)}\right) - \left(\bar{M}_2^{(E)}\right)^{-1}\bar{M}_1^{(E)}\right) \tag{4.58}$$

$$\bar{T}_{12} = \left(\bar{M}_2^{(E)}\right)^{-1}\bar{M}_1^{(E)}\left(\bar{I} + \bar{R}_{12}\right). \tag{4.59}$$

The next step is to calculate the modes for region 2. This is done with a similar approach as for region 1 but yields a different result. Inserting the expression for a single-mode m of the electric field into the wave equation

$$0 = \sum_n \left(-k_{x,n}^2 - (k_{z,m}^{(2)})^2 + k_0^2\varepsilon(x)\right)E_m^{(n,2)}\,\mathrm{e}^{\mathrm{i}k_{x,n}x}\,\mathrm{e}^{\pm\mathrm{i}k_{z,m}z} \tag{4.60}$$

and since that the structure is periodic along the x-axis with period Λ then the approximation is $\varepsilon(x) \approx \sum_n \varepsilon_n \, \mathrm{e}^{inGx}$ valid. Then it is possible to derive the following equation

$$(k_{z,m}^{(2)})^2 \sum_n E_m^{(n,2)} \, \mathrm{e}^{i(nG+k_x)x} =$$

$$-\sum_n (nG+k_x)^2 E_m^{(n,2)} \, \mathrm{e}^{i(nG+k_x)x} + k_0^2 \sum_{n'} \sum_{n''} \varepsilon_{n''} E_m^{(n',2)} \, \mathrm{e}^{i(n''+n')Gx} \, \mathrm{e}^{ik_x x} \quad (4.61)$$

$$\implies -(nG+k_x)^2 E_m^{(n,2)} + k_0^2 \sum_{n'} \varepsilon_{n-n'} E_m^{(n',2)} = (k_{z,m}^{(2)})^2 E_m^{(n,2)}. \quad (4.62)$$

The above equation can be written on matrix form by using vector eq. (4.55) and the matrices

$$\bar{A} = \begin{bmatrix} (-NG+k_x)^2 & 0 & \cdots & 0 \\ 0 & ((-N+1)G+k_x)^2 & \ddots & 0 \\ \vdots & \ddots & \ddots & \vdots \\ 0 & 0 & \cdots & (NG+k_x)^2 \end{bmatrix} \quad (4.63)$$

and

$$\bar{B} = \begin{bmatrix} \varepsilon_0 & \varepsilon_{-1} & \cdots & \varepsilon_{-2N} \\ \varepsilon_1 & \varepsilon_0 & \cdots & \varepsilon_{-2N+1} \\ \vdots & \vdots & \ddots & \vdots \\ \varepsilon_{2N} & \varepsilon_{2N-1} & \cdots & \varepsilon_0 \end{bmatrix}. \quad (4.64)$$

To calculate the Fourier coefficients given in the above matrix for the dielectric function, one should keep in mind that the dielectric function is a piecewise constant function given by (see fig. 4.5 for reference)

$$\varepsilon(x) = \begin{cases} \varepsilon_2, & 0 \le x < a \\ \varepsilon_1, & a \le x < \Lambda \end{cases}. \quad (4.65)$$

Then the Fourier coefficients can be calculated by integrating the dielectric function over a single period

$$\varepsilon_n = \frac{1}{\Lambda} \int_0^\Lambda \varepsilon(x) \, \mathrm{e}^{-i\frac{2\pi}{\Lambda}nx} \, \mathrm{d}x \quad (4.66)$$

$$= \frac{1}{\Lambda} \left(\int_0^a \varepsilon_2 \, \mathrm{e}^{-i\frac{2\pi}{\Lambda}nx} \, \mathrm{d}x + \int_a^\Lambda \varepsilon_1 \, \mathrm{e}^{-i\frac{2\pi}{\Lambda}nx} \, \mathrm{d}x \right), \quad (4.67)$$

which leads to two different results, one for $n = 0$ and one for $n \neq 0$

$$\varepsilon_n = \begin{cases} \frac{a}{\Lambda}\varepsilon_2 + (1-\frac{a}{\lambda})\varepsilon_1, & n = 0 \\ \frac{\varepsilon_2-\varepsilon_1}{inG\Lambda}(1 - \mathrm{e}^{-inGa}), & n \neq 0 \end{cases}. \quad (4.68)$$

The eigenvalue problem can then be formulated as

$$(k_0^2 \bar{B} - \bar{A}) \mathbf{E}_m^{(2)} = (k_{z,m}^{(2)})^2 \mathbf{E}_m^{(2)}. \quad (4.69)$$

After solving the eigenvalue problem and finding the eigenmodes, then $\bar{M}_2^{(E)}$ and $\bar{M}_2^{(H)}$ can be found as

$$\bar{M}_2^{(E)} = \left(\mathbf{E}_1^{(2)}, \mathbf{E}_2^{(2)}, ..., \mathbf{E}_{2N+1}^{(2)} \right) \tag{4.70}$$

$$\bar{M}_2^{(H)} = \left[k_{z,1}^{(2)} \mathbf{E}_1^{(2)} \quad k_{z,2}^{(2)} \mathbf{E}_2^{(2)} \quad \cdots \quad k_{z,2N+1}^{(2)} \mathbf{E}_{2N+1}^{(2)} \right]. \tag{4.71}$$

The same goes for the corresponding matrices for region 1, but since this region only consist of free space we can just write the solutions as

$$\bar{M}_1^{(E)} = \bar{I} \tag{4.72}$$

$$\bar{M}_1^{(H)} = \text{diag}(k_{z,1}^{(1)}, k_{z,2}^{(1)}, ..., k_{z,2N+1}^{(1)}). \tag{4.73}$$

Figure 4.6 shows the electric field distribution for the two-layer structure given in fig. 4.5. The calculation was performed with $\Lambda = 400\,000\,\mu\text{m}$, $a = 200\,\mu\text{m}$, $\lambda = 700\,\mu\text{m}$ and 4001 plane waves. It was assumed the rods had a dielectric value of $\varepsilon_2 = 1.96^2$ and the surrounding air with $\varepsilon_1 = 1$. The incident field in layer 1 was chosen to be the normal plane wave to the interface. We see that the field is scattered in all directions at the interface. The transmitted field excites the guided mode of the waveguide and the semi-radiation modes.

4.3.2 Multiple interfaces

The FMM can be expanded to handle multiple layers using S-matrix theory described in section 4.2.1. Instead of having semi-infinite rods in layer 2 as in fig. 4.5, we will consider a three-layer structure where layer 2 has a finite length L_2 as shown in fig. 4.7. The third layer is identical to layer 1, that is they are both solely consisting of air.

The electric field on each of the layers can be represented as

$$E^{(i)}(x,y) = \sum_{n=-N}^{N} e^{ik_{x,n}x} \sum_{m=1}^{2N+1} E_m^{(n,i)} \left(a_m^{(i)} e^{-ik_{z,m}^{(i)}(z-z_{i-1,i})} + b_m^{(2)} e^{+ik_{z,m}^{(i)}(z-z_{i-1,i})} \right), \tag{4.74}$$

where i can take the values 1, 2 and 3. Before we take into account the multiple reflections that appears in layer 2, we will first consider a propagation matrix which describes the propagation of the modes along the z-axis. This matrix is given by

$$\bar{P}^{(i)} = \begin{bmatrix} \exp\left(ik_{z,1}^{(i)}L_i\right) & 0 & \cdots & 0 \\ 0 & \exp\left(ik_{z,2}^{(i)}L_i\right) & \ddots & 0 \\ \vdots & \ddots & \ddots & \vdots \\ 0 & 0 & \cdots & \exp\left(ik_{z,2N+1}^{(i)}L_i\right) \end{bmatrix}. \tag{4.75}$$

The scatter matrix between each layer can then be calculated using the method outlined in section 4.2.1. To calculate the eigenmodes, we can use eq. (4.69), since it was derived using the general expression for the electric field.

In fig. 4.8 the real, imaginary and absolute values of the electric field are plotted for the geometry given in fig. 4.7. Layer 1 and 3 consist of air while layer 2 consist of air
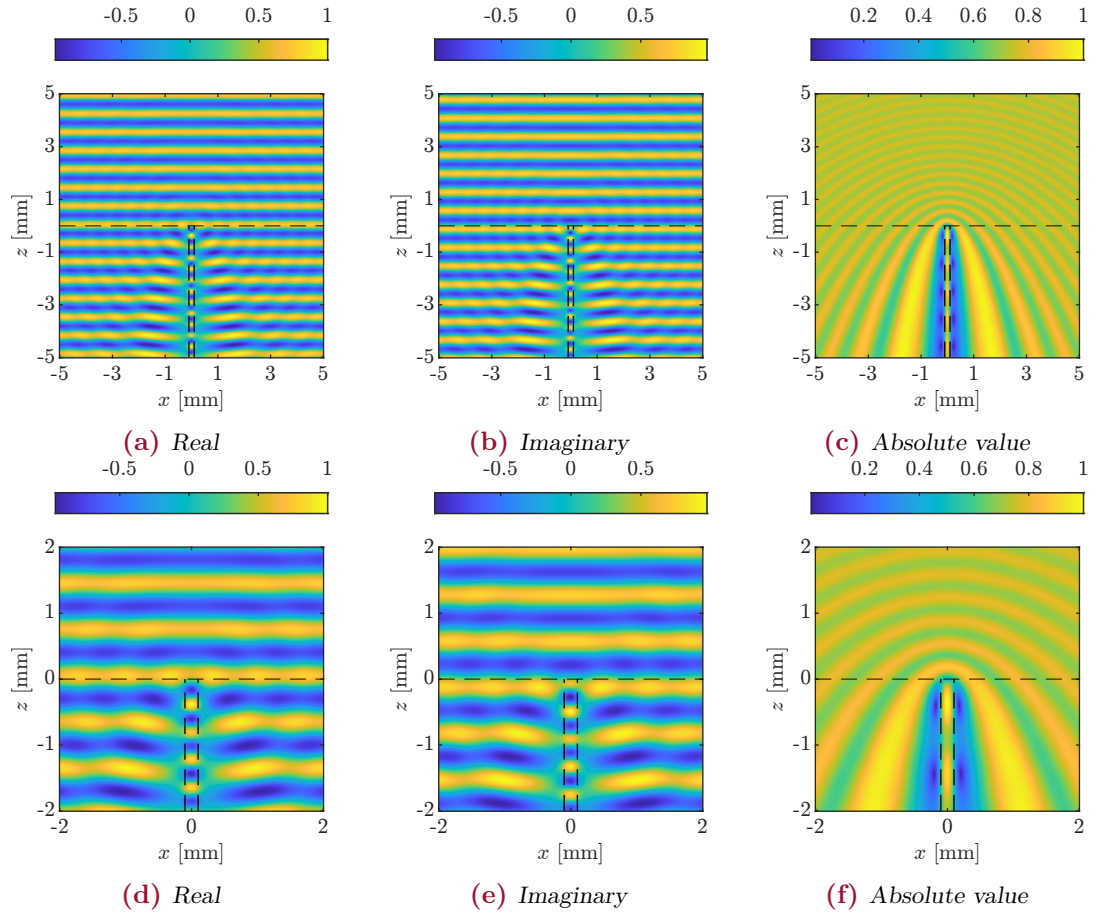
(a) *Real*   **(b)** *Imaginary*   **(c)** *Absolute value*

(d) *Real*   **(e)** *Imaginary*   **(f)** *Absolute value*

Figure 4.6: *The figures show the electric field distribution for a propagation field along the z-axis. The waveguide in the lower centre has $\varepsilon_2 = 1.96^2$, whereas the surrounding air has $\varepsilon_1 = 1$.*
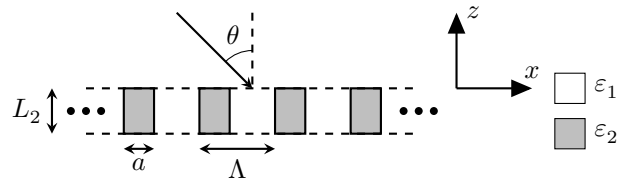

Figure 4.7: *An illustration of field incident from above in a three-layer structure with two interfaces. Each layer is invariant along the z axis and the middle layer is periodic along x.*

(a) *Real*   **(b)** *Imaginary*   **(c)** *Absolute value*

(d) *Real*   **(e)** *Imaginary*   **(f)** *Absolute value*
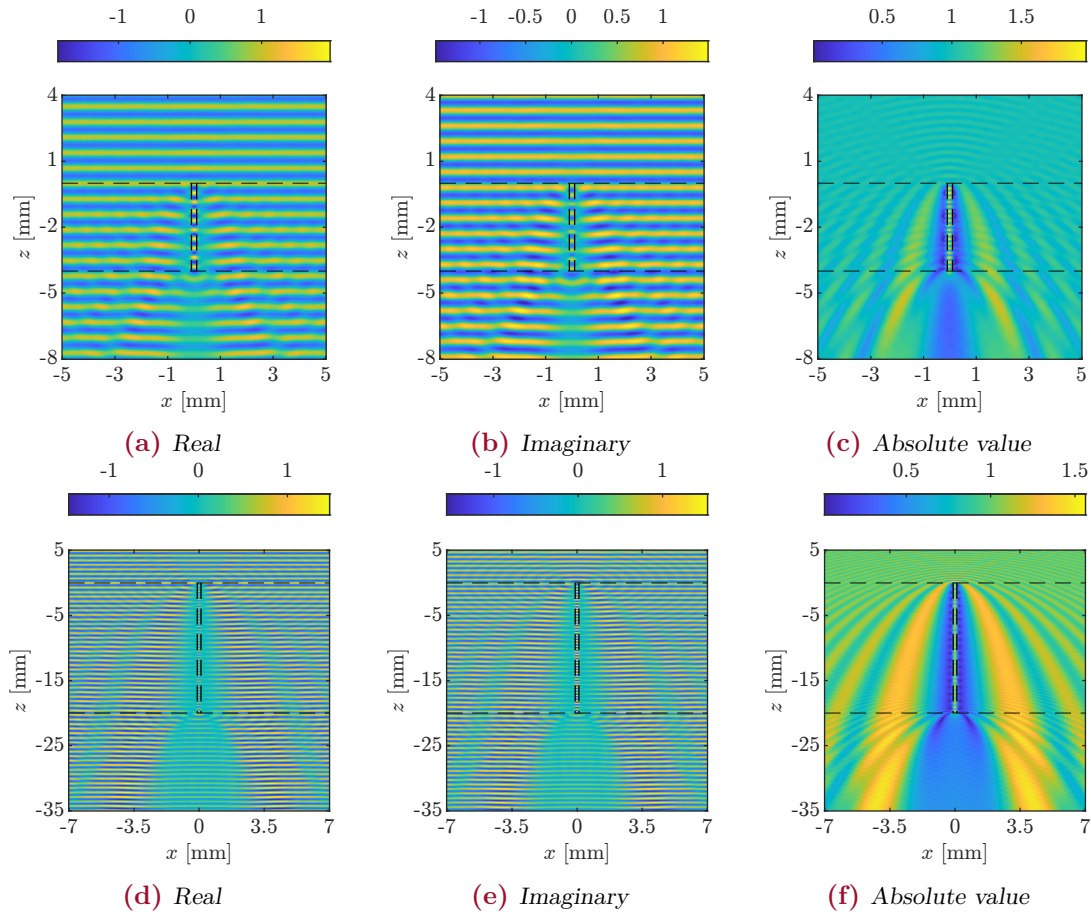
Figure 4.8: *The figures show the electric field distribution of fig. 4.7 with a normal incident plane wave from above. The parameters was $\varepsilon_1 = 1$, $\varepsilon_2 = 1.96^2$, $\Lambda = 400\,000\,\mu m$, $a = 200\,\mu m$, $\lambda = 700\,\mu m$ and 4001 plane waves.*

and rods with $\varepsilon_2 = 1.96^2$. The plots was calculated with $\Lambda = 400\,000\,\mu\text{m}$, $a = 200\,\mu\text{m}$ and 4001 plane waves. The incident field was chosen to be a normal incident plane wave from above. We see that the field is scattered in all directions at the first interface. The transmitted field excites the guided mode of the waveguide and the semi-radiation modes. A rather advanced interference pattern is formed in the middle layer due to the multiple reflections. The field transmitted through the second interface is largely scattered. The field in the middle layer becomes more similar to the field in fig. 4.6 as L_2 increases.

4.3.3 Transmission and Reflection

The transmission and reflection of the fields at the interfaces can be found by calculating the power of each mode and taking their ratio. The m'th backwards propagating mode in layer i' can be expressed as

$$E_{y,m}^{(i)}(x,z) = \left(\sum_n E_{y,m}^{(n,i)} \, \mathrm{e}^{\mathrm{i}k_{x,n}x} \right) \mathrm{e}^{-\mathrm{i}k_{z,m}^{(i)}z}. \tag{4.76}$$

The power can then be calculated by integrating the time-averaged Poynting vector over an interface, where the time-average Poynting vector is given by

$$\left\langle \mathbf{S}_m^{(i)} \right\rangle = \frac{1}{2} \, \mathrm{Re}\!\left(\mathbf{E}_m^{(i)} \times \left(\mathbf{H}_m^{(i)} \right)^* \right). \tag{4.77}$$

Since we are only interested in the energy flux along the z-direction we can multiply both sides of this equation with $\hat{\mathbf{n}} = \hat{\mathbf{z}}$. Then the only relevant part of $\mathbf{E}_m^{(i)}$ and $\left(\mathbf{H}_m^{(i)} \right)^*$ are the former's y component and the latter's x component. Note that we are still assuming that the electric field is polarised along the y-axis. This allows us to write the x-component of the magnetic field as

$$H_{x,m}^{(i)} = \frac{-1}{\mathrm{i}\omega\mu_0} \frac{\partial}{\partial z} E_{y,m}^{(i)} = \frac{k_{z,m}^{(i)}}{\omega\mu_0} E_{y,m}^{(i)}. \tag{4.78}$$

This enables us to write

$$-\hat{\mathbf{z}} \cdot \langle \mathbf{S}_m \rangle = \frac{1}{2} \, \mathrm{Re}\!\left(E_{y,m}^{(i)} \left(H_{x,m}^{(i)} \right)^* \right) \tag{4.79}$$

$$= \frac{1}{2} \, \mathrm{Re}\!\left(\frac{k_{z,m}^{(i)}}{\omega\mu_0} \right) \left| E_{y,m}^{(i)} \right|^2. \tag{4.80}$$

The power of the field propagating across the interface into region i can then be calculated by integrating the time-averaged Poynting vector over a single period at the interface

$$P_m^{(i)} = \int_0^\Lambda \frac{1}{2} \, \mathrm{Re}\!\left(\frac{k_{z,m}^{(i)}}{\omega\mu_0} \right) \left(\sum_n E_{y,m}^{(n,i)} \, \mathrm{e}^{\mathrm{i}k_{x,n}x} \right) \left(\sum_{n'} \left(E_{y,m}^{(n',i)} \right)^* \mathrm{e}^{-\mathrm{i}k_{x,n'}x} \right) \mathrm{d}x \tag{4.81}$$

$$= \frac{1}{2} \sqrt{\frac{\varepsilon_0}{\mu_0}} \, \mathrm{Re}\!\left(\frac{k_{z,m}^{(i)}}{k_0} \right) \Lambda \sum_n \left| E_{y,m}^{(n,i)} \right|^2, \tag{4.82}$$

where we have used $ck_0 = \omega$ and $c = 1/\sqrt{\varepsilon_0\mu_0}$ is the speed of light in vacuum. Note that this result is build upon the electric field presented in eq. (4.76). If we used a forward travelling mode i.e. $\exp(+\mathrm{i}k_{z,m}z)$, then we would have to use $\hat{\mathbf{n}} = \hat{\mathbf{z}}$ as the unit normal vector to the interface. In this case, eq. (4.82) is unchanged. In order to get the power for the forward or the backward mode the above result needs to be multiplied with either $\left|a_m^{(i)}\right|^2$ or $\left|b_m^{(i)}\right|^2$.

To calculate the transmission into layer i and the reflection of an incident beam $\mathbf{a}^{(1)}$, we will need to sum over the modes of interest, because of power orthogonality (eq. (2.70))

$$T = \frac{\sum_m P_m^{(i)}\left|a_m^{(i)}\right|^2}{\sum_n P_n^{(1)}\left|a_n^{(1)}\right|^2} \tag{4.83}$$

$$R = \frac{\sum_m P_m^{(1)}\left|b_m^{(1)}\right|^2}{\sum_n P_n^{(1)}\left|a_n^{(1)}\right|^2}. \tag{4.84}$$

For the two-layer geometry in fig. 4.5, it can be interesting to determine how much of the incident field is transmitted into the guided modes of the waveguide. In case of a single-mode slab waveguide, we can calculate this transmission as

$$T_{\text{guided}} = \frac{P_i^{(2)}\left|a_i^{(2)}\right|^2}{\sum_{m=1}^{2N+1} P_m^{(1)}\left|a_m^{(1)}\right|^2}, \tag{4.85}$$

where i corresponds to the index of the guided mode of the waveguide. The total transmission and reflection through a n-layer structure is found by summing over all modes as

$$T_{\text{total}} = \frac{\sum_{m=1}^{2N+1} P_m^{(n)}\left|a_m^{(n)}\right|^2}{\sum_{m=1}^{2N+1} P_m^{(1)}\left|a_m^{(1)}\right|^2} \tag{4.86}$$

$$R_{\text{total}} = \frac{\sum_{m=1}^{2N+1} P_m^{(1)}\left|b_m^{(1)}\right|^2}{\sum_{m=1}^{2N+1} P_m^{(1)}\left|a_m^{(1)}\right|^2}. \tag{4.87}$$

When calculating the last two equations, we should check the condition $T_{\text{total}} + R_{\text{total}} = 1$ is satisfied.

4.4 Absorbing Boundary Condition

In the Fourier modal method the field is expanded in a set of plane waves under the assumption that the structure is periodic. In the case where one is interested in a non-periodic structure, the period can be made large enough such that each waveguide does not interact with each other. However since large period requires a large number of plane waves for the expansion, one cannot necessarily make the period large enough

to avoid any interaction from the neighbouring waveguides, which results in parasitic reflections. In the non-open geometries, Te parasitic reflections will lead to advanced interference patterns. They are an artefact of having a non-open geometry and will not be present in an open geometry [3].

The parasitic reflections can be suppressed by introducing an absorbing layers also known as perfectly matched layers (PML) [3], which leads to less interference. The electric field for a plane wave propagating in a medium of thickness L with refractive index n can be described as

$$\mathbf{E}(L) = \mathrm{e}^{ik_0 nL}\mathbf{E}(0) \tag{4.88}$$

by allowing the refractive index to assume complex values, the field contains a damping effect which reduces the amplitude of the field. For large complex values of n the amplitude tends to move towards zero. However the index difference between the absorbing layer and the inner layer can create reflection as can be seen from eq. (4.9) [3]. Another approach is to make L in eq. (4.88) complex, which will yield as similar result as by making n complex [3]. It can be used to describe the field near a single waveguide.

5 Coupled waveguides

5.1 Coupled waveguides

This section will go into detail with the coupling between waveguides. This will initially be done through the examination of a slab waveguide consisting of 5 layers, i.e. 2 waveguides with air around and between them as seen in fig. 5.1. It will be assumed that a TE wave is propagating along with the uniform z-axis of the waveguide. Such a wave can be described with an electric field, which is polarised along the y-direction

$$E_{y,i}(x,z) = \left(E_{i,R}\, e^{ik_{i,x}(x-x_{i-1,i})} + E_{i,L}\, e^{-ik_{i,x}(x-x_{i-1,i})}\right) e^{i\beta z}, \tag{5.1}$$

where the subscript i is used to indicate the layer for which the electric field is to be calculated and hence it can assume the values $1,2,3,4,5$.

Since the dielectric function is piecewise constant along the x-axis, the electric field needs to satisfy the Helmholtz equation, eq. (2.32) in each region, hence

$$0 = (\nabla^2 - \beta^2 + k_0^2 \varepsilon_i)E_i(x,z), \tag{5.2}$$

from which it can be concluded that $k_{i,x} = \sqrt{k_0^2 \varepsilon_i - \beta^2}$ for each region i. Furthermore, the transverse components of the electric and magnetic fields are continuous across the boundary. By looking at the transverse electric field at the interface between layer i and layer $j = i + 1$ one can obtain the following equation

$$E_{i,R}\, e^{ik_{i,x}d_i} + E_{i,L}\, e^{-ik_{i,x}d_i} = E_{j,R} + E_{j,L}, \tag{5.3}$$

where $d_i = x_{i,j} - x_{i-1,j-1}$ is the width of layer i. From Maxwell's equations, eq. (2.24), it can be found that the z-component of the magnetic field is given by $H_z = (i\omega\mu_0)^{-1}\partial E_y/\partial x$, hence by the requirement that H_z is continuous across the interface one can obtain

$$E_{i,R}\, e^{ik_{i,x}d_i} - E_{i,L}\, e^{-ik_{i,x}d_i} = \frac{k_{j,x}}{k_{i,x}}\left(E_{j,R} - E_{j,L}\right). \tag{5.4}$$
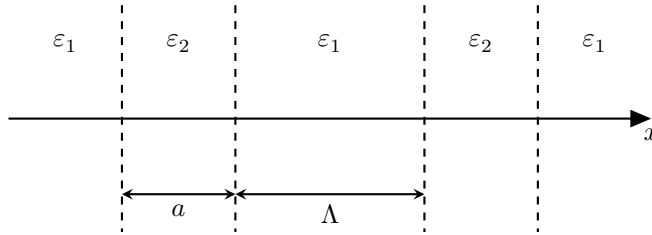

Figure 5.1: *Two waveguides that are coupled together if the separation distance Λ is sufficiently small.*

Solving eqs. (5.3) and (5.4) for $E_{j,R}$ and $E_{j,L}$ by adding and subtracting the equations yields

$$
\begin{bmatrix} E_{j,R} \\ E_{j,L} \end{bmatrix} = \frac{1}{2} \begin{bmatrix} 1 + \frac{k_{i,x}}{k_{j,x}} & 1 - \frac{k_{i,x}}{k_{j,x}} \\ 1 - \frac{k_{i,x}}{k_{j,x}} & 1 + \frac{k_{i,x}}{k_{j,x}} \end{bmatrix} \begin{bmatrix} \mathrm{e}^{\mathrm{i}k_{i,x}d_i} & 0 \\ 0 & \mathrm{e}^{-\mathrm{i}k_{i,x}d_i} \end{bmatrix} \begin{bmatrix} E_{i,R} \\ E_{i,L} \end{bmatrix}. \tag{5.5}
$$

The first matrix, in the above equation, describes how the field changes across an interface and the second matrix describes how the field propagates inside a single layer of the structure. Assuming the coefficient $E_{1,L}$ and $E_{1,R}$ are known, this equation can be used to calculate the field in the second layer and henceforth. Introducing the notation $\bar{H}_{ij}$ for the first matrix (including the factor $1/2$) and $\bar{L}_i$ for the second matrix, we shall write

$$
\begin{bmatrix} E'_{i,R} \\ E'_{i,L} \end{bmatrix} = \bar{L}_i \begin{bmatrix} E_{i,R} \\ E_{i,L} \end{bmatrix}. \tag{5.6}
$$

Then it is possible to set up an equation for the coefficients for the five-layer structure

$$
\begin{bmatrix} E_{5,R} \\ E_{5,L} \end{bmatrix} = \bar{H}_{45}\bar{L}_4\bar{H}_{34}\bar{L}_3\bar{H}_{23}\bar{L}_2\bar{H}_{12} \begin{bmatrix} E'_{1,R} \\ E'_{1,L} \end{bmatrix} \tag{5.7}
$$

$$
= \bar{S} \begin{bmatrix} E'_{1,R} \\ E'_{1,L} \end{bmatrix}. \tag{5.8}
$$

To determine the guided eigenmodes of the coupled waveguides, we look at the case where there are no incoming field i.e. $E_{1,R} = E_{5,L} = 0$. Then it follows from eq. (5.8) that

$$
E_{5,L} = S_{21}E'_{1,R} + S_{22}E'_{1,L} \implies S_{22}E'_{1,L} = 0, \tag{5.9}
$$

where S_{21} and S_{22} are components of $\bar{S}$. Since the fields in region 1 and 5 are evanescent waves, then $E'_{1,L} \neq 0$, we require therefore that

$$
S_{22}(\beta) = 0, \tag{5.10}
$$

which can be solved for β numerically.

5.2 Coupled Mode Theory

In this section, we will be looking into the coupling of waveguides approximately as opposed to the exact model introduced in section 5.1. Consider two isolated waveguides oriented along the z-axis with refractive index n_1 and n_2, respectively as in fig. 5.2. Furthermore, the electric field is polarised along the y-direction and it is required that this electric field satisfy the scalar equation for each waveguide isolated

$$
\nabla^2 E_{y,i}(x,y,z) + n_i^2(x,y)k_0^2 E_{y,i}(x,y,z) = 0. \tag{5.11}
$$

In the case where both waveguides are uniform along the z-axis the electric field will only change with a phase-factor along the z-axis

$$
E_{y,i}(x,y,z) = E_i(x,y)\,\mathrm{e}^{-\mathrm{i}\beta_i z}, \tag{5.12}
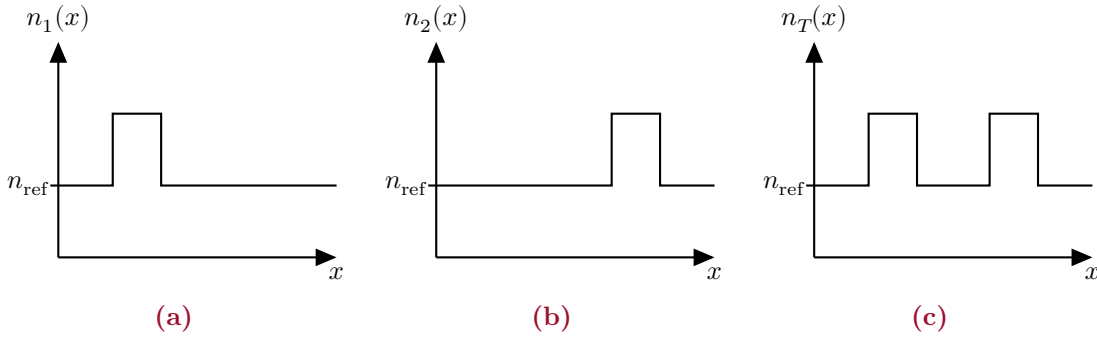$$

Figure 5.2: *(a-b) Two refractive index distributions of two isolated waveguides. (c) The refractive index of the same two waveguides in the same geometry.*

where $i \in \{1, 2\}$ and $E_i(x, y)$ and β_i is the transverse field and the propagation constant for the i'th waveguide respectively. These solution should also fulfil the scalar equation

$$\nabla_\perp^2 E_i(x, y) + [n_i(x, y)k_0^2 - \beta_i]E_i(x, y) = 0, \tag{5.13}$$

where $\nabla_\perp$ denotes the transverse part of the nabla operator. These equations can be solved for β_i and $E_i(x, y)$ and we will in the following assume they are known.

Consider now two waveguides in the same geometry as in fig. 5.2c. The electric field will need to satisfy the scalar equation

$$\nabla^2 E(x, y, z) + n_T^2(x, y)k_0^2 E(x, y, z) = 0, \tag{5.14}$$

where n_T^2 is the combined refractive index distribution of waveguides, i.e. $n_T = n_1 + n_2 - n_{\text{ref}}$. Assume that the electric field in this geometry can be described as a superposition of the electric fields for the two isolated waveguides

$$E(x, y, z) = A_1(z)E_1(x, y)\,\mathrm{e}^{-\mathrm{i}\beta_1 z} + A_2(z)E_2(x, y)\,\mathrm{e}^{-\mathrm{i}\beta_2 z}, \tag{5.15}$$

where A_1 and A_2 are the amplitude of the two modes [9]. Using this solution with eq. (5.14) and simplifying the resulting expression using eq. (5.11), then the following equation can be obtained

$$0 = \left[A_1(n_T^2 - n_1^2)k_0^2 E_1 + \frac{\mathrm{d}^2 A_1}{\mathrm{d}z^2}E_1 - 2\,\mathrm{i}\beta_1\frac{\mathrm{d}A_1}{\mathrm{d}z}E_1 \right]\mathrm{e}^{-\mathrm{i}\beta_1 z}$$
$$+ \left[A_2(n_T^2 - n_2^2)k_0^2 E_2 + \frac{\mathrm{d}^2 A_2}{\mathrm{d}z^2}E_2 - 2\,\mathrm{i}\beta_2\frac{\mathrm{d}A_2}{\mathrm{d}z}E_2 \right]\mathrm{e}^{-\mathrm{i}\beta_2 z}. \tag{5.16}$$

The above expression introduced two new functions; $n_T^2 - n_1^2$ and $n_T^2 - n_2^2$. One should remember that the dielectric constant and the refractive index is connected through $n^2 = \varepsilon_r$, therefore can $n_T^2 - n_1^2$ be interpreted as a perturbation in dielectric constant $\Delta\varepsilon_{r,1}$ to waveguide 1 caused by the neighbouring waveguide. A similar interpretation can be made for $n_T^2 - n_2^2$ [9].

To move forward with the calculations, it will be assumed that the second-order derivatives of the amplitude can be neglected. Applying this approximation and multiplying eq. (5.16) with the complex conjugated solutions of waveguide 1 and integrating over the device cross-section gives the first of the two following equations whereas the other is obtained by multiplying with the complex conjugated solutions of waveguide 2

$$
k_0^2 \langle E_1 | A_1(n_T^2 - n_1^2) | E_1 \rangle - 2\,\mathrm{i}\beta_1 \frac{\mathrm{d}A_1}{\mathrm{d}z} \langle E_1 | E_1 \rangle
$$
$$
+ \left[k_0^2 \langle E_1 | A_2(n_T^2 - n_2^2) | E_2 \rangle - 2\,\mathrm{i}\beta_2 \frac{\mathrm{d}A_2}{\mathrm{d}z} \langle E_1 | E_2 \rangle \right] \mathrm{e}^{-(\beta_2 - \beta_1)z} = 0 \tag{5.17}
$$

$$
k_0^2 \langle E_2 | A_2(n_T^2 - n_2^2) | E_2 \rangle - 2\,\mathrm{i}\beta_2 \frac{\mathrm{d}A_2}{\mathrm{d}z} \langle E_2 | E_2 \rangle
$$
$$
+ \left[k_0^2 \langle E_2 | A_1(n_T^2 - n_2^2) | E_1 \rangle - 2\,\mathrm{i}\beta_2 \frac{\mathrm{d}A_1}{\mathrm{d}z} \langle E_2 | E_1 \rangle \right] \mathrm{e}^{-\mathrm{i}(\beta_1 - \beta_2)z} = 0. \tag{5.18}
$$

Here we have used $\langle \cdot | \cdot \rangle$ to denote the integrals. These equations can be simplified by making several approximations. It will be assumed that the overlap terms are small, hence the overlap integral $\langle E_2 | E_1 \rangle$ and $\langle E_1 | E_2 \rangle$ can be neglected. This is a reasonable approximation as long as the guides are not too close together. The self-coupling terms $\langle E_1 | A_1(n_T^2 - n_1^2) | E_1 \rangle$ and $\langle E_2 | A_2(n_T^2 - n_2^2) | E_2 \rangle$ can be neglected as well, since they are only non-zero in regions of the perturbations $\Delta\varepsilon_{r1}$ and $\Delta\varepsilon_{r2}$, respectively. That is in the regions where the evanescent fields of E_1 and E_2 are already small, hence

$$
-2\,\mathrm{i}\beta_1 \frac{\mathrm{d}A_1}{\mathrm{d}z} \langle E_1 | E_1 \rangle + A_2 k_0^2 \langle E_1 | A_2(n_T^2 - n_1^2) | E_2 \rangle \, \mathrm{e}^{-\mathrm{i}(\beta_2 - \beta_1)z} = 0 \tag{5.19}
$$

$$
-2\,\mathrm{i}\beta_2 \frac{\mathrm{d}A_2}{\mathrm{d}z} \langle E_2 | E_2 \rangle + A_1 k_0^2 \langle E_2 | A_2(n_T^2 - n_2^2) | E_1 \rangle \, \mathrm{e}^{-\mathrm{i}(\beta_1 - \beta_2)z} = 0. \tag{5.20}
$$

Due to the symmetry of the geometry, it stands to reason that the coupling between the waveguides should not change if the positions of the waveguides are swapped, hence it will be assumed that the following equation will hold

$$
k_0^2 \langle E_1 | n_T^2 - n_1^2 | E_2 \rangle / \langle E_1 | E_1 \rangle \approx k_0^2 \langle E_2 | n_T^2 - n_2^2 | E_1 \rangle / \langle E_2 | E_2 \rangle. \tag{5.21}
$$

Furthermore the propagation constants will be assumed to be approximately equal i.e. $\beta_1 \approx \beta_2 \approx \beta_0$. With these simplifications eqs. (5.19) and (5.20) can be rewritten into

$$
\frac{\mathrm{d}A_1}{\mathrm{d}z} + \mathrm{i}\kappa A_2 \, \mathrm{e}^{-\mathrm{i}(\beta_2 - \beta_1)z} = 0 \tag{5.22}
$$

$$
\frac{\mathrm{d}A_2}{\mathrm{d}z} + \mathrm{i}\kappa A_1 \, \mathrm{e}^{+\mathrm{i}(\beta_2 - \beta_1)z} = 0, \tag{5.23}
$$

where κ is the coupling coefficient given by

$$
\kappa = \frac{k_0^2}{2\beta_0} \frac{\langle E_1 | n_T^2 - n_1^2 | E_2 \rangle}{\langle E_1 | E_1 \rangle}. \tag{5.24}
$$

The change in amplitudes of the waveguides' fields are connected, as seen from eqs. (5.22) and (5.23) in the case of non-zero coupling coefficient κ. The coupling length can be found by $\pi/(2\kappa)$ and describes the distance for which guided modes are transferred from one waveguide to the other [10].

6 Results

In this project, the waveguides that are examined is an air-silica step-index optical fibre with radius $a = 100\,\mu$m and slab waveguide of the same compound with thickness $a = 200\,\mu$m. The air-silica step-index waveguide can be obtained by stripping away the cladding of a commercially available multi-mode optical fibre which leaves only the core [1]. Usually, the core has a slightly higher refractive index than the cladding (about 1 %). Since the cladding has been removed and therefore effectively been replaced by air the difference in refractive index becomes much larger.

According to [1] this makes the step index fibre able to support guided modes in the terahertz band. Particularly, in the frequency range 0.3 THz to 1 THz, corresponding to the wavelength range 300 µm to 1000 µm, the refractive index of the core has a nearly constant value of 1.96. With the parameters given above, one can calculate from the V parameter

$$V = k_0 a \sqrt{n_2 - n_1^2} \tag{6.1}$$

that frequencies above 0.6807 THz results in multiple guided modes in the air-silica step-index fibre.

6.1 Step index fibre

In this section, we will examine the step-index fibre waveguide using finite-difference frequency-domain described in section 3.2. To use the Yee mesh, the first step is to choose a method to calculate the dielectric function at the grid points. The easiest method is to check whether a grid point is inside or outside the core and assign the respective dielectric constant, the so-called staircase approximation (fig. 3.4b). This approach may be adequate when the resolution of the waveguide is large enough. To significantly improve convergence of the eigensolutions to eqs. (3.27) and (3.28), a tensor averaging scheme was implemented as described in section 3.3. An example of this averaging scheme is shown in fig. 6.1. It should be noted that the axes are different for each diagonal component of the dielectric tensor, as they are needed to be determined at different grid points.

In fig. 6.2 the magnitude of the fundamental mode has been plotted for two different wavelengths. The first thing to notice is both plots show substantial evanescent waves in agreement with [1], which becomes more substantial with increasing wavelength. This can also be expressed through the full width half maximum (FWHM) which has been calculated as a function of the V-parameter in the range 1 to 3.5 as shown in fig. 6.3a. For the examined step-index fibre, $V = 1$ corresponds to the frequency $f = 0.283$ THz and scales linearly with frequency. The FWHM was calculated by averaging the radius from
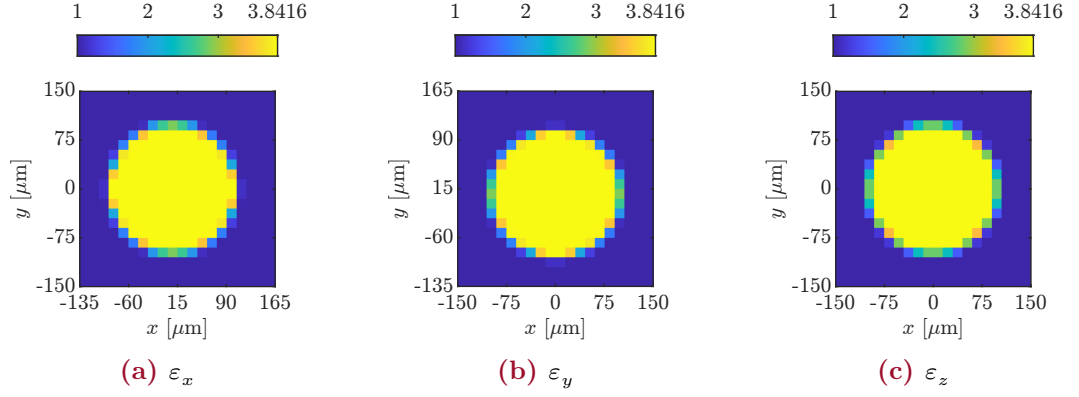
(a) ε_x　　　　(b) ε_y　　　　(c) ε_z

Figure 6.1: *An example of the tensor averaging scheme of the dielectric tensor. Here a Yee grid of size 20×20 and each box at the circle edge was split up into 1000×1000 grid points and the permittivity was determined at each point and averaged together.*

the fundamental mode's centre to all points that are positioned in a small range around half maximum e.g. all the points in the red band in fig. 6.3b was used. It should be noted that there are some bumps between $V = 2$ and $V = 3$. These bumps are non-physical and their origin is not clear. Possible explanations could be the eigensolutions were not fully converged or the grid length should have been chosen smaller. The other thing to notice is that the fundamental mode has an approximately Gaussian distribution.

For wavelengths larger than $500\,\mu$m, the grid length of $800\,\mu$m (as in fig. 6.2) is no longer sufficient to calculate the eigenmodes of the waveguide. This is because the outer grid boundary acts as a closed boundary and the field drops to zero outside. Ideally, an open boundary should be used, however, limited by memory it is enough to choose a grid length for which the field is sufficiently close to zero near the border. The field is not close to zero at the border in fig. 6.2b, however, it is adequate to give a good result.

An investigation has been performed to check at which grid length gives eigenvalues closes to those obtained from the analytical method presented in section 2.6. It was found that a grid length of $2000\,\mu$m was the most optimal for *V*-parameters in the range 1 to 7 for the examined step-index fibre.

With the optimal parameters found, the mode indices as a function of *V*-parameter have been calculated and presented in fig. 6.4a using finite difference frequency domain outlined in section 3.2. For comparison, fig. 6.4b have been calculated with the analytical expression outlined in section 2.6. We see that the modes indices in fig. 6.4a have fully converged except some tails (low β/k_0). The tails of the smoothly bending curves are not fully converged. This is most noticeable when looking at the orange curve just above $V = 4$.
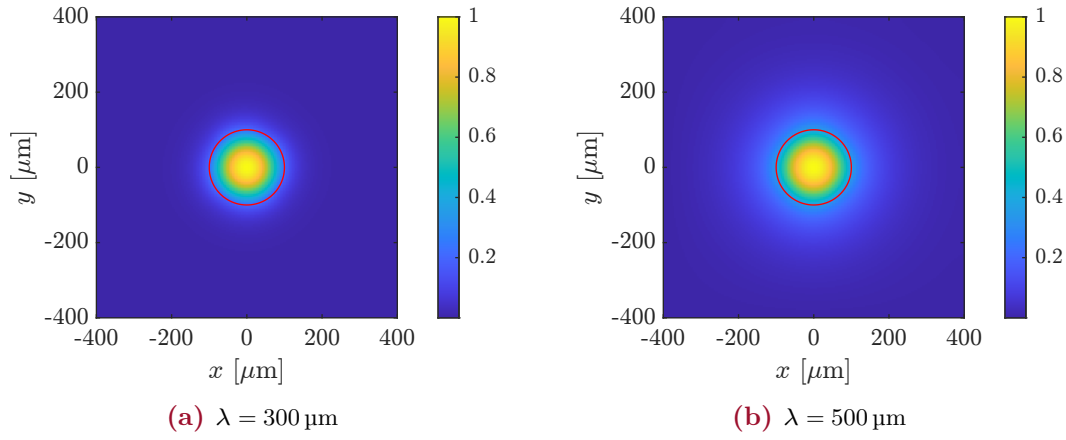
(a) $\lambda = 300\,\mu\mathrm{m}$ **(b)** $\lambda = 500\,\mu\mathrm{m}$

Figure 6.2: *A surface plot of $|\mathbf{H}_\perp|$ fundamental mode for two different wavelength. The red circle represents the $200\,\mu\mathrm{m}$ diameter waveguide.*
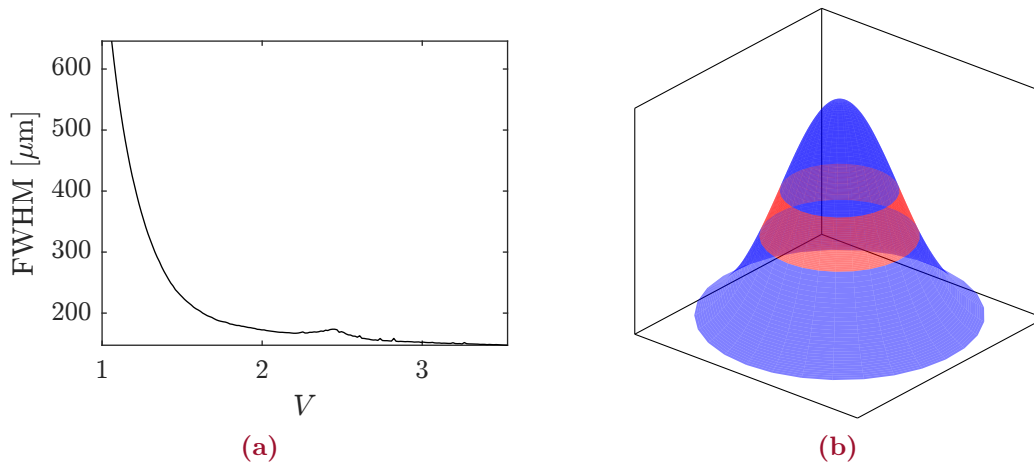

(a)   **(b)**

Figure 6.3: *(a) A plot of the FWHM as a function of the V-parameter of the air-silica step index fiber. (b) The red band illustrates where the FWHM averaging was carried out.*
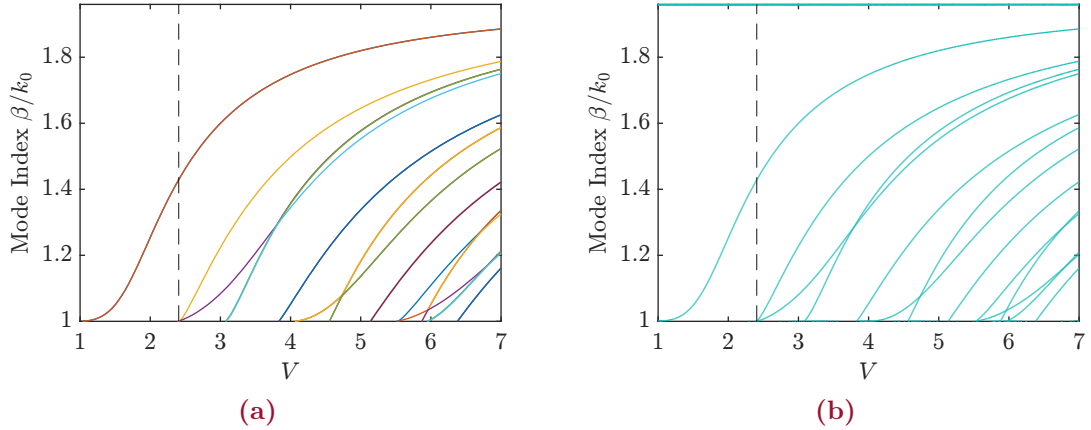
Figure 6.4: *Plots of the effective mode index for the air-silica step-index fiber. (a) Calculated with FDFD and a Yee mesh of $2000\,\mu m$ by $2000\,\mu m$ and discretised in 300×300 was used. (b) Calculated with the analytical expression in* eq. (2.113).

6.2 Mode coupling of slab waveguides

Mode coupling addresses the means of power transfer. One way to transfer power between two distinct waveguides is through evanescent waves [1, 5, 9, 10], which we will be examined in this section. The modal profiles of interest are the two modes with the highest real β. Additionally, we shall look into the coupling between these two modes.

6.2.1 Finding the mode indices

The mode indices β/k_0 was found by solving eq. (5.10) using several numerical methods. The first step is to discretise the line $\varepsilon_1 k_0 < \beta < \varepsilon_2 k_0$ for which guided modes exist and S_{22} is calculated and plotted in fig. 6.5. It is seen there exist modes where the curve crosses the dashed line around $\beta/k_0 = 1.05$, meaning that the modes can be identified by looking for sign changes in S_{22}. However these are not the modes of interest, but higher-order modes. Effectively, not all modes can be found like this as the peak around $\beta/k_0 = 1.77$ does not cross the dashed line, and the two modes that can be found there are the modes of interest. More grid points could be used, but this would require heavier computational resources and is rather time-consuming. As Λ increases, the problem will occur again and would require more grid points. A smaller discretization range $\varepsilon_1 k_0 < a < \beta < b < \varepsilon_2 k_0$ could be used, however the modes are not guaranteed to lie in the new range.

After calculating S_{22} over the grid $\varepsilon_1 k_0 < \beta < \varepsilon_2 k_0$, we decided to look for local extremas in the following way: For $S_{22} > 0$ look for local minimums and for $S_{22} < 0$ look for local maximums. This can be done for even a low number of grid points. A small grid of β-values around the corresponding extrema points is made. These sets of modes are then converged toward the true mode indices iteratively by the Newton-Raphson method.
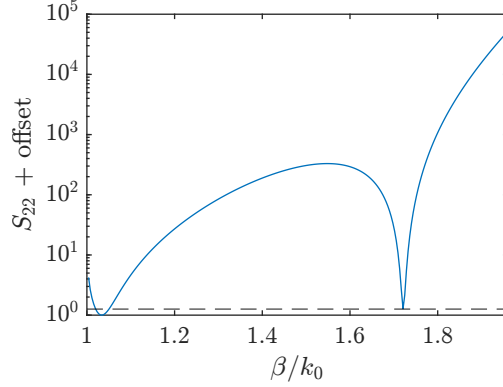
Figure 6.5: *A logaritmic plot of $S_{22}(\beta)$. The plot have been shifted upward with the offset $\min\{S_{22}\} + 1$ before taking the logarithm. The dashed line shows where the solution may be found.*

6.2.2 Result

We will compare the two coupled-mode theories describes in sections 5.1 and 5.2, where one of the methods is exact and the other is an approximation.

    Consider the geometry with two slab waveguides of width $a = 200\,\mu\text{m}$ and separation distance Λ as in fig. 5.1. Firstly we consider the exact theory from section 5.1 and look into how the isolated waveguides' fundamental modes split into the coupled waveguides' supermodes as the distance between the waveguides Λ decreases. Figure 6.6 shows the mode indices for the two supermodes with the highest real mode indices. As the Λ increases the effective mode indices of the two supermodes converges toward the mode index of a single waveguide of width $a = 200\,\mu\text{m}$ for each wavelength, because the coupling between the waveguides decreases. They converge toward the same mode in the limit as $\Lambda \to \infty$ [11]. While for small separation distances the coupling increases leading to a large separation in the mode indices. In the limit that $\Lambda \to 0$, the two supermode indices converge toward the two highest mode indices for a single waveguide of width $a = 400\,\mu\text{m}$ [11].

    Figure 6.7a shows the field amplitudes of the two supermodes waves for different wavelength. As the wavelength increases, the modes become less bounded to the waveguide and creating substantial evanescent fields. In fig. 6.7b, the fields have been calculated with the approximate coupled-mode theory. It can be seen that this method accurately depicts the fields compared with the exact calculations.

    If both super modes are exited then the field can be described as

$$\mathrm{e}^{i\beta_0 z}E_{y,0}(x) + \mathrm{e}^{i\beta_1 z}E_{y,1}(x) = \mathrm{e}^{i\beta_0 z}(E_{y,0}(x) + \mathrm{e}^{i(\beta_1 - \beta_0)z}E_{y,1}(x)), \tag{6.2}$$

with the exact method. Here $\beta_1 - \beta_0$ can be viewed as the coupling coefficient and have an important property; power transfer between waveguides. Assume the field is entirely located in waveguide 1 at $z = 0$. The field amplitudes are simply summed together here. Then after travelling some distance say, $z = \pi/|\beta_1 - \beta_0|$, then the field amplitude $E_{y,1}(x)$ is multiplied with a factor -1. This results in the field are cancelled in waveguide 1 and
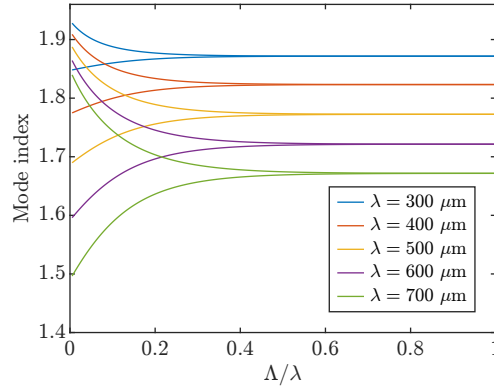
Figure 6.6: *The super mode indices for the two highest real mode indices for two coupled waveguides.*

are now entirely located in waveguide 2. Through evanescent waves, the power has been transferred from one waveguide to the other. This is shown in fig. 6.9 for weakly and strongly coupled waveguides. The distance over which such transfer occurs is highly dependent on wavelength and separation distance.

For the exact model, we call

$$\delta = \frac{\pi}{|\beta_1 - \beta_0|} \tag{6.3}$$

the coupling length and it describes the distance for which the guided modes is transferred from one waveguide to the other. In the approximate model, the coupling length can be found through eq. (5.24) as

$$\frac{\pi}{2\kappa}, \tag{6.4}$$

where κ is found by eq. (5.24). The coupling lengths as a function of the separation distance Λ is shown in fig. 6.8. The coupling length's dependence on wavelength and separation distance is clearly shown, and the power transfer can occur over distances as small as a few hundred micrometres to several meters. We also see that the approximate coupled-mode theory can accurately describe the coupling length over various separation distance Λ. Thought the approximate model predicts a slightly higher value at a very low Λ/λ value.
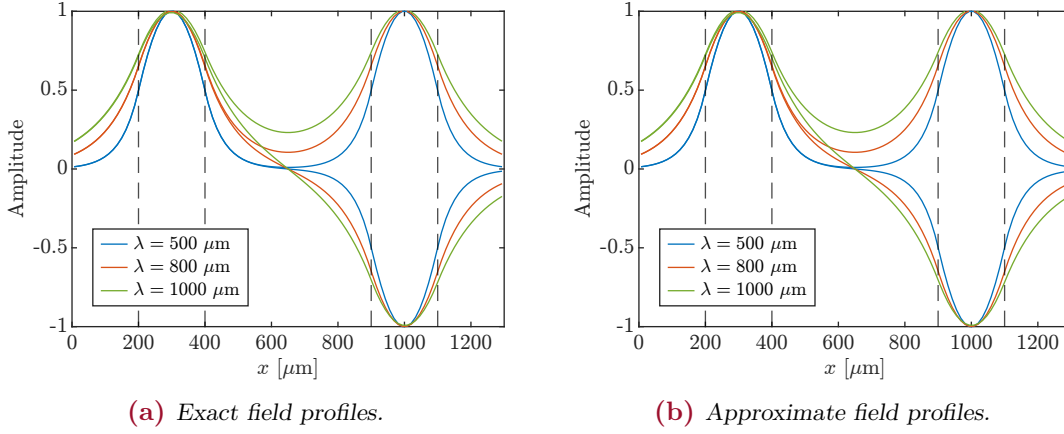
(a) *Exact field profiles.*

(b) *Approximate field profiles.*

Figure 6.7: *The field profiles of the two highest real modes in two coupled waveguides.*

(a) *Exact coupling length.*

(b) *Approximate coupling length.*
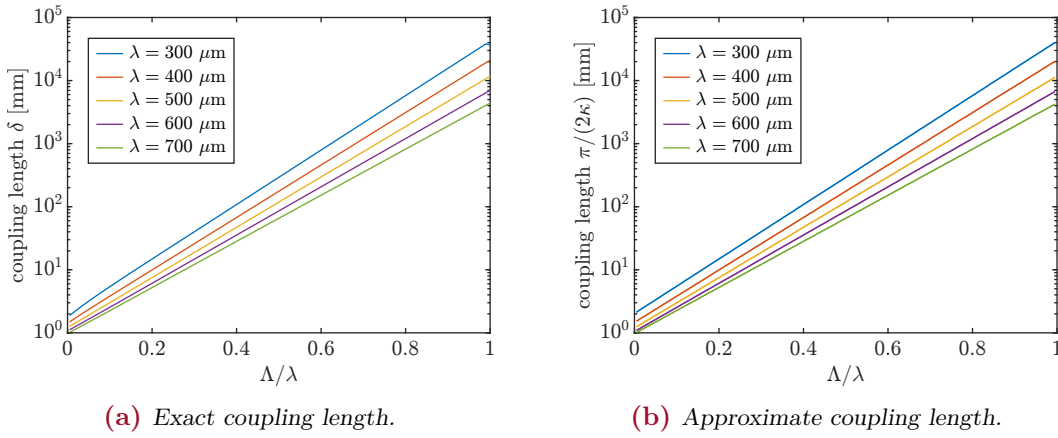
Figure 6.8: *The coupling between two waveguides is highly dependent on wavelength λ and separation distance Λ.*

(a) *Weakly coupled waveguides. $\lambda = 500\,\mu\text{m}$.*

(b) *Strongly coupled waveguides. $\lambda = 1000\,\mu\text{m}$.*
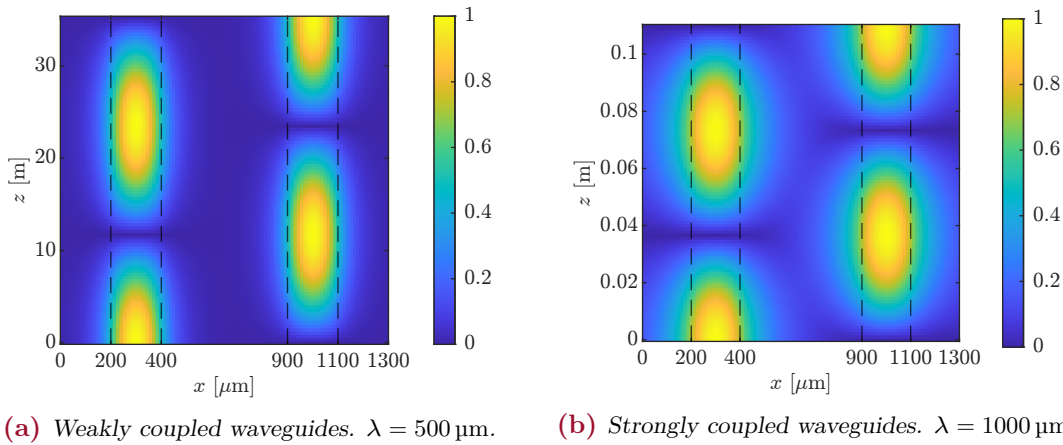
Figure 6.9: *Both plots shows power transfer with separation distance $\Lambda = 500\,\mu\text{m}$ for two different wave length. Higher wavelength leads to a smaller coupling length δ.*
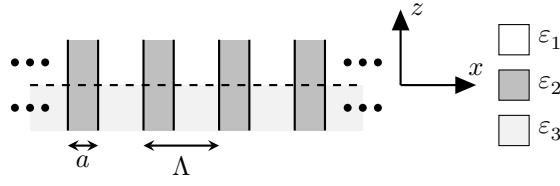
Figure 6.10: *An illustration of a two-layer structure. Each layer is invariant along the z-axis and periodic along the x-axis.*

6.3 Analysis of slab waveguides with FMM

We shall in this section discuss the use of the Fourier modal method to analyse slab waveguides in different geometries. Additionally, we shall look into the transmission and reflection of guided mode, plane wave and Gaussian beam through the geometries.

In the following subsections, we will assume that the air has permittivity $\varepsilon_1 = 1$, the slab waveguide has permittivity $\varepsilon_2 = 1.96^2$ and thickness has permittivity $a = 200\,\mu$m. Additionally, we will work with the wavelength of $\lambda = 700\,\mu$m. All other parameters will be specified in the figure captions.

6.3.1 2 layers with waveguides suspended in air and foam

Consider the geometry in fig. 6.10 wherein layer one we have semi-infinite long waveguides placed in air. In layer two the air is replaced with another material, which we will call foam. In practice, we cannot have the waveguides suspended in the air. The foam may act as supporting pillars to keep the waveguide suspended in air over long distances. However, the foam's presence will influence the field propagating in the waveguides. We will study how much influence the foam has on the transmitted field.

In fig. 6.11 the electric field have been plotted for the geometry in fig. 6.10 for various refractive indices of the foam. Here we have a backward propagating guided mode incident from the upper layer. At the interface, the field is largely transmitted and is only slightly reflected. The transmitted field is slightly, fairly, and greatly scattered in the foam for low, medium, and high refractive index, respectively. This is contributed by the reduction of confinement of the guided mode in the waveguide in the bottom layer. Whereas in fig. 6.12 the electric field has been plotted for the geometry in fig. 6.10 for various refractive indices of the foam. Here we have a forward propagating guided mode incident from the bottom layer. At the interface, the field is largely transmitted and the reflection varies with ε_3. The transmitted field is slightly, fairly, and greatly scattered in the air for low, medium, and high refractive index, respectively.

In fig. 6.13 the transmission and reflection are plotted with the guided mode incident from the top layer. In fig. 6.14 the transmission and reflectance are plotted with the guided mode incident from the bottom layer. The blue curves describe the total reflection and transmission, whereas the red curves only account of the reflection and transmission into the guided mode of layer one and two, respectively. Note that the reflection for the two graphs in fig. 6.13a and fig. 6.14a are similar for small values of n_3. As n_3 increases,

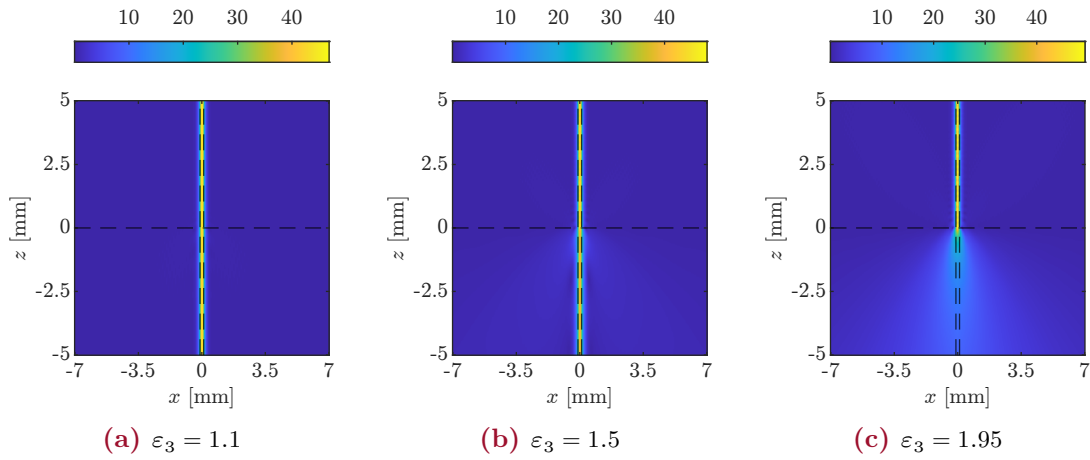**(a)** $\varepsilon_3 = 1.1$ **(b)** $\varepsilon_3 = 1.5$ **(c)** $\varepsilon_3 = 1.95$

Figure 6.11: *The field distribution of fig. 6.10 with a guided mode incident from the upper layer. We used $\Lambda = 400\,000\,\mu$m and 4001 plane waves.*

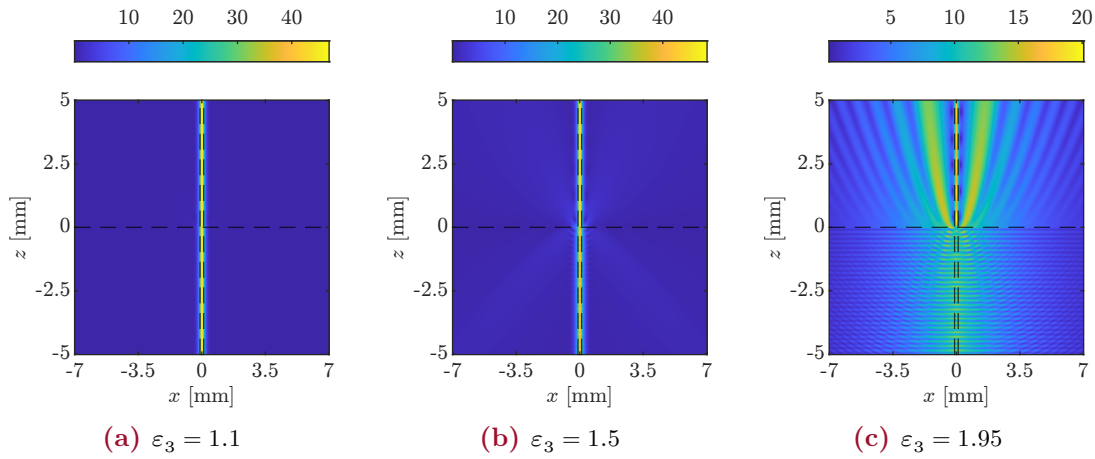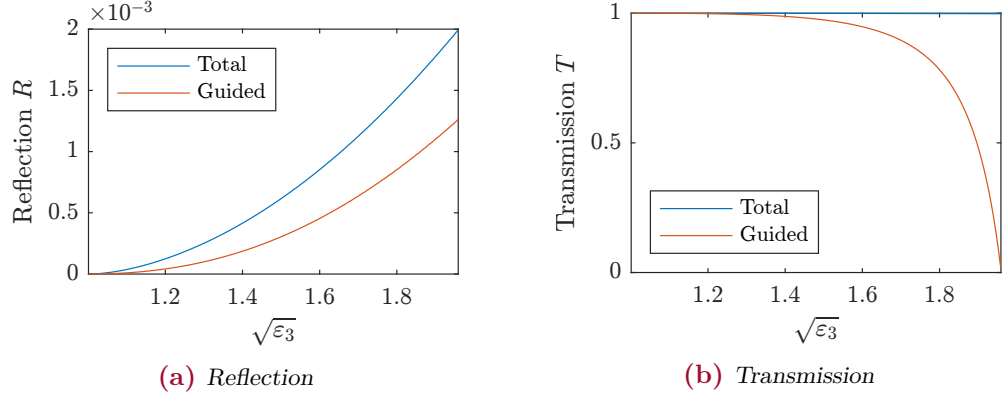**(a)** $\varepsilon_3 = 1.1$ **(b)** $\varepsilon_3 = 1.5$ **(c)** $\varepsilon_3 = 1.95$

Figure 6.12: *The field distribution of fig. 6.10 with a guided mode incident from the bottom layer. We used $\Lambda = 400\,000\,\mu$m and 4001 plane waves.*

(a) *Reflection*

(b) *Transmission*

Figure 6.13: *The reflection and transmission of fig. 6.10 with a guided mode incident from the upper layer. We used $\Lambda = 40\,000\,\mu\text{m}$ and 1001 plane waves.*
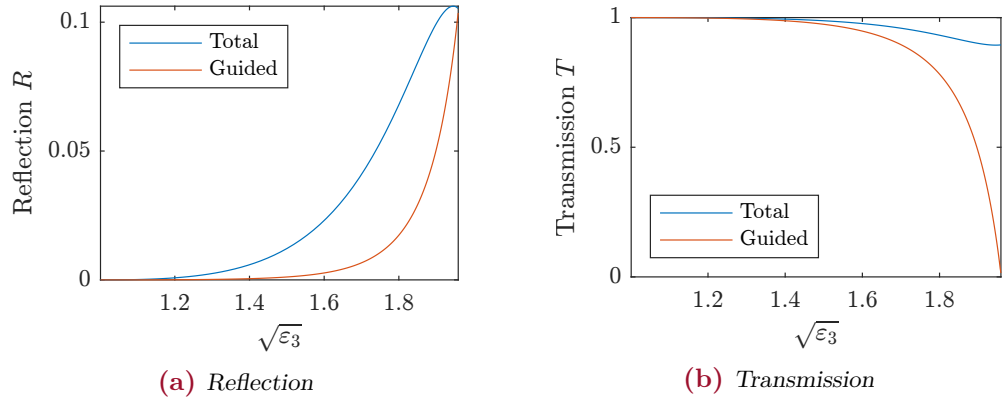

(a) *Reflection*

(b) *Transmission*

Figure 6.14: *The reflection and transmission of fig. 6.10 with a guided mode incident from the bottom layer. We used $\Lambda = 40\,000\,\mu\text{m}$ and 1001 plane waves.*

the difference becomes more prominent. This is due to the fact that the mode incident in the bottom layer becomes more loosely bound due to the difference between the refractive index of the waveguide and the foam becomes smaller. For the mode incident towards the upper layer, the modes remain strongly bounded due to the difference between the refractive index of the waveguide and air remain the same.

6.3.2 3 layers with waveguides suspended in air and foam

The illustration, fig. 6.16, shows the electric field distribution for the three-layer structure given in fig. 6.15. The calculation was performed with $\Lambda = 20\,000\,\mu\text{m}$. For the incident mode in layer 1, we choose the mode with the largest real propagation constant β. The first thing to notice is the scattering of the incoming mode when it crossed into layer 2 grows larger as ε_3 grows. When $\varepsilon_3 < 1.2$ then the scattering is fairly low and the field inside the waveguide is only slightly disturbed. For large values of ε_3, the field has been scattered significantly and the transmission of the field into the guided mode is
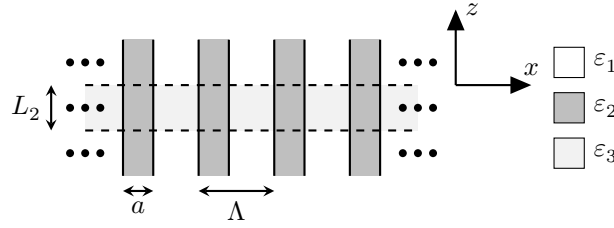
Figure 6.15: *An illustration of a three-layer structure. Each layer is invariant along the z axis and periodic along the x axis.*
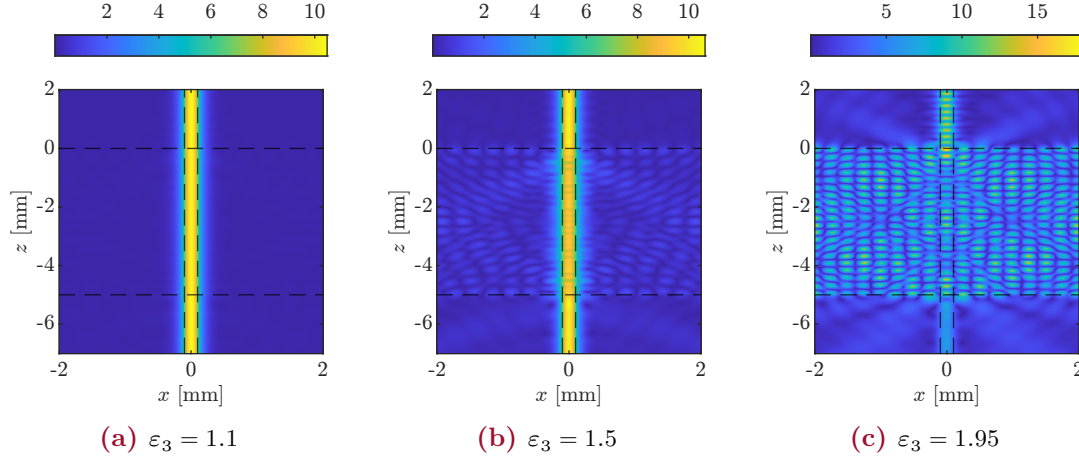

(a) $\varepsilon_3 = 1.1$ **(b)** $\varepsilon_3 = 1.5$ **(c)** $\varepsilon_3 = 1.95$

Figure 6.16: *The field distribution of fig. 6.15 with the upper layer's guided mode incident from above. We used $\Lambda = 20\,000\,\mu m$ and 1001 plane waves in the calculation. The fields are affected by substantial parasitic waves.*

significantly lowered.

It should be noted that the field in figs. 6.16b and 6.16c are both subject to substantial parasitic waves from neighbouring waveguides leading to advanced interference patterns. It shows that the choice of Λ should have been much larger in order to describe the field for a single waveguide accurately. As shown in fig. 6.17, even at $\Lambda = 400\,000\,\mu m$ the effect of the parasitic waves is still too large to approximate the field for a single waveguide. Calculation with so large a period requires a very large number of plane waves and is very computationally heavy in terms of both time and memory.

As mentioned in section 4.4, there are several methods to reduce the parasitic waves. The method we tried out is using a complex period $\Lambda = \Lambda_R + i\Lambda_I$, where we can control the dampening with Λ_I. The field is shown in fig. 6.18. Thought the field near the waveguide look to be unaffected by parasitic waves and give a nice field. However, from around $|x| > \Lambda_R/2$ the field is greatly disturbed by Λ_I due to exponential increasing waves. For a smaller Λ_I, this occur first at a larger $|x|$-values. Therefore to use a complex period, one should choose a large Λ_R and small Λ_I.

The transmission and reflectance of an incident guided mode through the three-layer structure fig. 6.15 was investigated. The transmission and reflectance depends on refractive
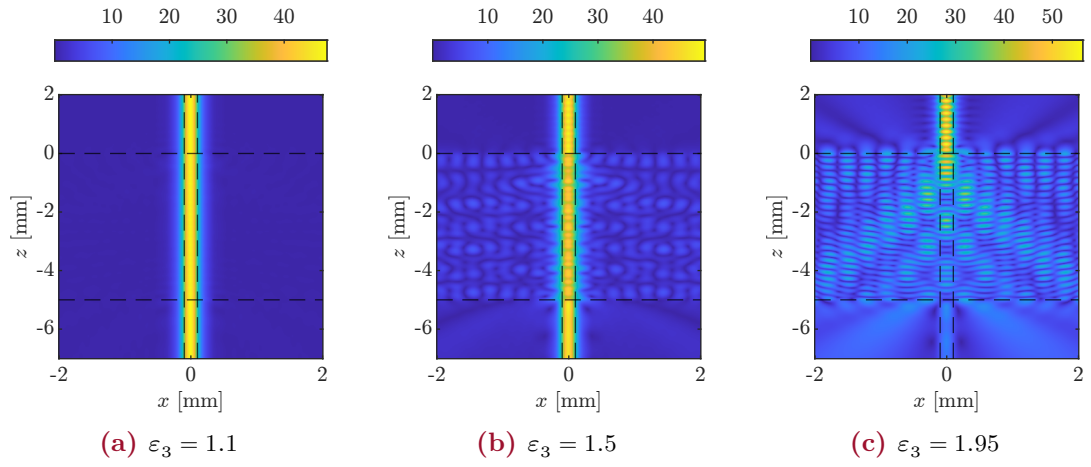
(a) $\varepsilon_3 = 1.1$ **(b)** $\varepsilon_3 = 1.5$ **(c)** $\varepsilon_3 = 1.95$

Figure 6.17: *The field distribution of fig. 6.15 with the upper layer's guided mode incident from above. We used $\Lambda = 400\,000\,\mu m$ and 4001 plane waves in the calculation. The fields are affected by substantial parasitic waves.*

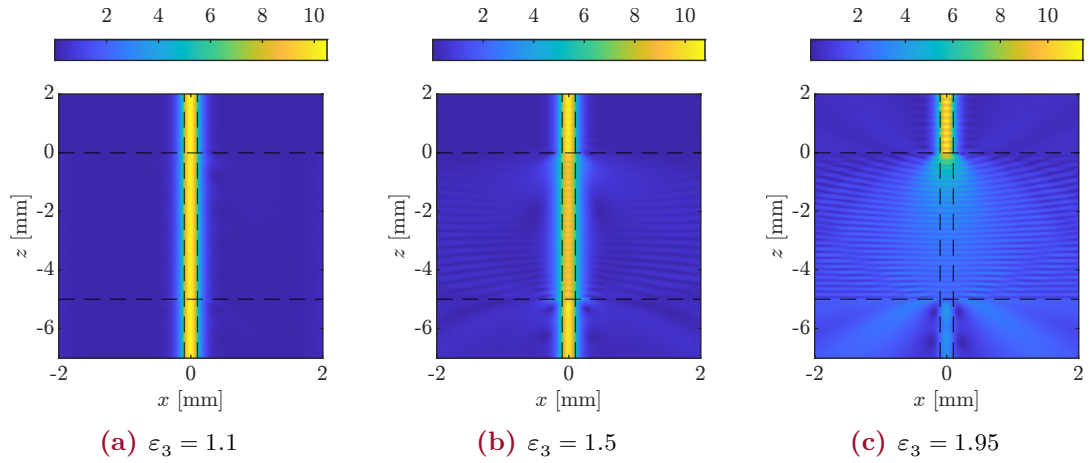**(a)** $\varepsilon_3 = 1.1$ **(b)** $\varepsilon_3 = 1.5$ **(c)** $\varepsilon_3 = 1.95$

Figure 6.18: *The field distribution of fig. 6.15 with the upper layer's guided mode incident from above. We used $\Lambda = (20\,000 + 600i)\,\mu m$ and 1001 plane waves in the calculation. The fields are not affected by parasitic waves.*

(a) *The reflection of a guided mode in layer 1 back into a forward propagating mode in layer 1.*

(b) *The total reflection of a guided mode in layer 1.*

(c) *The transmission of a guided mode in layer 1 to the guide mode in layer three.*

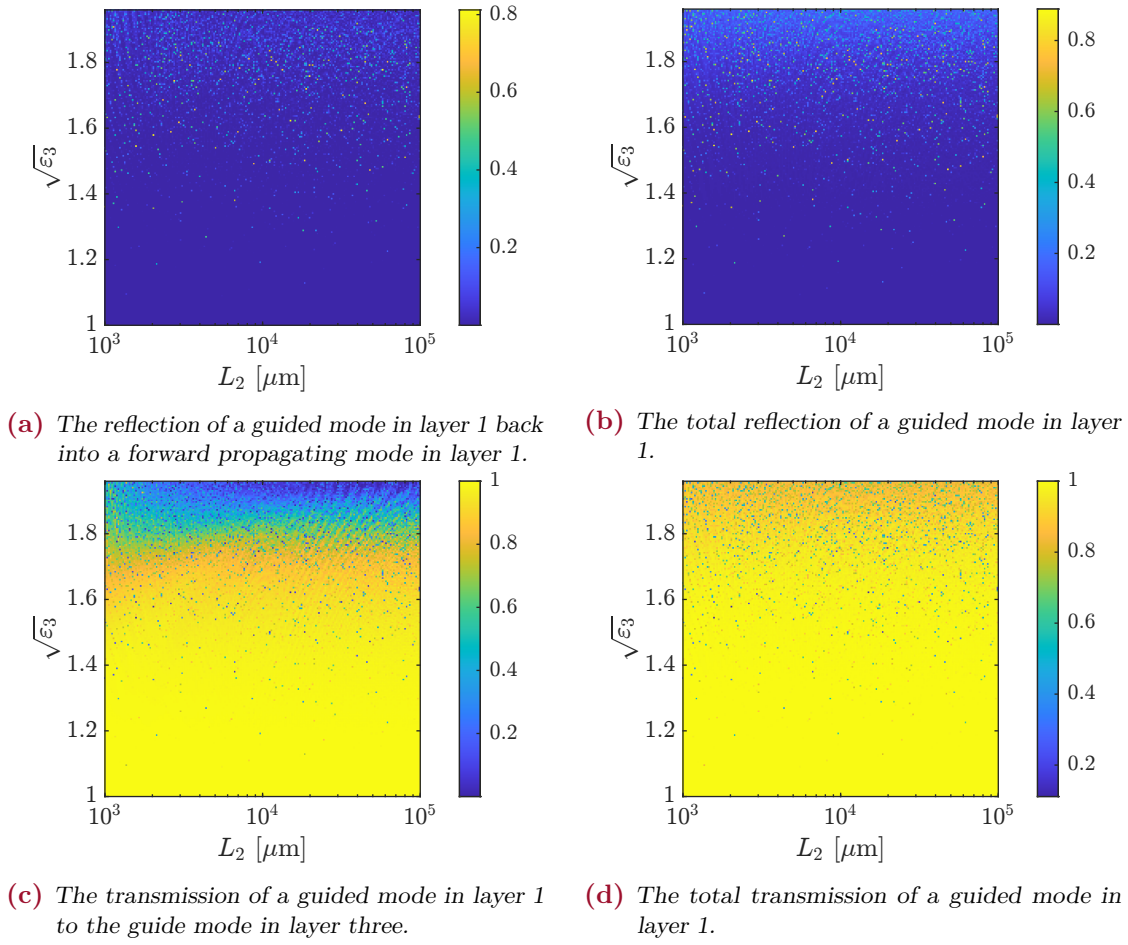**(d)** *The total transmission of a guided mode in layer 1.*

Figure 6.19: *A plot of the reflection and transmission of a guide mode from above for the structure in fig. 6.15.*

index of the surrounding foam in layer two and the length of layer two L_2 as seen in fig. 6.19. These plots are created with a period $\Lambda = 12\,000\,\mu\text{m}$. In fig. 6.19c it can be seen that the transmission is approximately equal one for $n_3 < 1.6$. However as $n_3 > 1.7$ the guided mode in the middle layer becomes loosely bounded resulting in less excitation of this mode. Figure 6.19b and Figure 6.19a indicates that there is a low loss due to reflection for most refractive indices of the form. However for large values of n_3 there seems to be introduced a small amount of loses due to an increase in reflection. It is found that the transmission and reflection is largely independent of L_2.

Gaussian beam

Here we will look at the 2-layer structure given in fig. 4.5 with a normal incident Gaussian beam from above. We have air in layer 1 and in layer 2 we have a periodic array of waveguides with air surrounding it.
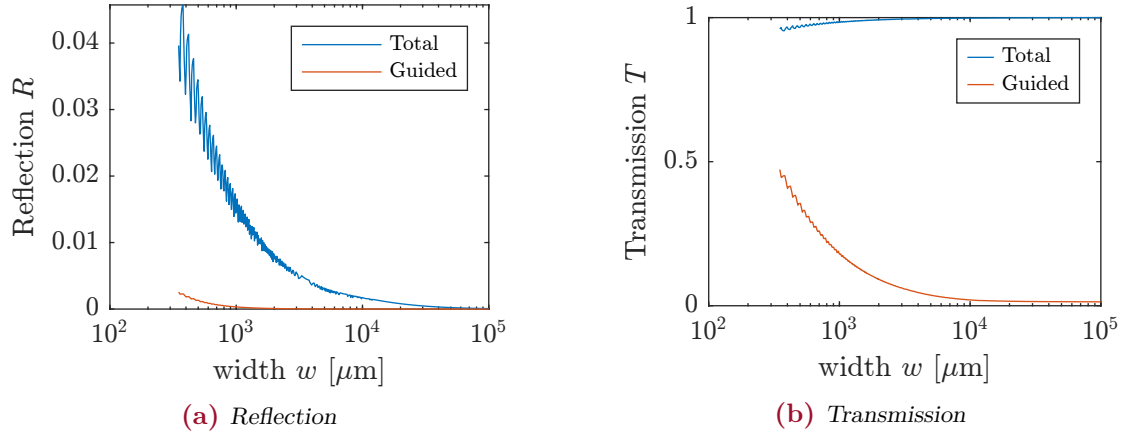
(a) *Reflection*

(b) *Transmission*

Figure 6.20: *Reflection and transmission of a Gaussian beam normal incident from above on a two-layer structure fig. 6.10.*

The transmission and reflection of the Gaussian beam through the interface depends on the beam width, w, as shown in fig. 6.20. The blue curves describe the total reflection and transmission, whereas the red curves only account of how much of the field is transmitted into the waveguide's guided mode. Since we used the approximation $w \ll \Lambda$ when the theory was derived in section 4.3.3, we need to make sure that this requirement is satisfied for every beam width w in fig. 6.20. This is done by scaling the period Λ with increasing w such that $\Lambda/w = 10$.

For the case of small $w \lessgtr 2000\,\mu\mathrm{m}$, the reflection develops chaotic, which may occur due to evanescent waves or parasitic scattering due to small period. As w increases, an increasing amount of the field propagates through the air outside of the waveguide which results in the total transmission goes towards 1. The guided transmission goes to zero for large ω. The latter is misleading because most of the power is transmitted through the air.

When looking at the field fig. 6.21 another interpretation arise. The field in the waveguides seems equal amplitude (it is in arbitrary units). From fig. 6.21a is can be seen that the field excites the guided mode of the waveguide while some of it is also scattered into to air. As the beam width increases, more of the field propagates in the air. Comparing the field in fig. 6.21c with the field infig. 4.6f, they are almost identical. For large w, the field is almost constant over a small interval along the x-axis i.e. $|x| \ll w$ and propagates in one direction. Hence they are similar in properties and therefore a single plane wave can approximate a wide Gaussian beam.
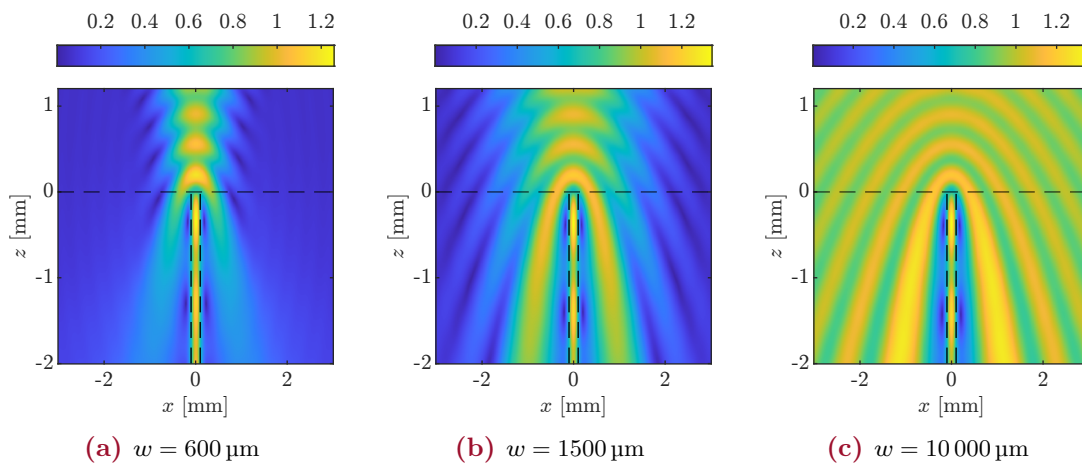
(a) $w = 600\,\mu\text{m}$ **(b)** $w = 1500\,\mu\text{m}$ **(c)** $w = 10\,000\,\mu\text{m}$

Figure 6.21: *The absolute electric field of fig. 4.5 with an normal incident Gaussian beam from the upper layer. We used $\Lambda = 400\,000\,\mu\text{m}$ and 4001 plane waves in the calculation.*

7 Conclusion

This project aimed to examine the air-silica step-index fibre presented in *Ultra-High Q terahertz whispering-gallery modes* [1]. One of the first things that where examined was the mode profile as a function of the *V*-parameter. It was found for the 200 μm diameter step-index fibre, that frequencies below 0.6807 THz result in single mode. For frequencies below this, the width of the fibre's fundamental mode greatly increased with decreasing frequencies leading to large evanescent waves.

Air-silica slab waveguides of thickness 200 μm were also studied. We investigated the mode coupling of two identical slab waveguides by evanescent waves and found that the coupling length ranges between a few hundred micrometres to several metres. Furthermore, the coupled-mode theory gave satisfactory results in terms of coupling length and field profiles compared to analytical calculations.

To study two-dimensional geometries, we used Fourier modal method to examine single slab waveguides in two-layer and three-layer geometries. The foam was introduced to hold the waveguides suspended in the air and the effect of its presence was investigated. Moreover, it is evident from the field plots that the field scattering at the interfaces between the layers is low for a low refractive index of the foam. For a high refractive index, the scattering is increased leading to a great loss of power. The thickness of the foam was not found to have any prominent influence of the transmission and reflection.

In an attempt to get rid of advance interference patterns which occurred due to parasitic scattering, we tried to see the effects of introducing a complex period, Λ, and increase the number of plane waves used in the plane-wave expansion. It was here found that due to the limitation of the computational equipment available, the dampening effect, due to the complex period, was found the be most effective. However, the field may be affected by exponential increasing waves for large $|x|$-values but unaffected by them near the waveguide. A similar course of action was performed but instead of sending in a guided mode towards the structure, a Gaussian beam was incident. It was found that the reflection of a Gaussian beam was low.

References

[1]   Dominik Walter Vogt and Rainer Leonhardt. 'Ultra-high Q terahertz whispering-gallery modes in a silicon resonator'. In: *APL Photonics* 3.5 (2018), p. 051702. DOI: 10.1063/1.5010364. eprint: https://doi.org/10.1063/1.5010364. URL: https://doi.org/10.1063/1.5010364.

[2]   Thomas Møller Søndergaard. *Green's Function Integral Equation Methods in Nano-Optics.* CRC Press, Jan. 2019. ISBN: 9781351260206. DOI: 10.1201/9781351260206.

[3]   Andrei V Lavrinenko et al. *Numerical Methods in Photonics.* eng. 1st ed. Vol. 1. CRC Press, 2015, pp. 1–334. ISBN: 9781466563889.

[4]   David J. Griffiths. *Introduction to Electrodynamics.* eng. 4. ed. New International Edition. Upper Saddle River NJ: Pearson, 2014. ISBN: 9781292021423.

[5]   Govind P. Agrawal. *Nonlinear fiber optics.* eng. 5th ed. Optics and Photonics. Amsterdam: Academic Press. ISBN: 0-12-397307-4.

[6]   Lukas Novotny and Bert Hecht. *Principles of Nano-Optics.* eng. Vol. 9781107005464. 2012, pp. 1–564. ISBN: 9781107005464.

[7]   Jorge. Nocedal. *Numerical Optimization.* eng. 2nd ed. Springer Series in Operations Research and Financial Engineering. New York, NY: Springer New York. ISBN: 0-387-40065-6.

[8]   Thomas Møller Søndergaard. *Modeling of photonic crystals and antirefelctive microstructured surfaces using the Fourier Modal Method.* eng. Mar. 2016.

[9]   Richard. Syms. *Optical guided waves and devices.* eng. London: McGraw-Hill. ISBN: 0077074254.

[10] Manfred Hammer. *Coupled Mode Theory.* 2019. URL: https://wmm.computational-photonics.eu/cmt.html.

[11] Michael L. Cooper and Shayan Mookherjea. 'Numerically-assisted coupled-mode theory for silicon waveguide couplers and arrayed waveguides'. In: *Opt. Express* 17.3 (Feb. 2009), pp. 1583–1599. DOI: 10.1364/OE.17.001583. URL: http://www.opticsexpress.org/abstract.cfm?URI=oe-17-3-1583.